

The copyright of this thesis vests in the author. No quotation from it or information derived from it is to be published without full acknowledgement of the source. The thesis is to be used for private study or non-commercial research purposes only.

Published by the University of Cape Town (UCT) in terms of the non-exclusive license granted to UCT by the author.

Characterization of gold catalysts for methanol synthesis

MSc Thesis

Tracey van Heerden

2012



Centre for Catalysis Research, Chemical Engineering Department, University of
Cape Town, Rondebosch, South Africa

ACKNOWLEDGEMENTS

I would like to extend my sincere gratitude to a number of people and organizations for their contributions to this project.

- Prof. Van Steen for his help and guidance in absolutely every aspect, for his patience, for always having an open door, for having a solution to all my unsolvable problems.
- Prof. Case for her enthusiasm and valuable input into the formation, development and eventual conclusion of this project.
- Helen, Suzanna, Lonwabo, and Stephanie for their work and help in the analytical laboratory in our department.
- Mohamed, Miranda and Franscious of the Electron Microscope Unit at UCT for helping me obtain all my TEM and SEM images.
- Cobus, Lucky, Waldo and Chris for always being prepared to spend their time giving me assistance and advice in the lab. The rest of the students and staff for the enjoyable and productive working environment this department has developed.
- Linda and Cindy for making me laugh when I wanted to cry and always having an ear (and an opinion) when I needed it. Marwan for being in the boat with me and for all the good coffee. Ivan for all the football videos when I needed a distraction (and when I didn't) and for introducing me to James.
- My family for being proud of me and for being understanding even when they don't understand.
- Mintek, UCT, and the NRF for financial assistance.

ABSTRACT

The activity (per mass of catalyst) of supported gold catalysts across a range of reduction and oxidation reactions is significantly affected by the average crystallite size of the gold crystallites in the catalyst. Supported gold catalysts are most commonly characterized for particle size using TEM and XRD. Both of these methods can have a large degree of inaccuracy associated with them at low metal loadings and for catalysts containing small gold crystallites. In this study oxygen chemisorption was used as an additional method to characterize supported gold catalysts to complement electron microscope techniques. Agreement between the results from these different methods was obtained only with regard to the order of magnitude range of crystallite size. The oxygen chemisorption can be used to estimate the mass fraction of gold present as nano-crystallites (typically less than 1%) implying a large room for improvement in catalyst preparation technique.

In this study a range of supported gold catalysts were prepared by ion exchange, varying a range of preparation variables, including gold concentration in the precursor solution, washing procedure using an aqueous ammonia solution, as well as drying and calcination procedures. The washing procedure and in particular the concentration of ammonia and the duration affected the final metal loading of the catalyst. TEM analyses show crystallite size distributions between 2-5nm for all catalysts excepting those which were not washed using an aqueous ammonia solution and which did not show any small crystallites. Only the total omission of the ammonia wash resulted in a significant change in the gold crystallite sizes observed on TEM-images. Further characterization with SEM showed that catalysts that appeared identical on the TEM-images also contained large 50-500nm crystallites. This additional method of characterisation using SEM allowed for the identification of significant differences between catalysts upon varying the preparation method. Catalyst drying was also shown to be a crucial step in the catalyst preparation method, with SEM images displaying only small well-distributed gold crystallites for catalysts dried in the rotary evaporator.

Two of the catalysts were then tested for their activity and selectivity in the hydrogenation of CO or CO₂. Although it has been shown that the production of methanol from CO (and CO₂) can be catalysed by gold particles with crystallite sizes below 5nm (Haruta, 1997), this reaction has received comparatively little attention compared to the more extensively studied CO oxidation reaction. Testing was done over a range of temperatures (200 - 350°C) at a pressure of 30bar. The obtained methanol yields and selectivities are comparable to reported values in literature. The hydrogenation of CO₂ was shown to have

higher yields and selectivities to methanol than the hydrogenation of CO over the same catalyst. The preparation of the catalyst was shown to have an effect on the activity and selectivity, with the catalyst dried in the rotary evaporator having a higher yield and selectivity to methanol, while also forming a larger variety of products than the catalyst dried in the oven.

University of Cape Town

TABLE OF CONTENTS

Acknowledgements.....	i
Abstract	ii
Table of Contents	v
List of Figures.....	viii
List of Tables	x
1 Literature Review	1
1.1 Methanol and its Synthesis.....	1
1.1.1 Background	1
1.2 Gold in Catalysis.....	4
1.3 Catalyst Preparation Methods.....	5
1.3.1.1 Deposition-Precipitation	5
1.3.1.2 Co-precipitation.....	6
1.3.1.3 Impregnation.....	6
1.3.1.4 Ion-exchange	6
1.4 Catalyst characterization	9
1.4.1 Electron Microscope techniques	9
TEM and HRTEM.....	9
1.4.2 XRD.....	12
1.4.3 Adsorption studies	13
1.4.3.1 CO-chemisorption	13
1.4.3.2 H ₂ – adsorption.....	15
1.4.3.3 O ₂ - chemisorption	16
1.5 Gold in Methanol synthesis.....	17
1.5.1 Effect of particle size on gold catalysts for methanol synthesis.....	17
1.5.2 Effect of catalyst support for methanol synthesis	19
2 Experimental.....	21
2.1 Catalyst preparation	21

2.1.1	Batch A.....	21
2.1.2	Batch B.....	22
2.1.3	Batch C	22
2.1.4	Batch D	22
2.2	Characterization of catalysts.....	24
2.2.1	Catalyst loading	24
2.2.2	Particle size distribution of gold crystallites	24
2.2.3	Temperature programmed adsorption and desorption of oxygen	26
2.3	Catalyst testing	26
2.4	Health and Safety	36
3	Results.....	37
3.1	Catalyst loading	37
3.2	Crystallite size distributions	39
3.2.1	TEM.....	39
3.2.1.1	Batch A – effect of gold concentration in precursor solution and calcination conditions	40
3.2.1.2	Batch B – effect of washing procedure	42
3.2.1.3	Batch C – effect of drying procedure	43
3.2.1.4	Batch D – effect of calcination temperature.....	45
3.2.2	HRTEM	47
3.2.3	SEM	50
3.2.3.1	Batch A – effect of gold concentration in precursor solution and calcination conditions	51
3.2.3.2	Batch B – effect of washing procedure	53
3.2.3.3	Batch C – effect of drying procedure	55
3.2.3.4	Batch D – effect of calcination temperature.....	58
3.3	Chemisorption	60
3.4	Catalyst testing	67

3.4.1	CO hydrogenation	67
3.4.2	CO ₂ hydrogenation	69
4	Discussion	72
4.1	Catalyst Characterization results	72
4.1.1	Crystallite size analysis.....	72
4.1.2	Effect of precursor concentration and calcination gas.....	79
4.1.3	Effect of washing procedure	82
4.1.4	Effect of drying procedure.....	84
4.1.5	Effect of calcination temperature	88
4.2	Catalyst testing.....	90
5	Conclusions	94
5.1	Oxygen chemisorption as an alternative to TEM.....	94
5.2	The effect of preparation method on catalyst characteristics	95
5.2.1	Loading efficiency.....	95
5.2.2	Gold crystallite size.....	95
5.2.3	SEM visible gold particles.....	96
5.3	Catalytic testing in CO and CO ₂ hydrogenation	96
7	References	98
8	Appendix A – Statistical Analysis	103
8.1	ANOVA and Tukey analysis of TEM	103
8.2	T-test comparison of TEM and HRTEM	114

LIST OF FIGURES

Figure 1-1: World consumption of methanol in 2008 (SRI Consulting, 2010).	2
Figure 1-2: Equilibrium conversion of carbon oxides to methanol based on reformed natural gas compositions of 73% H ₂ , 15% CO, 9% CO ₂ , 3%CH ₄ at 30, 20, 10 and 5 MPa (from top to bottom) (English <i>et al.</i> , 1992).	3
Figure 1-3 Speciation of gold as a function of pH in a 500 ml solution of 2.54 mmol H ₂ AuCl ₄ /litre solution (change in pH by addition of NaOH). Van Steen, 2009.....	8
Figure 1-4: Speciation of gold as a function of pH in a 500 ml solution of 2.54 mmol H ₂ AuCl ₄ /litre and 1 M NaNO ₃ solution (change in pH by addition of NaOH). Van Steen, 20098	
Figure 1-5: Speciation of gold as a function of pH in a 500 ml solution of 2.54 mmol H ₂ AuCl ₄ /litre and 1 M NaCl solution (change in pH by addition of NaOH). Van Steen, 2009 .	9
Figure 1-6: Diagram of interaction volume between an electron beam and the sample during SEM analysis.....	11
Figure 1-7: Hydrogen chemisorption on gold catalysts at different temperatures (Bus <i>et al.</i> , 2005)	15
Figure 1-8: Effect of particle diameter of gold in methanol synthesis from CO ₂ . ^o • d _{Au} determined by TEM observation, <input type="checkbox"/> ■ crystallite size of gold determined by XRD (Sakurai and Haruta, 1996).....	18
Figure 2-1: Catalyst testing rig flow diagram	28
Figure 2-2: Reactor configuration.....	29
Figure 2-3: Example GC-FID chromatogram.....	32
Figure 2-4: Example GC-TCD chromatogram	33
Figure 2-5: diagram to illustrate setup used to prepare a N ₂ /C ₆ mixture tank	35
Figure 3-1: Example TEM image (catalyst D200).....	39
Figure 3-2: Gold crystallite size distributions of Batch A obtained from TEM analysis	41
Figure 3-3: Gold crystallite size distributions of Batch B obtained from TEM analysis	42
Figure 3-4: Gold crystallite size distributions of Batch C obtained from TEM analysis	44
Figure 3-5: Gold crystallite size distributions of Batch D obtained from TEM analysis	46
Figure 3-6: Example HRTEM image (catalyst D400).....	47
Figure 3-7: Gold crystallite size distributions of Batch D obtained from HRTEM analysis....	49

Figure 3-8: Example SEM image (catalyst D100).....	50
Figure 3-9: Gold crystallite size 'distributions' of Batch A obtained from SEM analysis	52
Figure 3-10: Gold crystallite size 'distributions' of Batch B obtained from SEM analysis	54
Figure 3-11: Gold crystallite size 'distributions' of Batch C obtained from SEM analysis	56
Figure 3-12: SEM average particle sizes for catalysts C60, C80 and C100	56
Figure 3-13: SEM average particle sizes for catalysts of Batch D	58
Figure 3-14: Gold crystallite size 'distributions' of Batch D obtained from SEM analysis	59
Figure 3-15: Oxygen chemisorption isotherms on catalysts of Batch A at 200°C	61
Figure 3-16: Oxygen chemisorption isotherms on catalysts of Batch B at 200°C	62
Figure 3-17: Oxygen chemisorption isotherms on catalysts of Batch C at 200°C	62
Figure 3-18: Oxygen chemisorption isotherms on catalysts of Batch D at 200°C	63
Figure 3-19: Modelled and actual O ₂ chemisorption data of gold on alumina support	64
Figure 3-20: Modelled and actual O ₂ chemisorption data of gold on alumina support presented on a log scale.....	64
Figure 4-1: Comparison of gold crystallite sizes obtained from oxygen chemisorption using Vm ₁ and TEM	73
Figure 4-2: Monolayer volume plotted against gold loading	77
Figure 4-3: Gold loading vs crystallite sizes from SEM	77
Figure 4-4: Gold loading vs crystallite sizes from TEM.....	78
Figure 4-5: Effect of Au loading on volume % of small particles	79
Figure 4-6: Effect of gold precursor concentration, keeping Au : support ratio constant, on loading.....	80
Figure 4-7: Effect of gold precursor concentration, keeping Au : support ratio constant, on crystallite size of catalysts calcined at 200°C	81
Figure 4-8: Effect of gold precursor concentration, keeping Au : support ratio constant, on crystallite size of catalysts calcined at 500°C	81
Figure 4-9: Effect of washing procedure on obtained gold loading	82
Figure 4-10: Effect of washing procedure on crystallite size.....	83
Figure 4-11: Effect of washing procedure on size and frequency of large gold crystallites ..	84

Figure 4-12: Effect of drying procedure on crystallite size	85
Figure 4-13: effect of drying procedure on size and frequency of large gold crystallites	86
Figure 4-14: Example SEM images. Catalyst labels clockwise from top left - C80, C100, CDRY, CDRY	87
Figure 4-15: Effect of calcination temperature on gold loading.....	88
Figure 4-16: Effect of calcination temperature on crystallite size.....	89
Figure 4-17: effect of calcination temperature on size and frequency of large gold crystallites	90

LIST OF TABLES

Table 2-1: Catalyst preparation variables.....	23
Table 2-2: GC specifications.....	34
Table 3-1: Catalyst loading results from AAS analysis	38
Table 3-2: Parameters calculated for oxygen chemisorption models and particle size calculated from V_{m1} and V_{m2}	66
Table 3-3: Reaction parameters for testing supported gold catalysts in CO and CO ₂ hydrogenation.....	67
Table 3-4: Conversion in the CO hydrogenation reaction over a range of temperatures	68
Table 3-5: Product yield as a function of temperature over Au/Al ₂ O ₃ catalyst D400 in CO hydrogenation.....	69
Table 3-6: Product yield as a function of temperature over Au/Al ₂ O ₃ catalyst D400 in CO ₂ hydrogenation.....	70
Table 3-7: Product yield as a function of temperature over Au/Al ₂ O ₃ catalyst C80 in CO ₂ hydrogenation.....	71
Table 4-1: Bi-modal distribution	76
Table 4-2: Comparison of methanol yields and selectivity's for CO hydrogenation at 250°C of catalysts D400 and C80 with supported gold catalysts from literature.....	92
Table 4-3: Comparison of methanol yields and selectivity's for CO ₂ hydrogenation at 250°C of catalysts D400 and C80 with supported gold catalysts from literature.....	93

1 LITERATURE REVIEW

1.1 Methanol and its Synthesis

1.1.1 Background

Methanol is an industrially important chemical. Close to 40 million metric tons of methanol were produced in 2008 and this is expected to continue to grow (SRI Consulting, 2010). The primary usage of methanol is for the production of formaldehyde (see Figure 1-1) whose derivatives are primarily used in the building and automotive industry. Urea formaldehyde, melamine formaldehyde, and phenolic formaldehyde are examples of thermosetting resins, the largest use of formaldehyde. Methyl di-p-phenylene isocyanate is a chemical produced from formaldehyde for the use in polyurethane foams, binders, adhesives and sealants, and this is a growing use of formaldehyde (Reuss *et al.*, 2002). The fuel additives methyl tert-butyl ether (MTBE) and tert-amyl methyl ether (TAME) also represent a large portion of the use of methanol. They are oxygenates added to petrol to increase its octane number. While MTBE is being phased out in the USA due to it occurring in groundwater, as well as regulations that favour the use of ethanol, the growing Asian market, in particular China (Weirauch, 2006), who do not have regulations favouring ethanol, means the use of MTBE has been reasonably steady. Other uses and products of methanol are acetic acid and acetic anhydride, primarily used for the formation of various acetate esters, such as vinyl acetate which is polymerized to poly-vinyl acetate. Direct fuel usage includes applications such as direct methanol fuel cells, a type of proton exchange fuel cell where methanol is the fuel or direct addition to petrol. While the usage of methanol in some sectors is declining, and in particular in Europe and the United States, the overall demand is growing, especially in Asia, with China leading the growth in demand (the Methanol Institute, 2011).

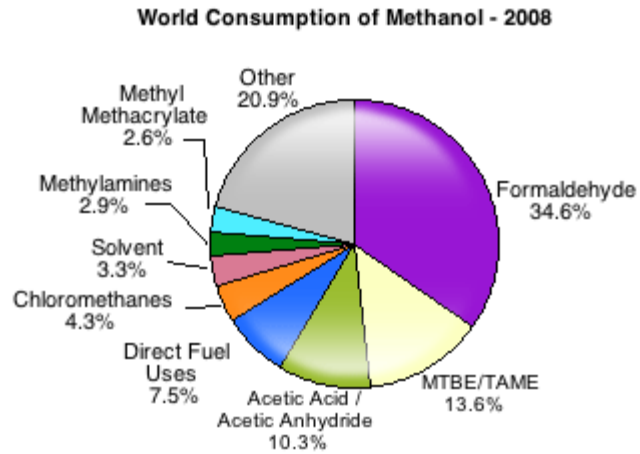


Figure 1-1: World consumption of methanol in 2008 (SRI Consulting, 2010).

Methanol was originally produced by distillation of wood and was referred to as wood alcohol. Today, however, methanol is commercially produced by the hydrogenation of CO and CO₂ (English *et al.*, 1992).



These reactions are exothermic and result in a net decrease in the number of moles. For this reason a low temperature and high pressure are more thermodynamically favourable for higher conversions (see Figure 1.2).

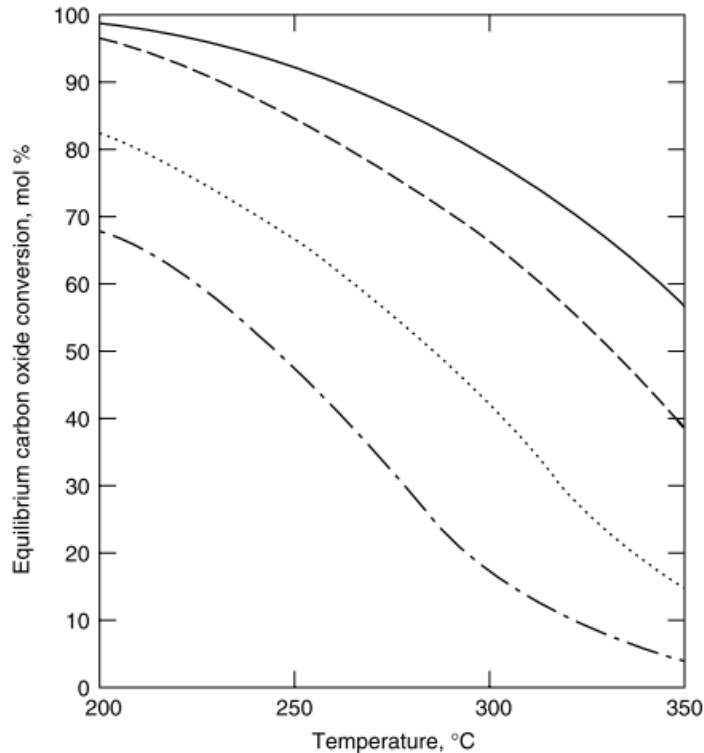


Figure 1-2: Equilibrium conversion of carbon oxides to methanol based on reformed natural gas compositions of 73% H₂, 15% CO, 9% CO₂, 3%CH₄ at 30, 20, 10 and 5 MPa (from top to bottom) (English *et al.*, 1992).

Methanol was first synthetically produced in 1923 by BASF in Germany. A Zn-Cr₂O₃ catalyst was used and operating conditions were typically 320-380°C and ca. 340bar. This high operating pressure resulted in very high capital and compression costs. In 1966 ICI introduced a process that operated between 50 and 100bar and 240-260°C. Using a Cu-Zn-Al-oxide catalyst they obtained better stability and selectivity. In 1973 Lurgi developed a CuO-ZnO catalyst and managed to bring the operating pressure down further to 50-80bar at similar temperatures.

As is mentioned previously (evident from Figure 1.2) the thermodynamically limited conversion is higher at lower temperatures and higher pressures. With the development of newer and better catalysts the operating temperatures of methanol synthesis have already been reduced to ~250°C and any further reduction would be detrimental to the efficient removal of the reaction heat for the production of high quality steam. However, while increasing pressures allow for higher conversions, the increasing costs associated with this

mean that lower pressures are still more desirable and one of the most effective ways to lower costs around this process would be to have an active catalyst that maximizes per pass conversion and lowers the recycle requirements.

Studies comparing the performance of various Cu catalysts in methanol synthesis yield some interesting and relevant observations. It is generally known that the specific Cu surface area affects the methanol production by CO and CO₂ hydrogenation. However, the material used as the support also plays a significant role in the methanol production. It has been shown that for methanol synthesis from both syngas (Kurtz *et al.*, 2003) and CO₂ (Fujitani *et al.*, 1994) that at the same specific Cu surface area, Cu catalysts supported on ZnO/Al₂O₃ are much more active than Cu/ZnO, and that this is more active than Cu supported solely on Al₂O₃.

Fujitani *et al.* (1994) obtained yields of just 0.13% of methanol at 250°C and 50atm on a Au/Al₂O₃ catalysts, while using ZnO as a support almost tripled the yield of methanol to 0.31% and the Cu/ZnO/Al₂O₃ catalyst performed the best with a 0.44% methanol yield. Space velocities in this study were on the high side (~18000 cm³ (STP) h⁻¹ g_{cat}⁻¹), hence the low yields. Alumina is believed to act as a structural promoter in this catalyst configuration, providing thermal stability to the Cu crystallites. This is also demonstrated in the deactivation studies done by Kurtz *et al.* (2003) where Cu/ZnO deactivates much more rapidly than Cu/ZnO/Al₂O₃ with increasing temperatures.

1.2 Gold in Catalysis

Gold has long been considered to be an inert substance and hence to have no value as a catalytic material. As a bulk material, gold adsorbs neither oxygen nor hydrogen at room temperature and it was thus concluded to be generally unsuitable in hydrogenation or oxidation reactions (Bond, 1972).

Studies involving supported gold have been conducted for many years. However, these catalysts were prepared by impregnation, as was common for the preparation of platinum group metals at the time. More recently, Haruta and co-workers (1989) showed that gold nanoparticles on high surface area oxidic support can be an effective catalyst for CO oxidation. This study led to the realization that dispersion played a significant role in catalytic activity. Having prepared their catalysts by deposition-precipitation instead of impregnation they achieved smaller well dispersed gold particles. Since then, more preparation methods and applications have been developed, and catalysis using gold

nanoparticles has become a rapidly expanding research area. Supported gold nanoparticles have been shown to be active in the selective oxidation of hydrocarbons, the water-gas shift reaction, the reduction of nitric oxide and the synthesis of polyvinyl chloride, amongst others (Bond *et al.*, 2006).

1.3 Catalyst Preparation Methods

There are various catalyst preparation methods that can be used in the preparation of supported gold catalysts. Together with the preparation method, the choice of support material and gold precursor plays a significant role in the resulting catalyst. The synthesis of gold catalysts is most commonly done via deposition-precipitation, based on the work by Haruta (1993). In addition to this, co-precipitation and impregnation are also commonly encountered (Bond and Thompson, 1999). However, alternate synthesis routes exist.

In general, the gold precursor is in the form of a gold chloride solution. The presence of the chloride ion may increase agglomeration of the gold crystallites during preparation (Oh *et al.*, 2002), but this can be mitigated. Precursors that don't contain chloride can be prepared (Beeming, 2008). However, their use in the synthesis of supported gold catalysts is generally expensive and complicated, making them impractical to use on a large scale.

1.3.1.1 *Deposition-Precipitation*

In deposition-precipitation the gold is precipitated on the surface of a catalyst support. The catalyst support and the gold precursor are placed together in solution. This solution is then mixed and aged after the pH is adjusted to the desired value. This method is quoted as being the easiest and is the method of choice in the production of commercial Au catalysts (Haruta, 2004). Chloroauric acid is typically used as the gold precursor, and this method can be applied to a number of catalyst supports (Wolf and Schüth, 2002). Supports with PZC's (point of zero charge or iso-electric point, IEP) of greater than 5 work well with this method, such as alumina, magnesia, titania, zirconia, ceria, etc. It is also suitable for zeolites (Bond *et al.*, 2006). The ζ -potential of a catalyst in a solution describes the charge of the surface of the catalyst. The charge of the surface is dependent on the pH of the solution. If the pH is low the surface is positively charged and if the pH is high the opposite is true as the surface becomes negatively charged due to deprotonation. The pH at which the surface charge is zero is the iso-electric point. An added advantage of this method is that no gold is embedded in the support (Beeming and Bialek, 2006), yielding a narrow gold particle size distribution (Bond and Thompson, 1999).

1.3.1.2 *Co-precipitation*

In co-precipitation both the support precursor and gold are precipitated simultaneously from solution. Haruta and colleagues have been pioneers in the application of this method to gold catalysis (Haruta *et al.*, 1989). This method, however, has the distinctive disadvantage that the gold particle size distribution has been shown to be less narrow than that of deposition-precipitation as well as the amount of gold that is 'buried' within the catalyst support (Bond and Thompson, 1999).

1.3.1.3 *Impregnation*

Impregnation is commonly used in the preparation of other metal catalysts, and was the first method used when production of supported gold catalysts was first attempted (see e.g. Shibata *et al.*, 1985). This method is now rarely used for gold catalyst preparation as it doesn't lead to well dispersed active catalysts and gold particle sizes larger than 10nm are obtained even for catalysts with low metal loadings (Haruta, 1997; Bond *et al.*, 2006). Impregnation occurs by suspending the support in a solution of a gold salt, such as chloroauric acid ($\text{HAuCl}_4 \cdot 3\text{H}_2\text{O}$). This is dried to remove the solvent, and then reduced with hydrogen or aqueous oxalic acid (Bond and Thompson, 1999). The only real benefit of this method is that it can be applied to essentially any support material and there are multiple precursors that can be used. Chloroauric acid (HAuCl_4) is most commonly used as the gold precursor; however, other compounds such as gold chloride (AuCl_3) or the ethylenediamine complex ($[\text{Au}(\text{en})_2]\text{Cl}_3$) have also been used (Bond *et al.*, 2006).

1.3.1.4 *Ion-exchange*

The use of ion-exchange as a catalyst preparation method has not been widely reported on in the literature. Agglomeration of small particles is typically seen during the precipitation step of most methods of preparation. Ion exchange eliminates this step, therefore reducing agglomeration. Any gold not attached to the surface of the catalyst is removed, this prevents the deposition of additional gold, and hence a highly dispersed catalyst is theoretically possible (Case, 2009). As with some other methods gold chloride solution is a commonly used precursor. The presence of chloride in the (adsorbed) ion-exchange species may result in sintering of the catalyst during calcination (Oh *et al.*, 2002; Ivanova *et al.*, 2004; Hugon *et al.*, 2010). Furthermore, residual chloride present in the catalyst may act as a poison (Oh *et al.*, 2002). However, Ivanova *et al.*, (2005) have shown that washing the catalyst with ammonia is an effective method to remove chlorine after ion-exchange.

When HAuCl_4 is in an aqueous solution the Cl^- ions can exchange with OH^- ions in solution. The extent of the exchange is in particular dependent on the pH of the solution. In the study by Ivanova *et al.* (2004) it was theorised that the $\text{AuCl}_2(\text{OH})_2^-$ species forms a stronger bond to the γ -alumina support than other species, due to its bonding as a bidentate species instead of a monodentate species. Ivanova *et al.* (2004) have investigated the speciation of gold in solution using UV-Vis spectroscopy. They deduced that $\text{AuCl}_2(\text{OH})_2^-$ is most prominent at a pH of approximately four.

Van Steen (2009) shows the distribution of gold species over a range of pH values with and without the presence of a NaNO_3 or NaCl background. These were calculated based on the equilibrium constants for dissociation of the relevant species. Activity coefficients were taken into account. The diagrams are shown as Figures 1-3-1-5, on the following pages.

It was found that the presence of a NaNO_3 background (1M) has almost no effect on the pH and a small effect on the speciation of gold in the precursor solution. It is noteworthy that the maximum concentration of the $\text{AuCl}_2(\text{OH})_2^-$ species occurs at a pH just above 5 and not near 4 as stated by Ivanova *et al.* (2004). The addition of a 1 molar NaCl background, however, has a significant effect on the equilibrium of gold complexes in the precursor solutions. The maximum concentration of $\text{AuCl}_2(\text{OH})_2^-$ now occurs at a pH above 7. This is shown in Figure 1-5. The presence of AuCl_4^- is also significant up to a pH of 5 to 6.

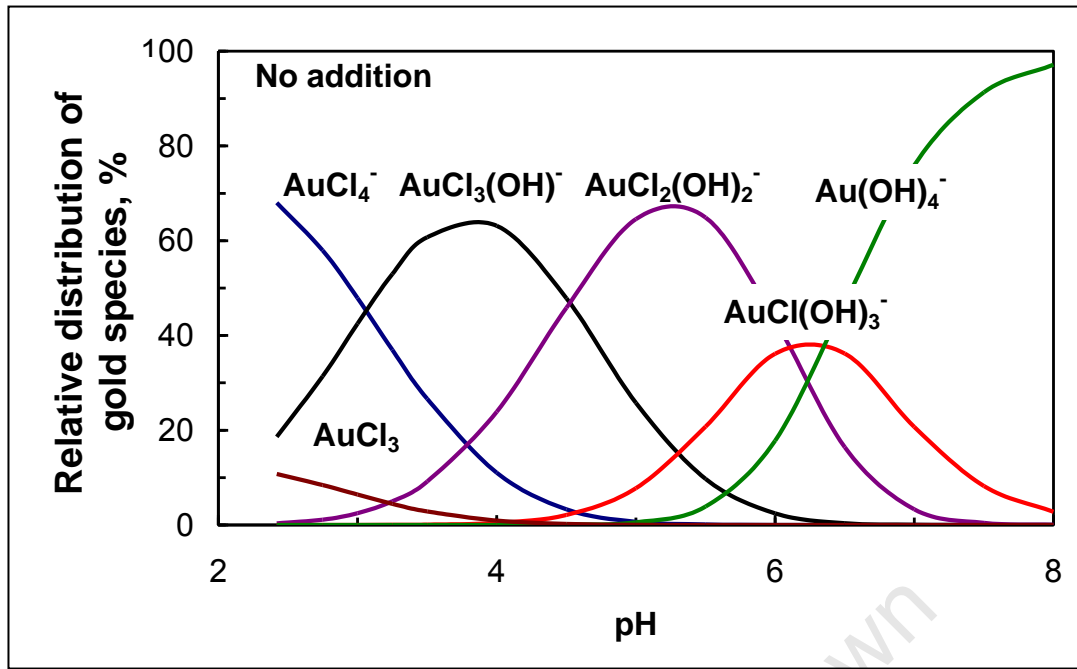


Figure 1-3: Speciation of gold as a function of pH in a 500 ml solution of 2.54 mmol HAuCl₄/litre solution (change in pH by addition of NaOH). Van Steen, 2009

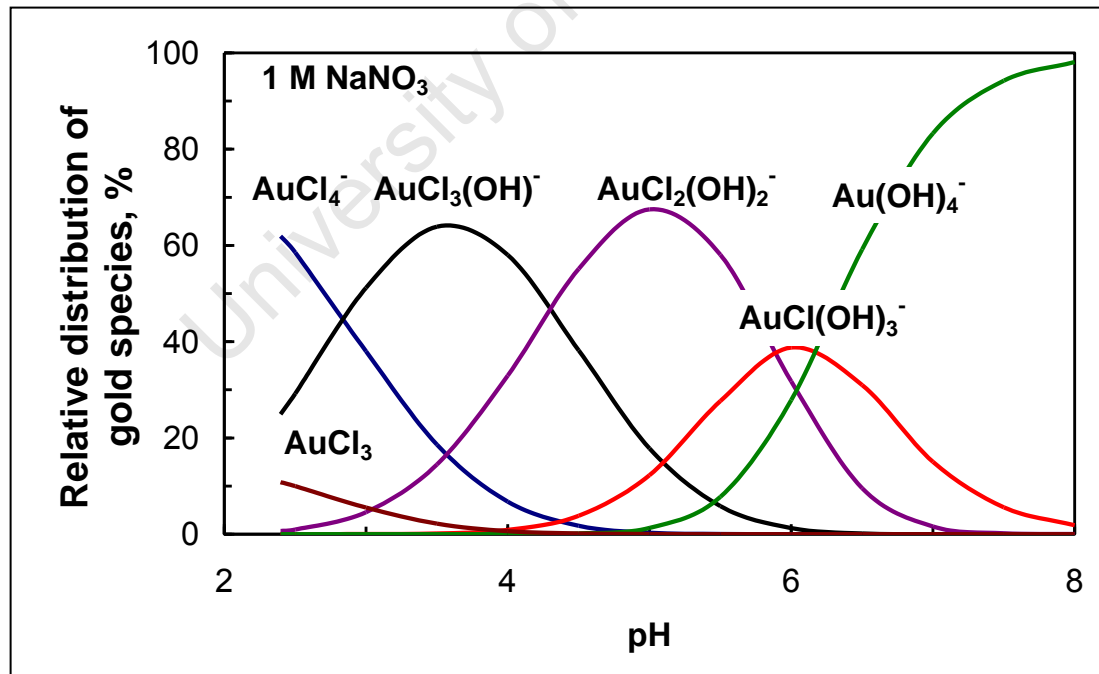


Figure 1-4: Speciation of gold as a function of pH in a 500 ml solution of 2.54 mmol HAuCl₄/litre and 1 M NaNO₃ solution (change in pH by addition of NaOH). Van Steen, 2009

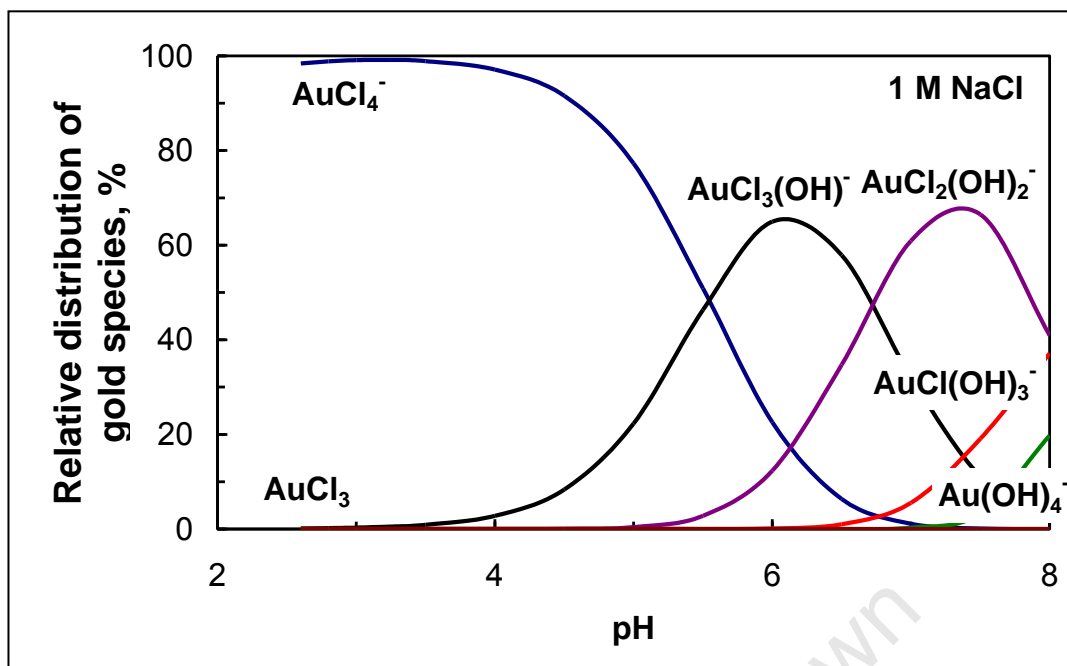


Figure 1-5: Speciation of gold as a function of pH in a 500 ml solution of 2.54 mmol HAuCl_4 /litre and 1 M NaCl solution (change in pH by addition of NaOH). Van Steen, 2009

In anionic ion-exchange the ions are negatively charged and will adsorb more easily onto a positively charged surface. Hence a pH below the IEP is favourable, this implies that a pH below 8 should be favourable for anionic ion-exchange with γ -alumina, while pH values above 8 are suitable for cationic ion-exchange (Brunelle, 1978). In anionic exchange the OH groups of γ -alumina are protonated by H^+ in the acidic solution. This complex then leaves the surface as H_2O , creating a cationic vacancy on the support. The OH groups on the gold complexes then interact with this vacancy. The $[\text{AuCl}_2(\text{OH})_2]^-$ is most prominent at a pH near 5 and this corresponds to the pH at which maximum gold loading was obtained in a previous study (Bergh and Van Heerden, 2009), as well as in a study by Yang *et al.* (2005).

1.4 Catalyst characterization

1.4.1 Electron Microscope techniques

TEM and HRTEM

Transmission electron microscopy (TEM) and high-resolution transmission electron microscopy (HRTEM) have been used extensively in the characterization of supported gold catalysts. From the images that are taken the size, shape and other factors such as crystallinity can be identified immediately. These are, however, qualitative data and

transforming these initial qualitative observations into meaningful quantitative results is not straightforward.

A beam of electrons is transmitted from an electron gun, containing an electron source (such as a tungsten filament or an LaB_6 crystal). This beam is focused using various lenses before being transmitted through the sample. Contrasts are formed by the adsorption and obstruction of electrons by the sample. Areas of the sample that are thicker or have a higher atomic number will appear darker, as more of the electrons in the beam are scattered or adsorbed in these regions. Areas of the specimen that are thinner or have low atomic numbers are more electron transparent and will appear as the lighter areas on the resulting images. Between the sample and the detector, objective lenses are used to magnify the beam that now contains the information about the sample. At every step in the process the information contained within the electron beam is degraded.

Although TEM is by far the most widely used method for characterizing particle size on supported gold catalysts, there are a number of drawbacks. It requires experience and skill in the sample preparation, use of the apparatus and the analysis of the images to use this method in an efficient and accurate manner (Williams and Carter, 2009).

The first most obvious drawback is the poor sampling associated with TEM. When looking at a sample under the microscope only a fraction of the sample is being investigated. As the resolution is increased the problem is exaggerated. The homogeneity of the catalyst cannot be assumed. The preparation of the sample is an important aspect of TEM studies as a very thin specimen is required. The preparation of these samples can affect the catalysts structure and chemistry. Generally methods where the catalyst is dispersed onto a grid are preferred when dealing with supported catalysts. Catalysts are dispersed in an alcohol (such as methanol) and are sonicated for some time. Information on the dispersion and distribution of the metal on the support would be lost if the support is broken up. As a small amount of the fluid (containing suspended catalyst) is dropped onto the grid, the homogeneity of the sample itself, (in addition to that of the catalyst as mentioned above), can be questioned as none of the catalyst that sinks to the bottom of the suspension makes it onto the grid. Furthermore, the support has a significant effect on the ease of obtaining information from TEM images, since supports with low atomic numbers (Al_2O_3 , SiO_2) have a higher contrast from the gold nano-particles making them easier to identify, especially when sizes are in the nanometer range.

Resolution on a TEM image is primarily limited by an effect called spherical aberration, however, newer, higher resolution TEM apparatus are fitted with aberration correctors to increase the resolution that can be obtained.

SEM

A Scanning Electron Microscope (SEM) utilizes an electron gun containing an electron source to produce an electron beam. The beam is focused using multiple condenser lenses. The final lens contains deflection coils such that the beam can be deflected (in the xy axis).

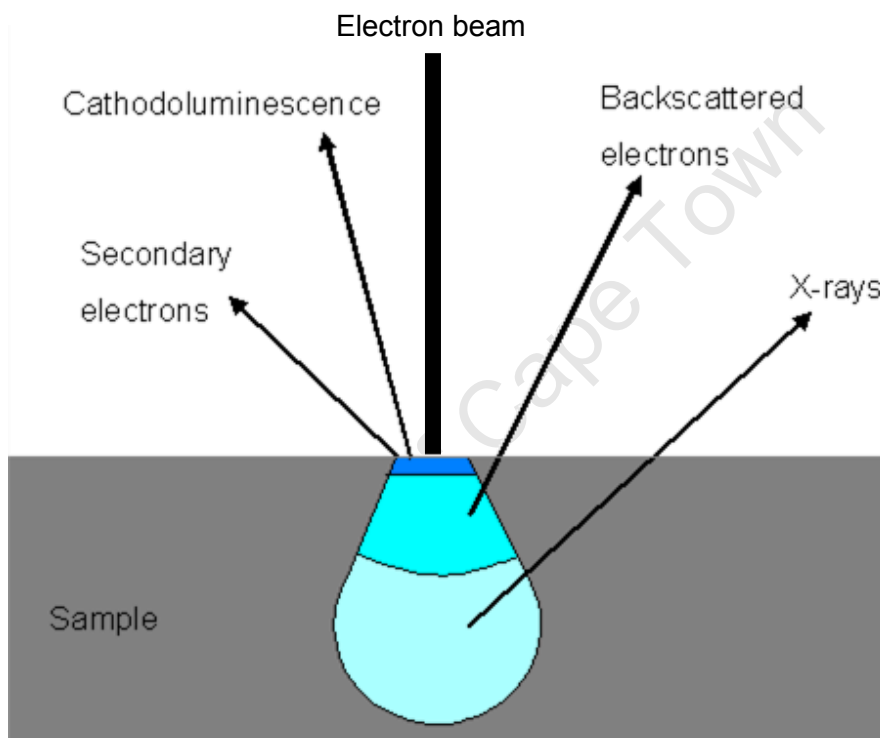


Figure 1-6: Diagram of interaction volume between an electron beam and the sample during SEM analysis

The beam scans over a rectangular area of the sample in what is referred to as a raster pattern. The electron beam interacts with a small volume of the sample (see Figure 1.6) with the result that low-energy secondary electrons and high-energy backscattered electrons are emitted as well as X-rays.

On the image formed from the backscatter electrons heavier atoms appear as brighter spots (as more electrons are backscattered) while lighter atoms appear as darker areas (less backscatter).

Unlike TEM, the resolution of SEM is not limited by spherical aberration. Rather, the spot size and interaction volume play a role in this; both are much larger than the distance between two atoms, and hence the high resolutions obtained in HRTEM machines cannot be achieved. SEM is usually considered more useful for imaging bulk materials.

1.4.2 XRD

During X-Ray Diffraction (XRD) a beam of X-rays (called the incident beam) pass through a powdered catalyst sample. Some of these X-rays are diffracted by the atomic planes in the crystalline material according to Bragg's law. The diffraction pattern is recorded. The resulting XRD pattern can be used to obtain information on average particle sizes of gold crystallites using the Scherrer equation (Scherrer, 1918):

$$B \ 2\theta = \frac{K\lambda}{L\cos\theta} \quad (1-1)$$

Where: L is the volume average of the crystal thickness in the direction normal to reflecting planes

B is the width of the relevant peak at half height

λ is the wavelength of the X-rays

K is a constant determined by the shape of the crystallites

θ the angle of incidence

Using this equation it is assumed that all crystallites are of a uniform shape and size, generally, however, this is not true.

As the particles of interest decrease in size the peak broadens. When particles are below a size of ~5nm the peak becomes so broad that the peak width cannot be accurately determined. Conversely, above a size of ~100nm the peak is so narrow that the same problem is encountered. Additionally, when loading is low (<1wt %) the signal becomes weak enough for the gold peak to disappear completely. This often limits the usefulness of

XRD for gold catalysis, and although it is often used to characterize catalysts in literature, it is rarely done without the additional characterization of TEM. These are two completely different measurements, each with their own shortcomings, and it would not be at all surprising if they resulted in different crystallite sizes for the same catalyst, particularly when crystallites are not of a uniform shape and size. It should be noted that the shape constant K in the Scherrer equation differs greatly for different shapes. Nonetheless, for supported gold catalysts with sufficient loading and/or large enough particle size, the average particle sizes obtained from TEM and XRD are often found to agree, with the average size obtained from XRD usually being the slightly larger of the two (Porta *et al.*, 2000; Grabowski *et al.*, 2004; Centeno *et al.*, 2006). There are many examples of literature where XRD and TEM are used in tandem without the results of both methods being given in the study, the author simply choosing to use one of results without displaying the other (for example Comotti *et al.*, 2006).

1.4.3 Adsorption studies

1.4.3.1 CO-chemisorption

Unlike oxygen, CO can be adsorbed onto thin films and single crystals of gold. This is usually investigated in two ways, viz. temperature programmed desorption (TPD) experiments, or Infra-red studies.

Temperature programmed desorption (TPD)

There are quite a number of studies dealing with CO adsorption on thin films and single crystals (for example Outka and Madix, (1987) and Ruggiero and Hollins, (1996)), but far fewer that conduct TPD on supported gold catalysts. When CO temperature programmable desorption is conducted on supported gold catalysts, two peaks are observed. The first peak occurs at a temperature between 130 and 140K (Lemire *et al.* 2004a; Lemire *et al.* 2004b). The second peak occurs at a higher temperature, although this temperature is dependent on the size of the gold crystallites. With a decrease in crystallite size it was found that the second peak would shift to a higher temperature (from 210K to 300K), implying that the smaller particles adsorb CO more strongly (Lemire *et al.* 2004a; Shaikhutdinov *et al.* 2003). It is possible that this second peak could correspond to an adsorption site on the metal-support interface. However, experiments done by Ruggiero & Hollins, (1996), on Au(332) also demonstrated a second peak in the same position indicating that the second peak could also belong to the gold particle. These catalysts (Lemire *et al.* 2004a) had not been treated at high temperatures, and when the authors proceeded to anneal their catalysts,

prior to conducting TPD, they obtained different results. The first thing that was observed is that the second peak no longer shifts with changes in particle size. Secondly, the intensity of the peak decreased for samples that had been annealed. CO adsorbed on the well-ordered Au(332) surface naturally displayed no shifts in its second peak. The best explanation for this is that the annealed catalysts had been transformed into more well-ordered structures and thus experienced a decrease in the amount of defects on the catalyst surface. Another possible explanation of this is that the particle size effect is only displayed for particles smaller than a certain size and that above that size the adsorption is size independent. If annealing the samples then causes the particles to go above that size, the observed effect would make sense. Unfortunately there is no clear indication of the sizes of the catalysts used in the TPD studies discussed above.

Another interesting result presented in Meyer *et al.* (2004), shows that the effect of the support does not have a significant effect on the adsorption of CO onto supported gold catalysts. This shows that any support effects that are observed in experimental studies do not arise from the adsorption of CO. It, however, does not exclude support effects as these may still manifest themselves in the adsorption of other species present in the reaction.

Infra-red Spectroscopy (IR)

Infra-red spectroscopy can provide additional information on the oxidation state of the gold as well as how molecules are adsorbed onto the gold surface. In literature, the catalytic activity of gold has been attributed to be the Au⁰, Au⁺, Au³⁺, or even the Au⁻ species. IR spectroscopy should be a useful tool in identifying which of these are present during reaction; however, there is no real consensus as to the assignments of carbonyl stretching bands for the different gold carbonyl species.

Most often in literature, carbonyl absorption bands between 2130 and 2090cm⁻¹ are assigned to metallic gold, negatively charged gold carbonyls are located in the lower frequencies, positively polarized gold is found between 2155 and 2130cm⁻¹ and Au⁺-CO species find themselves in the frequencies above this (Mihaylov *et al.*, 2007). The presence of Au³⁺ is generally not considered. However, it was shown that when preparing a sample from start to finish in the absence of air and water vapour, CO adsorption results in an IR band at 2207cm⁻¹ (Mihaylov *et al.*, 2007); this was assigned to Au³⁺. In normal catalyst preparations any Au³⁺ present will be coordinatively saturated by OH groups or water molecules. These cations are easily reduced in processes that remove OH or water, and are thus much more difficult to identify.

Most assignments made in literature are based on the relative stabilities of the different carbonyl species. For example Venkov *et al.*, (2006), assigned a band at 2167cm^{-1} to $\text{Au}^+\text{-CO}$ based on its stability and assigned the band at 2180cm^{-1} to $\text{Au}^{3+}\text{-CO}$ as it disappeared after evacuation. The reality, however, is that even the relative stabilities of the carbonyl species are not fully agreed upon in literature and is typically based on the relative stabilities of carbonyl species of other group 11 metals (Mihaylov *et al.*, 2007).

1.4.3.2 H_2 – adsorption

Hydrogen Chemisorption on Gold Catalysts			
TABLE 3: H/M Values of the Total and Strong Adsorption			
sample	T (K)	H/M total adsorption	H/M strong adsorption ^a
Pt/SiO ₂ –A	298	121%	57%
	373	117%	27%
	423	105%	19%
Pt/SiO ₂ –B	473	86%	
	298	28%	12%
	373	25%	4%
Au/Al ₂ O ₃ –A	423	23%	2%
	473	20%	
	298	41%	3%
Au/Al ₂ O ₃ –B	373	50%	8%
	473	47%	
	523	50%	
Au/Al ₂ O ₃ –C	298	10%	3%
	373	16%	4%
	473	27%	6%
Au/Al ₂ O ₃ –D	298	27%	4%
	373	27%	
	473	27%	
Au/Al ₂ O ₃ –E	298	66%	16%
	373	73%	18%
Au/Al ₂ O ₃ –E	298	41%	4%

^a Strongly adsorbed hydrogen that does not desorb during 2 h evacuation at the analysis temperature.

Figure 1-7: Hydrogen chemisorption on gold catalysts at different temperatures (Bus *et al.*, 2005)

Not many studies involving the interactions of gold and hydrogen exist. The reason for this may partially be due to oxidation reactions being the most studied reactions in gold catalysts. In hydrogenation reactions, hydrogen is adsorbed, dissociates and then takes part in the reaction. When hydrogen chemisorption studies are conducted on gold films, adsorption is not always observed (Sault *et al.*, 1986; Claus, 2005) or the coverage is low. It has been shown (see Figure 1.7) that for supported gold catalysts, hydrogen uptake during chemisorption experiments increases with temperature (Bus *et al.*, 2005; Kartusch *et al.*,

2009). This suggests that the process of hydrogen chemisorption is an activated process, most likely due to the dissociation step.

Gold crystallite size has been shown to have a significant effect on both the amount of hydrogen adsorption as well as the strength of adsorption. Both the amount of hydrogen adsorbed and the amount of strongly adsorbed hydrogen increase with a decrease in particle size. As these nano-sized crystals consist primarily of corner and edge sites, it is suggested that steps and corner sites are where the hydrogen adsorbs. This is supported by the fact that most model surfaces don't adsorb hydrogen and that on those that do coverage is very low and adsorption is weak, which is attributed to the lack of low coordination atoms on the surface. Essentially very little is known about the interaction of hydrogen with nanoparticles of gold and whether there is any sort of effect by the support. However, there is mention in literature of the presence of oxygen aiding the dissociation of hydrogen during the H₂ - D₂ exchange reaction (Claus, 2005). It is possible that the oxidic support plays a similarly important role in the dissociation of hydrogen on supported gold catalysts.

1.4.3.3 O₂ - chemisorption

For other metal catalysts (Pt, Rh, Ir, etc.) chemisorption of simple molecules has been used successfully to characterize the average crystallite size, dispersion and surface area. Although TEM is also useful for obtaining particle size distributions, chemisorption is a much simpler and easier technique to use. Due to the chemical inertness of bulk gold, chemisorption of simple molecules on gold has failed to give any sort of meaningful result. However, more recently the chemisorption of oxygen on supported gold catalysts which are highly dispersed has given results that can be directly related to the sizes obtained using more established methods such as TEM (Berndt *et al.*, 2003; Bond *et al.*, 2006). Fukushima, Galvagno, & Parravano performed oxygen chemisorption experiments on supported gold catalysts (Au/Al₂O₃, Au/SiO₂, and Au/MgO). Chemisorption was conducted between 170 and 450°C. Together with TEM experiments they concluded that an adsorption stoichiometry of 2 (Au^s/O) describes the oxygen monolayer. At 300°C a stoichiometry of 1 was applicable. Although mentioning some doubts over the experimental methods followed by Fukushima *et al.*, (1979), Berndt *et al.*, (2003) showed that for oxygen chemisorption on Au/Al₂O₃ at 200°C the particle sizes calculated from the oxygen chemisorption do agree with those obtained by TEM when a stoichiometry of 2 is assumed.

Berndt *et al.* (2003) also observed the occasional large gold crystallite in their TEM analysis. Assuming a bi-modal distribution and making use of the gold surface area obtained from the

oxygen chemisorption experiments they attempted to calculate the contribution of large and small gold crystallites in the sample and found that only a very small portion of large particles are present and that they contribute to less than 1% of the total surface area. They calculate the total volume of gold present per gram of catalyst using the density of gold and the loading. It can then be said that the total volume is made up of contributions by the small particles as well as the large particles. They then use the same approach to the surface area (essentially creating a set of simultaneous equations).

1.5 Gold in Methanol synthesis

In comparison to the work done investigating the oxidation of CO, very little has been published on the use of gold for the hydrogenation of CO/CO₂. It is commonly believed that the presence of ZnO plays an important role in the yield of methanol when using the industrial Cu/ZnO/Al₂O₃ or other Cu/ZnO containing catalysts (Choi *et al.*, 2001; Grabowski *et al.*, 2004), as well as having a similar effect on gold catalysts (Sakurai and Haruta, 1995, 1996). For this reason most research groups are using gold supported on ZnO as a starting point for their research (Sakurai and Haruta, 1995; Zhao *et al.*, 2007).

1.5.1 Effect of particle size on gold catalysts for methanol synthesis

It has been demonstrated in many studies that the activity of supported gold catalysts shows a dependency on the particle size. Even before the well-known Haruta study, (Haruta *et al.*, 1989), CO hydrogenation over a supported gold catalyst had been attempted (Shibata *et al.*, 1985). In this study the usefulness of supported gold was immediately dismissed, as the amorphous gold-zirconium alloy catalyst had a conversion that was more than three times greater. In preparing their catalysts these researchers had used impregnation, a method used at the time for preparation of platinum catalysts. Thus, the behaviour they observed was probably due to the large particle sizes produced.

This size effect caused by the choice of preparation method was demonstrated again with an Au/ZnO catalyst (Sakurai and Haruta, 1995). Two catalysts were prepared, one by co-precipitation and the other by impregnation. When characterising these two catalysts they found that the primary difference between them is that the average particle size on the impregnated catalyst was almost 10 times larger (33.9 nm vs. 3.5nm). At a temperature of 250°C and 50atm, the catalyst prepared by impregnation showed no activity for CO₂ hydrogenation while the other catalyst achieved a conversion of 8.2%. Meanwhile, at a temperature of 400°C the impregnated catalyst only improved to a 3.7% conversion in comparison to the 37.7% of the co-precipitation catalyst (Sakurai and Haruta, 1995).

In another article by the same authors, (Sakurai and Haruta, 1996), the effect of particle size was explored further, again on a ZnO supported gold catalyst. The results they obtained are illustrated in Figure 1-8 below. There is a clear effect of increased conversion with a decrease in particle size.

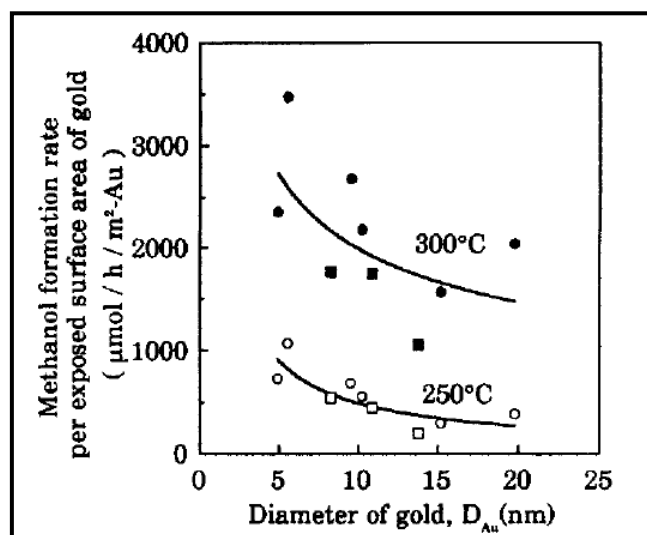


Figure 1-8: Effect of particle diameter of gold in methanol synthesis from CO_2 . \circ d_{Au} determined by TEM observation, \square \blacksquare crystallite size of gold determined by XRD (Sakurai and Haruta, 1996)

This particle size effect may depend on the location of the active site. If the active site is situated on the surface of the gold particle then by decreasing the size of the particles one will obtain a greater total surface area of catalyst and thus a greater activity (when defined in terms of the mass of the catalyst). In a similar manner if we consider step and corner sites to be the active sites, a decrease in particle size would result in an increase in the total number of these sites. The final option generally considered is that the metal-support interface is the active site. Thus a decrease in particle size would result in a greater total number of gold atoms being situated on the perimeter of a gold nanoparticle and in contact with the catalyst support.

Each of these possibilities has a similar consequence in terms of the effect of particle size on catalyst performance. Smaller particles will increase the activity per mass of catalyst. However, they have different implications in other areas of the catalyst, such as the effect that the support has on the behaviour of the catalyst.

There are other factors that influence how particle size affects the catalyst activity. For example the heat of adsorption of the reactant molecules is not constant with a change in particle size. As the particle size decreases the heat of adsorption generally increases in magnitude. There are multiple reasons for this occurring. As the particle size decreases the adsorbed particles are brought closer together and will then interact with each other. This however, is believed to only play a small role. A greater effect is seen due to a catalyst with smaller particles having more edge and corner sites in total, these sites having a greater heat of adsorption as the corner and edge sites have a lower co-ordination number.

1.5.2 Effect of catalyst support for methanol synthesis

It is very difficult to isolate the effect of the catalyst support on activity from other variables such as particle size and dispersion. Even in studies dedicated to understanding the influence of the support on the catalyst or vice versa a size effect cannot be excluded.

Attempting to compare the few CO/CO₂ hydrogenation studies with each other is further complicated as they differ in too many ways. Catalysts do not have the same particle sizes or dispersions even in one article, let alone across articles. Reactions are carried out under different conditions of temperature and pressure, as well as using different feed gas compositions and space velocities. Despite this difficulty, the relevant literature is discussed below.

In the studies by Sakurai and Haruta (1995, 1996), of all the catalysts that were tested, those that contained ZnO always resulted in the highest methanol yield and selectivity. Both the effect of the catalyst support and particle size was attributed to a synergistic effect at the gold-oxide interface. The authors, however, went no further than this, and offered no explanation for this effect.

The idea that ZnO containing catalysts show an increased selectivity to methanol has been demonstrated in other studies. Au/ZnO was shown to have a higher selectivity to methanol (and other alcohols) in comparison to Au/Fe₂O₃, Au/SiO₂ and Au/TiO₂ (Zhao *et al.*, 2007). The Au/SiO₂ catalyst was inactive at the chosen reaction conditions. Au/TiO₂ produced methane, ethane and propane; this was also shown in other studies (Sakurai and Haruta, 1995, 1996; Zhao *et al.*, 2007). Au/Fe₂O₃, although active, was not as selective to alcohols as Au/ZnO and did not suppress the formation of hydrocarbons.

They also compared these catalysts to catalysts without the gold to see if the gold improved the activity of the metal oxide. It was found that for the Fe₂O₃ catalysts the addition of gold

caused a slight shift in selectivity away from the alcohols. For the ZnO catalysts, the addition of gold increased the selectivity to alcohols and higher alcohols; however, the conversion of CO decreased from 20% to 6%.

In a paper by Strunk *et al.*, (2009), the importance of oxygen vacancies on the support are highlighted. The presence of oxygen vacancies on ZnO are demonstrated, giving a possible reason for the more favourable activity and selectivity of ZnO containing catalysts for methanol synthesis.

University of Cape Town

2 EXPERIMENTAL

2.1 Catalyst preparation

Ion exchange has been used to prepare well-dispersed active catalysts (Ivanova *et al.*, 2004; Beeming, 2008; Case, 2009). For anionic exchange to occur, a pH below the iso-electric point (IEP) of the support is favoured, and for cationic exchange a pH above the IEP. Cationic precursors have the advantage over anionic precursors of not containing chloride, which is believed to cause sintering and/or blockage of the catalytically active sites (Oh *et al.*, 2002; Yang *et al.*, 2005). However, these chloride species can be removed by washing the catalyst in a concentrated ammonia solution (after washing it in water to remove any unattached gold complexes, see section 2.4 Health and Safety) (Xu *et al.*, 2003; Ivanova *et al.*, 2005). Due to aurochloric acid being readily available anionic exchange is generally preferred.

Anionic ion-exchange was used to prepare well-dispersed gold catalysts supported on γ - Al_2O_3 (Puralox SCCa 5/150, Sasol Germany; $S_{\text{BET}} = 162 \text{ m}^2/\text{g}$, $V_{\text{pore}} = 0.47 \text{ cm}^3/\text{g}$, $d_p < 500 \text{ m}$). The IEP of $\gamma\text{-Al}_2\text{O}_3$ is approximately 8 (Zwane, 2004). The catalysts were typically prepared by contacting a 1 l solution containing 0.5 g Au (prepared from a stock solution containing 250 g Au/l supplied by MINTEK), whose pH was adjusted to ca. 5 (unless otherwise stated) using a dilute NaOH solution, with 10 g of the support. The suspension was aged for 22 hours at room temperature under stirring. The catalyst precursor was filtered off and washed with 1 l deionized water. The catalyst precursor was subsequently redispersed in 500 ml of an aqueous 25 wt.-% NH_3 -solution to remove the chloride ions. The catalyst precursor was filtered off after 20 minutes and washed with 500 ml deionized water. The supported material was then dried and subsequently calcined in a fluidized bed reactor.

A variety of catalyst synthesis conditions were used (see Table 2.1).

2.1.1 Batch A

The influence of the concentration of the gold in the initial supernatant solution was investigated in Batch A. The initial gold concentration was varied between 1 and 50 g Au/l at an initial pH of ca. 5.0. The catalyst precursors were dried in an oven at 60 °C for 16 hrs. The catalysts were subsequently calcined for 16-18 hours in either hydrogen, air or argon (6-9 ml(NTP)/min/g_{cat}) at temperatures ranging from 200-500 °C.

2.1.2 Batch B

The influence of the contact time in the ammonia washing step was investigated in Batch B, which was prepared by contacting the support with a precursor solution containing initially 1 g Au/ / at an initial pH of ca. 5.0. The concentration of the ammonia solution was varied between 0 and 25 wt.-%, and the duration of the ammonia wash was varied between 0 and 20 minutes.

2.1.3 Batch C

The effect of the drying conditions was investigated with Batch C, which was prepared using a precursor solution containing 0.5 g Au/ / at a pH of ca. 5.0. The catalyst precursor was dried either in a fluidized bed reactor or under reduced pressure in a rotary evaporator. Dry air (50 ml(NTP)/min) or air (50 ml(NTP)/min) saturated with water at room temperature ($y_{\text{H}_2\text{O}} = 0.03$) was used for the drying process in the fluidized bed reactor at 200°C for 2 hrs. Drying in the rotary evaporator was performed at 110 mbar and 60, 80 and 100 °C, respectively. Subsequently, the catalyst was either calcined in dry hydrogen (6-9 ml(NTP)/min/g_{cat}) or in hydrogen (6-9 ml(NTP)/min/g_{cat}) saturated with water at room temperature ($y_{\text{H}_2\text{O}} = 0.03$) at 200°C for 2 hrs.

2.1.4 Batch D

The influence of the calcination temperature was investigated for Batch D, which was prepared using a precursor solution containing 0.5 g Au/ / at a pH of ca. 3.2. The catalysts were dried in an oven at 200°C for 2hrs. Each batch of the catalysts was calcined in hydrogen (6-9 ml(NTP)/min/g_{cat}) for 2 hours at 100, 200, 300, 400, and 500 °C, respectively.

Table 2-1: Catalyst preparation variables

catalyst code	Precursor		Aging		support		Washing			drying			Calcination				
	Au conc. (g/L)	pH	pH (initial)	concentration (g/L)	duration (hrs)	pH (final)	1st water wash water volume (ml/gcat)	duration (min)	Ammonia wash ammonia concentration (g/g)	catalyst/ammonia ratio (g/L)	2nd water wash water volume (ml/gcat)	duration (hours)	temperature (°C)	environment	duration (hrs)	temperature (°C)	environment
A1-200	1	4.90	5.25	20	22	5.03	50	20	25%	20	50	overnight	60	air	16	200	hydrogen
A1-500	1	4.90	5.25	20	22	5.03	50	20	25%	20	50	overnight	60	air	16	500	hydrogen
A2-200H	25	5.20		500	22		50	20	25%	20	50	overnight	60	air	16	200	hydrogen
A2-200Ar	25	5.20		500	22		50	20	25%	20	50	overnight	60	air	16	200	argon
A2-500H	25	5.20		500	22		50	20	25%	20	50	overnight	60	air	16	500	hydrogen
A2-500Ar	25	5.20		500	22		50	20	25%	20	50	overnight	60	air	16	500	argon
B-base	1	4.96	5.38	20	22	5.08	50	20	25%	20	50	overnight	60	air	4	200	hydrogen
B-time	1	4.96	5.38	20	22	5.08	50	5	25%	20	50	overnight	60	air	4	200	hydrogen
B-conc	1	4.96	5.38	20	22	5.08	50	20	0.2%	20	50	overnight	60	air	4	200	hydrogen
B-ratio	1	4.96	5.38	20	22	5.08	50	20	25%	2	50	overnight	60	air	4	200	hydrogen
B-none	1	4.96	5.38	20	22	5.08	50	0	-	-	50	overnight	60	air	4	200	hydrogen
C-Dry	0.5	4.98	4.63	10	22	4.80	100	20	25%	20	50	2	200	flowing dry air	2	200	hydrogen
C-Wet	0.5	4.98	4.63	10	22	4.80	100	20	25%	20	50	2	200	flowing wet air	2	200	wet hydrogen
C60	0.5	5.02	4.85	10	22	5.01	100	20	25%	20	50	-	60	rotavap 110mbar	2	200	hydrogen
C80	0.5	5.02	4.85	10	22	5.01	100	20	25%	20	50	-	80	rotavap 110mbar	2	200	hydrogen
C100	0.5	5.02	4.85	10	22	5.01	100	20	25%	20	50	-	100	rotavap 110mbar	2	200	hydrogen
D100	0.5	3.11	3.27	10	22	3.99	100	20	25%	20	50	2	200	air	18	100	hydrogen
D200	0.5	3.08	3.21	10	22	3.96	100	20	25%	20	50	2	200	air	18	200	hydrogen
D300	0.5	3.06	3.14	10	22	3.74	100	20	25%	20	50	2	200	air	18	300	hydrogen
D400	0.5	3.10	3.24	10	22	4.27	100	20	25%	20	50	2	200	air	18	400	hydrogen
D500	0.5	3.27	3.37	10	22	3.96	100	20	25%	20	50	2	200	air	18	500	hydrogen

2.2 Characterization of catalysts

2.2.1 Catalyst loading

The gold loaded onto the catalyst was analysed for all catalysts by conducting AAS (Atomic Adsorption Spectroscopy) on liquid samples of digested catalyst. The AAS was calibrated with known concentrations of standards, and a calibration curve was plotted such that the concentrations in the liquid samples could be determined.

Each catalyst was acid digested to produce liquid samples using a standard method. An Erlenmeyer flask was placed on a heating plate, to which 0.3 - 0.4g of sample and 10 ml of 3:1 (by volume) HCl:HF mixture was added. The mixture was heated until it began to boil, at which point 10ml of HNO₃ was added. The mixture is allowed to continue boiling until the volume is reduced to approximately 2ml, after which 5ml HClO₄ was added. The mixture was again reduced to 2ml. This mixture was then removed from the hot plate and allowed to cool. Finally, the mixture was made up to a standard volume of 100ml with deionised water before being analysed by AAS.

The resultant gold loading (in wt%) of each catalyst is calculated from the concentrations obtained for the digested liquid samples using the equation shown below.

$$Au \text{ loading } wt\% = \frac{100 \times C_{Au} \times V_s}{m_s} \quad (2-1)$$

Where C_{Au} is the concentration of gold in the liquid sample analysed by AAS (in g/L),

V_s is the total volume of the liquid sample (in L), and

m_s is the mass of catalyst that is digested to the liquid sample (mg)

2.2.2 Particle size distribution of gold crystallites

Transmission electron microscopy

To prepare the samples for TEM, each catalyst was dispersed in methanol. This mixture was then sonicated, and spotted onto a carbon-coated copper grid. The microscope used for analysis was a JEM 1200EXII (JEOL) TEM and was operated at 120kV. For catalysts investigated on the higher resolution microscope, a holey copper grid was used instead.

Scanning Electron Microscopy

SEM was conducted on all of the catalysts. Catalysts are prepared in a different manner to that of TEM preparation. A small amount of catalyst sample is placed onto the stub (which is covered in carbon-based glue). Excess catalyst is blown off the stub before it is placed in the machine. A Nova NanoSEM 230 operated at between 15 and 20 keV was used for all images. Images are formed from the detection of backscattered electrons, as heavier elements backscatter electrons more strongly; gold appears as a bright spot on a darker background. A number of images were taken for each sample and in addition to some qualitative observations; the particle size of any gold particles found was measured.

Oxygen chemisorption

When compared to its use in the characterisation of other metal catalysts, oxygen chemisorption is not widely used as an analysis technique for supported gold catalysts.

It has been shown that reductive pre-treatment in hydrogen is required to sufficiently remove all oxygen from the catalyst surface (Berndt *et al.*, 2003). Furthermore, it was shown in this study that this treatment did not significantly alter the crystallite size of the catalysts. The authors found good agreement for the particle size obtained through chemisorption measurements and that of their TEM analysis by assuming that the adsorption of oxygen was dissociative.

Oxygen chemisorption of the catalysts in all batches were performed on a Micrometrics ASAP 2020C. Approximately 0.1g of the catalyst was subjected to a flow of hydrogen at 200°C for 16 hours. The sample was then evacuated for 2 hours before oxygen chemisorption was conducted at 200°C. Chemisorption was conducted between pressures of 0.1mmHg and 700mmHg. An equilibration time of 20 seconds was used.

Measurements on catalyst D100 were repeated three times. The first repeat ran with an equilibration time of 40 seconds. The second ran with an equilibration time of 20 seconds and was followed by a 60 seconds run. The run with the 60 second equilibration time used the same sample as that at 20 seconds (the sample was not removed from the sample tube, however, all pre-treatment steps were repeated). The purpose of this was to ensure that the equilibrium time was appropriate and not affecting the results.

Catalyst D300 was also used for additional measurements at successively increasing temperatures (35, 90, 150 and 200°C).

2.2.3 Temperature programmed adsorption and desorption of oxygen

Temperature programmed experiments were conducted to complement the chemisorption experiments. 0.1-0.15g of catalyst was pre-treated at 400°C in helium for 2 hours. Thereafter the sample was allowed to cool to 50°C.

Temperature programmed oxidation was then conducted as follows. The gas was changed to an oxygen helium mixture (5.1% O₂). After a minimum of one hour, but only once the baseline of the signal on the TCD was stable, the temperature was ramped up to 400°C, held at that temperature for 30 minutes, before returning to 50°C.

Temperature programmed desorption then follows by switching the gas back to pure helium and repeating the temperature ramp described above.

All experiments used a ramp rate of 20°C/min. Gas flows for all gases were 50 cm³/min during analysis, and 40 cm³/min during pre-treatment steps. Experiments were conducted on a Micromeritics AutoChem 2950 HP or, where mass spectrometer results are given, a Micromeritics AutoChem 2910 together with an OmniStar GSD 301 C quadrupole mass spectrometer. Both AutoChem machines made use of a cold trap at temperatures between -20 and -40°C to significantly reduce the water content of the vapours prior to the analysis of the gas stream.

2.3 Catalyst testing

Rig description

The gold catalysts were tested for their activity and selectivity in CO/CO₂ hydrogenation. A flowsheet of the rig used is shown in Figure 2.1. All lines are stainless steel with an outer diameter (OD) of 1/8in and a nominal wall thickness of 0.028in unless otherwise stated. Each of the four gases (H₂, N₂, CO, Ar) enters the rig setup *via* a gas manifold system at high pressure. All gases that come through the manifold system are of 99.999% purity unless otherwise stated. An N₂/C₆ mixture gas tank and a CO₂ gas tank are also connected via the manifold system. The preparation of the N₂/C₆ mixture tank is described in greater detail in a later section. With the use of a three way valve, a selection between N₂ or the N₂/C₆ mixture is made. Gas filters (0.5 micron) are installed ahead of the pressure regulators for each of the five gases. From here the H₂, CO, CO₂ and N₂ are each sent to their respective mass flow controllers. Argon does not pass through a mass flow controller but is pressure controlled and controls the pressure of the rig. One-way valves are

installed immediately after each mass flow controller. H₂, CO and CO₂ each pass through an open / close valve before the lines are combined with two T-pieces and the mixture is referred to as synthesis gas after this point. The synthesis gas goes to a three-way valve allowing it to either pass through the reactor or through the bypass line. Argon also goes to a three-way valve. The lines from the two three- way valves to the reactor are joined, as are the two lines going to the bypass.

The line enters the reactor at the top. A vent line (to the atmosphere) is also connected to the top of the reactor, a pressure indicator is installed on this line, and an open/close valve is fitted to its end. The thermocouple enters at the top of the reactor fits into the thermowell inside the reactor.

The reactor consists of a 220mm long 1in OD stainless steel tube with a 45mm long piece of 1/2in OD tubing welded to both the inlet and outlet. A copper frit is situated in the 1/2in tube at the bottom of the reactor.

The line leaving the reactor passes through an open/close valve before being joined with the bypass line. A pressure indicator is situated between the reactor and the open/close valve. After the join between the line leaving the reactor and the bypass line a needle valve is installed followed by an open/close valve. At this point the nitrogen line joins the exit line before encountering a split. One line passes through the ampoule sampling point before exiting to the vent via a bubble flow meter. The other line goes to an open/close valve before it passes through an online gas chromatogram [Varian 3300 GC-TCD] and subsequently exiting to the vent.

All the lines from the top of the reactor up until the ampoule sampling point are heated with heating lines and insulated with glass wool. The reactor is situated inside an oven with four heating elements which are used to control the temperature within the reactor. The temperature of the exit lines from the reactor to the ampoule sampling point are controlled separately.

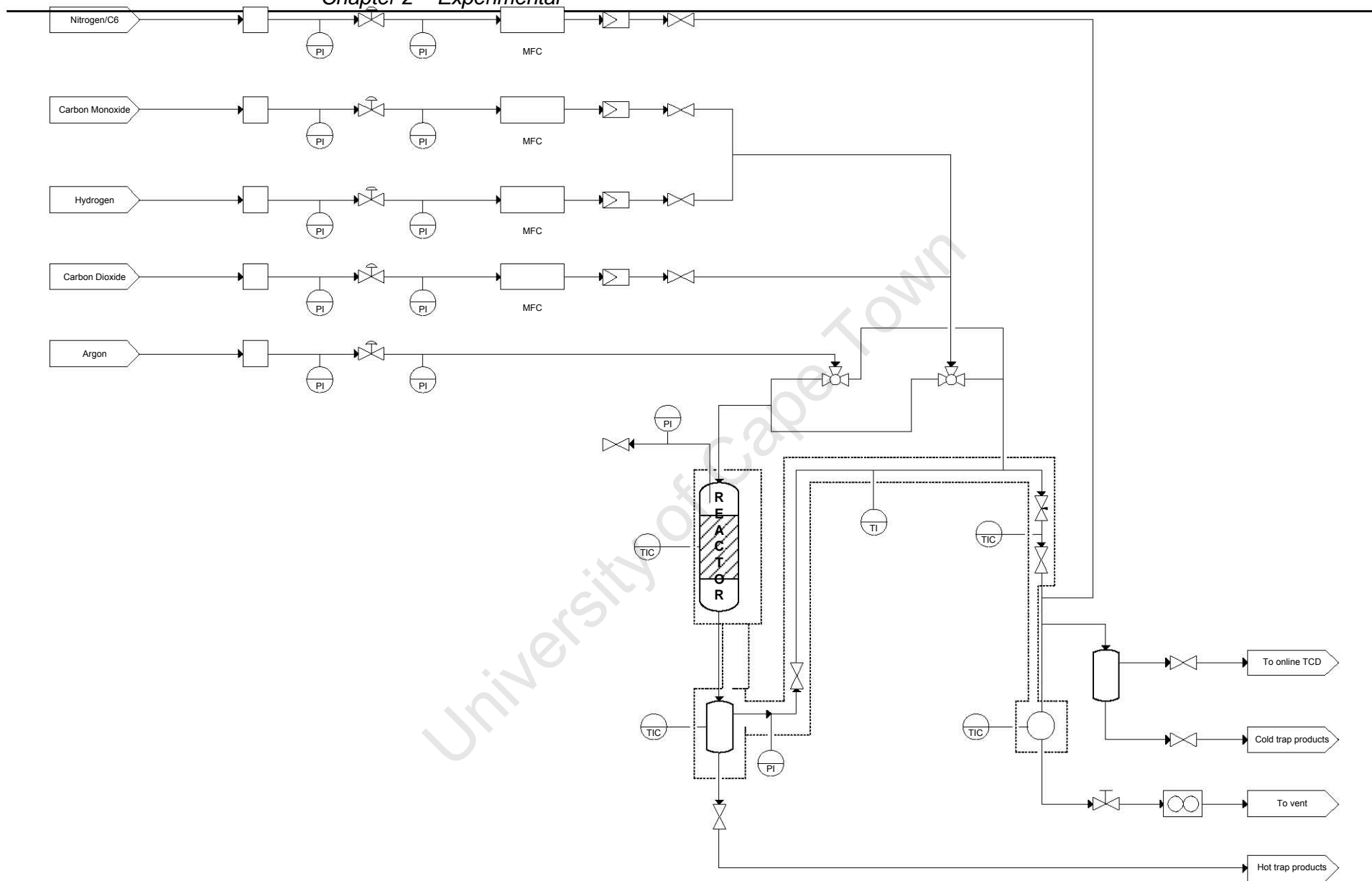


Figure 2-1: Catalyst testing rig flow diagram

Loading the catalyst

The tubular reactor (described in previous section) was loaded with a bed of 1g of catalyst for each run. Silicon carbide ($d_p = 200\text{-}250\mu\text{m}$) was used as a spacer to fill up the remainder of the reactor tube and is separated from the catalyst bed using glass wool. The location of the catalyst bed is such that it coincides with the location of the thermocouple. The gases flow from top to bottom. A diagram of the reactor is shown in Figure 2.2.

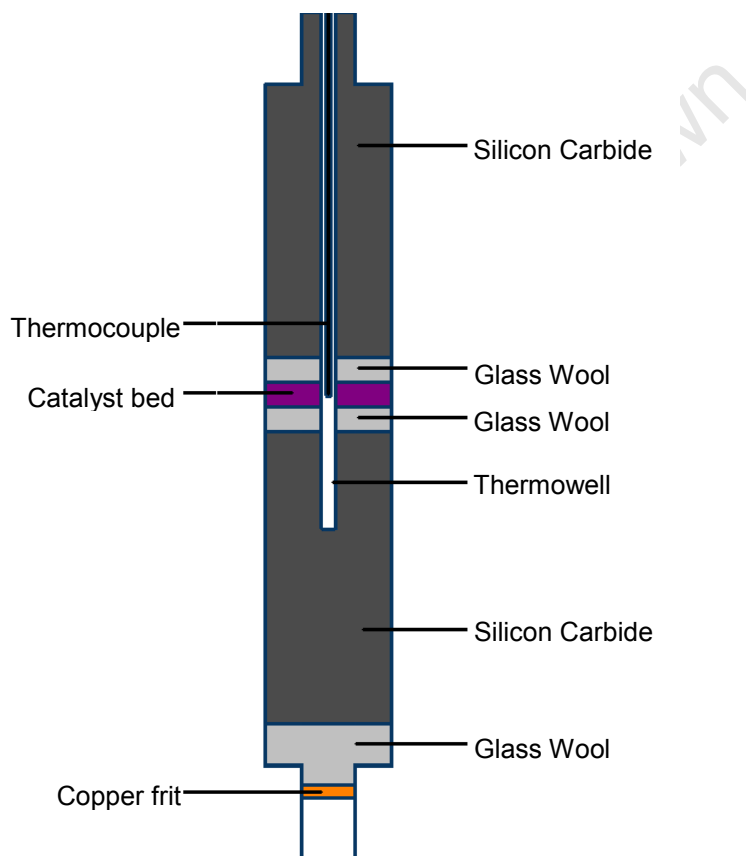


Figure 2-2: Reactor configuration

Reactor start up

After the catalyst has been loaded into the reactor, the reactor is refitted onto the rig. A pressure test is then conducted. All gases and their inlet valves are shut. The open/close valve after the reactor is in the closed position. The argon valve is then opened (and the three way valve is set

such that it flows through the reactor). While checking for leaks, the pressure of the argon, and thus in the reactor, is gradually increased to 55 bar. If no leaks are found the inlet valve is closed, thus isolating the reactor, and left for a minimum of an hour. If the pressure in the reactor does not drop then the pressure test is passed and start-up can begin.

Once the pressure test is passed the exit valves are slowly opened to allow the argon to vent out of the reactor. The inlet valves for the relevant gases are opened and the MFC's are used to set the flow rates to the appropriate values. Argon is used to pressurize the reactor and the needle valve is adjusted to control the total flow rate of syngas plus argon. The temperature program is started and once this as well as the flow rate/pressure has stabilized samples are taken on bypass. Thereafter the two valves at the top of the reactor are switched over such that the syngas flows through the reactor and the argon through the bypass. At this point the reaction has begun.

Running reaction and sampling procedure

Samples were regularly taken and analysed using gas chromatography in two different ways:

- An online TCD was used to monitor conversion and/or formation of H_2 , CO , CO_2 and CH_4 (using Ar as the carrier gas and N_2 as the reference).
- Gas ampoule samples were taken and subsequently analysed off-line with an FID (Flame Ionization Detector). Evacuated glass ampoules are inserted into the ampoule breaker. The tip of the ampoule is then broken and the gas enters the ampoule. The ampoule is sealed using a butane torch before being removed from the ampoule breaker.

Reactor shutdown

Once the reaction is complete, the gases are switched over to bypass. The pressure is returned to atmospheric and the temperature is returned to ambient. Finally the gases are shut off and the reactor is removed to recover the catalyst and reload for the next run.

GC analysis and data manipulation

An online TCD (details in Table 2.2) is used to monitor the formation/consumption of CO, CO₂, H₂, and CH₄. The TCD also detects N₂ and this is used as the reference compound. Ar is the carrier gas and thus does not appear on the chromatogram. A reference cylinder with known concentrations of all the relevant compounds is used to obtain calibration factors. These are then used to calculate flow rates of unknown gas mixtures where the flow rate of nitrogen is known.

$$f_i = A_{N_2}/A_i \times C_i/C_{N_2} \quad (2-2)$$

$$F_i = f_i \times F_{N_2} \times A_i/A_{N_2} \quad (2-3)$$

Where F_i = molar flow rate of compound i

f_i = calibration factor of compound i relative to the reference N₂

A_i = carbon number of compound i

C_i = molar concentration of compound i

An example diagram of a TCD chromatogram is shown below in Figure 2.4. The areas under the peaks are given by the integrator (and used in the equations discussed above) and the retention time determines the compound.

Using the flow rates/concentrations obtained from the GC analysis the conversions and yields can be calculated. Yield and conversion are defined in the following manner throughout this thesis.

$$\text{Yield (\%)} = 100 \times F_i / (F_{CO} + F_{CO_2})_{\text{inlet}} \quad (2-4)$$

$$X = 100 \times (F_{i0} - F_i) / F_{i0} \quad (2-5)$$

Where F_i = molar flow rate of compound i

X = conversion of compound i as a percentage

A GC-FID is used for offline product analysis. More details on the specifications of the column and the operating conditions can be found in Table 2.2.

A labelled example of a chromatogram obtained from the offline GC-FID is shown below in Figure 2.3. The peak position, (molecules are separated based on boiling point in the column prior to the FID analysis) and shape are used to determine what molecule it represents and the area under the peak is used to calculate the concentration of that molecule in the gas mixture relative to that of the reference compound. The FID can only detect molecules that are ionized upon combustion (i.e. hydrocarbons) and thus not all components of the exit stream are detected (i.e. H₂O, CO, H₂, CO₂, N₂, Ar).

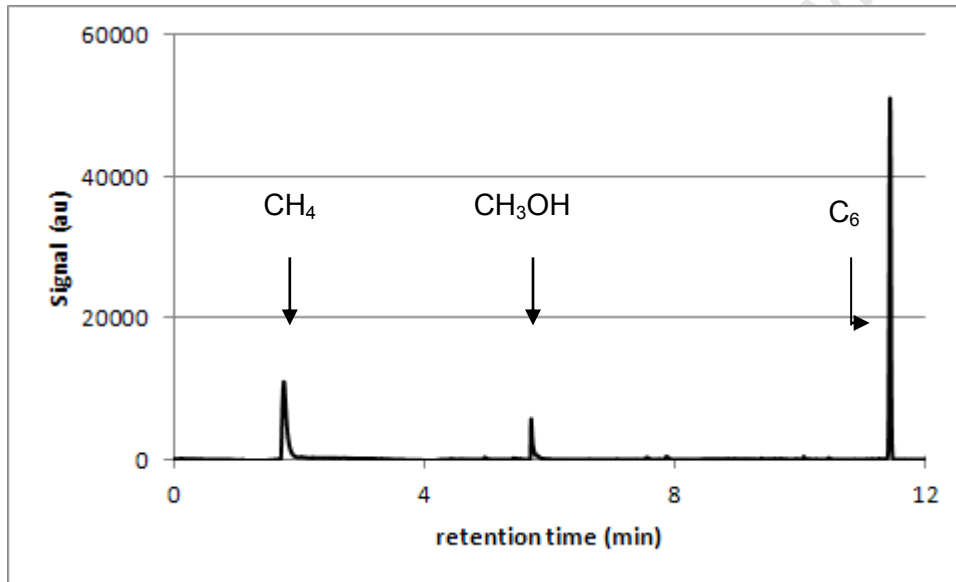


Figure 2-3: Example GC-FID chromatogram

Knowing the concentration and flow rate of the reference compound (cyclohexane, also referred to as C₆) in the gas sample and the response factors of the relevant compounds enables us to calculate the concentration of these compounds in the following manner.

$$F_i = f_i \times A_i / CN_i \times CN_{C_6} / A_{C_6} \times F_{C_6} \quad (2-6)$$

Where F_i = molar flow rate of compound i

f_i = carbon based response factor of compound i

A_i = area under the peak assigned to compound i

CN_i = carbon number of compound i

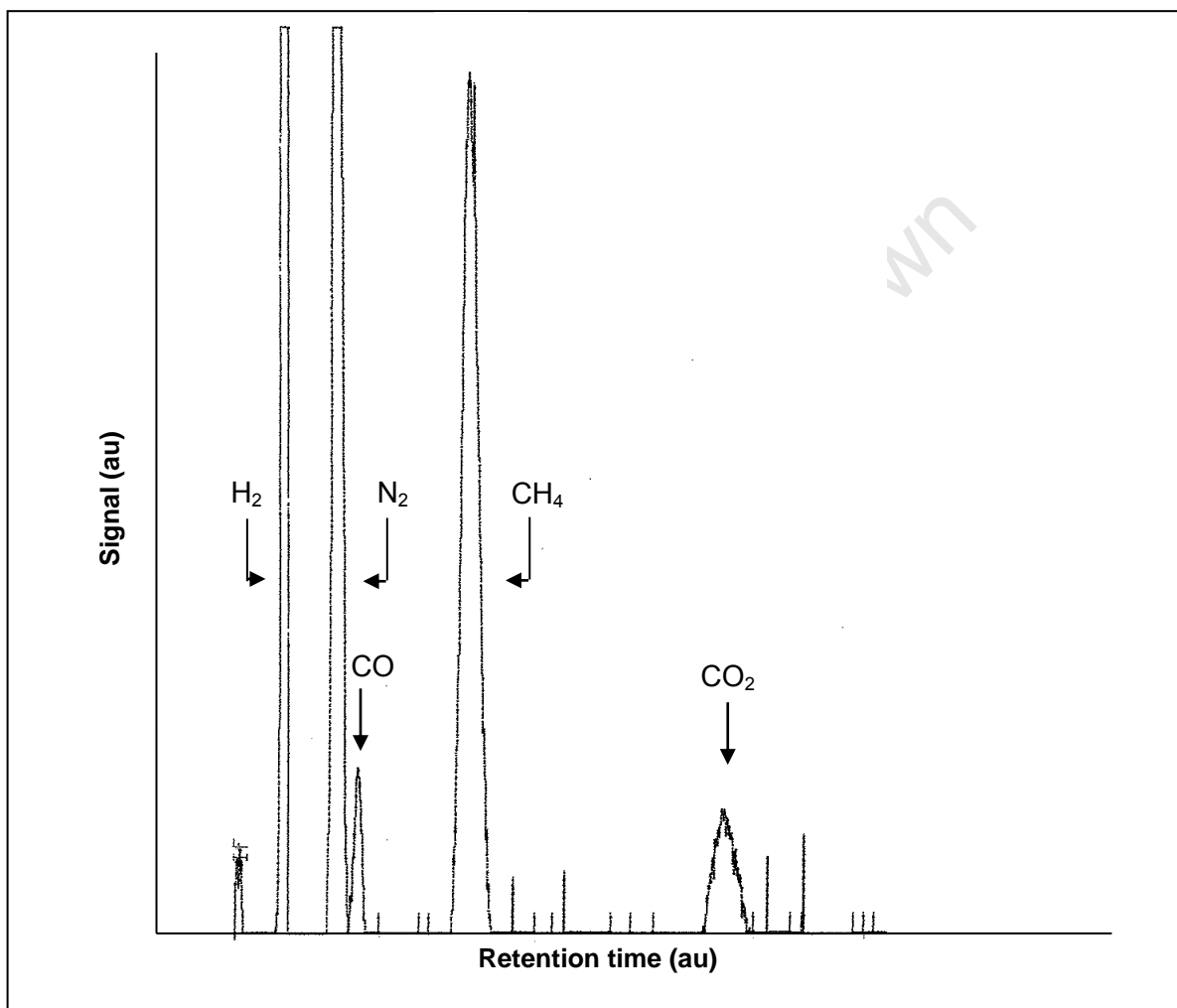


Figure 2-4: Example GC-TCD chromatogram

Table 2-2: GC specifications

	GC-FID (offline)	GC-TCD (online)
Type of GC	Varian CP-3800 gas chromatogram	Varian 3300 GC-TCD and HP3396 series II integrator
Column	Varian Chrompack Capillary GC Column CP-SIL 5CB 25 x 0.15 x 0.12µm	Carbosieve™ SII packed stainless steel column 10' x 1/8"
Split ratio	0.4	splitless
Carrier gas	300ml/min air	30ml/min Ar
Make up gas	30ml/min N ₂	-
H ₂ flowrate	30ml/min	-
Injector temperature	200°C	200°C
Detector temperature	200°C	200°C
Column temperature	Temperature program	120°C

Preparation of N_2/C_6 mixture tank

A N_2/C_6 mixture tank is needed as the C_6 is used as the reference compound when doing GC-FID analysis of the reactor products. A tank initially filled with Nitrogen at 1bar is connected to a high pressure nitrogen tank. The tubing that is used to connect the two tanks features a pressure regulator and indicator, a one way valve and a long U-shaped tube. This is shown in the schematic in Figure 2.5 prior to connecting the tanks the U-shaped tube is filled with approximately 8 ml of liquid cyclohexane. Once the setup is ready the nitrogen tank is opened and the valve on the pressure regulator is gradually opened until the previously atmospheric pressure tank is at the desired pressure (~ 40 bar).

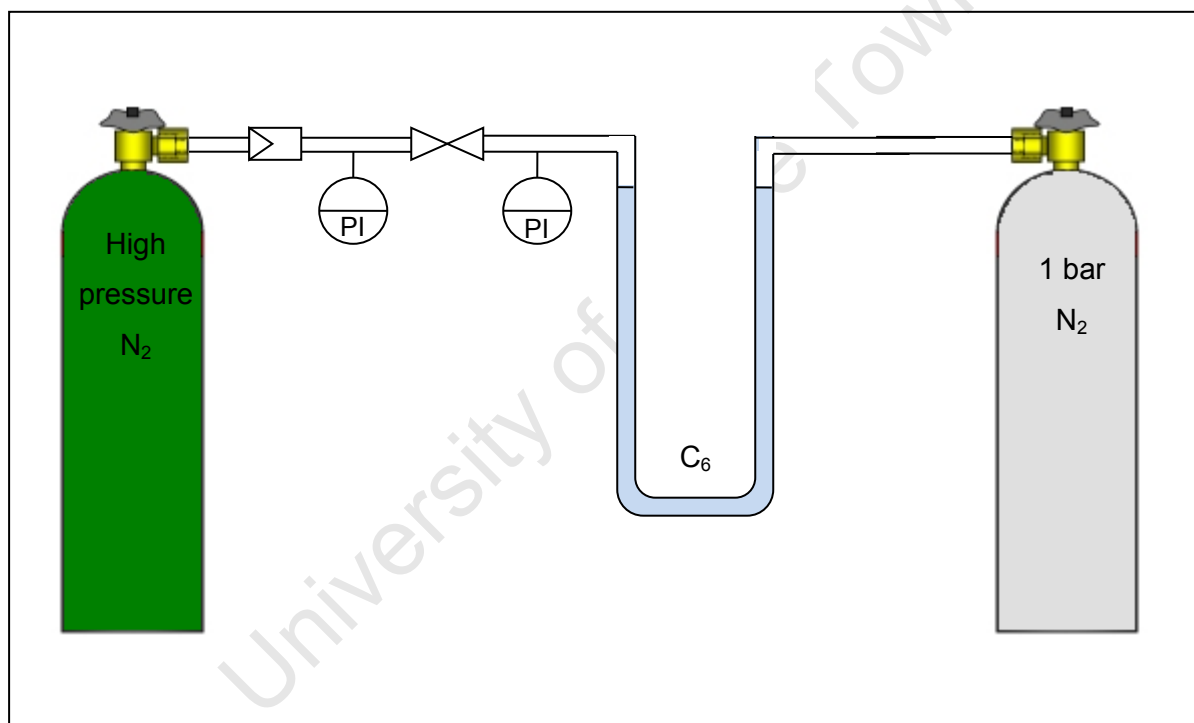


Figure 2-5: diagram to illustrate setup used to prepare a N_2/C_6 mixture tank

The valves are then closed and heaters are placed around the bottom section of the mixture tank. This causes convection currents that aid in obtaining a homogenous C_6/N_2 mixture.

The concentration of C_6 is analysed using the GC-FID. Known volumes of reference gas (containing a known concentration of methane) are injected after which identical volumes of the C_6/N_2 mixture are injected into the GC to establish the concentration of C_6 to be used as the

reference compound.

2.4 Health and Safety

One must check that no gold remains in the solution prior to the ammonia washing step of catalyst preparation to prevent the formation of gold ammonia complexes. Gold ammonia complexes are explosive and therefore a great safety risk in the laboratory (Steinhauser *et al.*, 2008).

Chemicals such as sodium hydroxide, nitric acid, hydrochloric acid and ammonia were used in these experiments. Caution was taken and a laboratory coat, safety glasses and latex gloves were worn. The chemicals mentioned above are toxic; with vapours which are strong irritants therefore experiments were performed within a fume cupboard. Special care was taken when working with concentrated acids as they are strong oxidising agents and can cause severe burns. Any contact with skin requires immediate washing with water.

Great care was taken when disposing of substances after use. All bottles were labelled clearly and mixing of waste was prevented. Gold containing samples were disposed of separately for the future recovery of gold.

Catalyst testing took place at temperatures and pressures that can be hazardous, additionally CO and H₂ were being used as reactants. Both of these gases are dangerous and the appropriate care was taken when operating the rig, as well as adhering to all the safety rules in the laboratory.

3 RESULTS

3.1 Catalyst loading

The gold loading on the synthesized catalyst samples was determined by AAS analysis of the digested liquid samples as described in the experimental chapter.

The resultant gold loading in each of the synthesized catalyst samples as determined using AAS is given in Table 3.1. The theoretical loading is based on the gold content in the precursor solution assuming a 100% uptake during the ion-exchange and no gold loss in the subsequent washing steps. All catalysts were prepared at pH values close to 5 with the exception of Batch D which was prepared at a pH between 3 and 4. Previous work (Yang *et al.*, 2005) has demonstrated that pH can have a significant effect on the loading obtained when using ion-exchange (or deposition precipitation) as the preparation method for supported gold catalysts. A maximum uptake of ca. 40-50% can be obtained at pH values close to 5.

Most catalysts were prepared together and split at a later stage of the preparation such as the washing, drying or calcination step. For example all the catalysts in the A2 series were prepared together and at the calcination step were divided and calcined separately at various conditions. This means the gold metal loading is the same for all catalysts in this series. Thus the variation in the gold loading is due to errors associated with the digestion and AAS analysis. In this case the average gold loading is 2.31 wt%, with a %RSD (relative standard deviation) of 4%. On the other hand, catalysts in Batch D were each prepared separately from the first step and the deviation in the gold loadings from the mean in this batch is due to the repeatability of the catalyst preparation in addition to that of the analysis. The average gold loading of 2.17 wt% was obtained with this batch with a % RSD of 9.8%.

Batch B was split at the washing step, with the exception of B-none, which was prepared separately. C-WET and C-DRY were separated at the drying step, as was C60, C80 and C100. Variations in the precursor concentration (keeping the support - Au ratio constant), the drying and calcination conditions had no visible effect on the gold uptake by the support. Changes in the washing procedure, however, caused a gold loss during washing that resulted in a gold uptake of as little as 27%.

Table 3-1: Catalyst loading results from AAS analysis

	Catalyst code	pH of preparation	Gold loading (wt%)	Gold uptake (% of theoretical loading)
Variation in precursor Au concentration (and calcination procedure)	Batch A average	~	2.3 ± 0.08	46
	A1-200H	5.03	2.25	45
	A1-500H	5.03	2.29	46
	A2-200H	5.20*	2.31	46
	A2-200Ar	5.20*	2.40	48
	A2-500H	5.20*	2.19	44
	A2-500Ar	5.20*	2.35	47
Variation in washing procedure	Batch B average	~	1.8 ± 0.35	37
	B-base	5.08	1.83	37
	B-time	5.08	1.70	34
	B-conc	5.08	1.37	27
	B-ratio	5.08	1.91	38
	B-none	5.08	2.34	47
Variation in drying procedure	Batch C average	~	2.7±0.03	53
	C-Dry	4.80	2.01	40
	C-Wet	4.80	2.65	53
	C60	5.01	2.65	53
	C80	5.01	2.68	54
	C100	5.01	2.62	52
Variation in calcination temp.	Batch D average	~	2.2 ± 0.20	43
	D100	3.99	2.42	48
	D200	3.96	2.18	44
	D300	3.74	1.95	39
	D400	4.27	2.34	47
	D500	3.96	1.97	39

*pH before addition of support

3.2 Crystallite size distributions

3.2.1 TEM

A sample TEM image is shown in Figure 3.1. The grey background is the carbon on the grid, while the broken up alumina appears as the darker grey shapes. Gold is relatively easy to identify, having a much larger electron density, it appears as the small black circular type shapes.

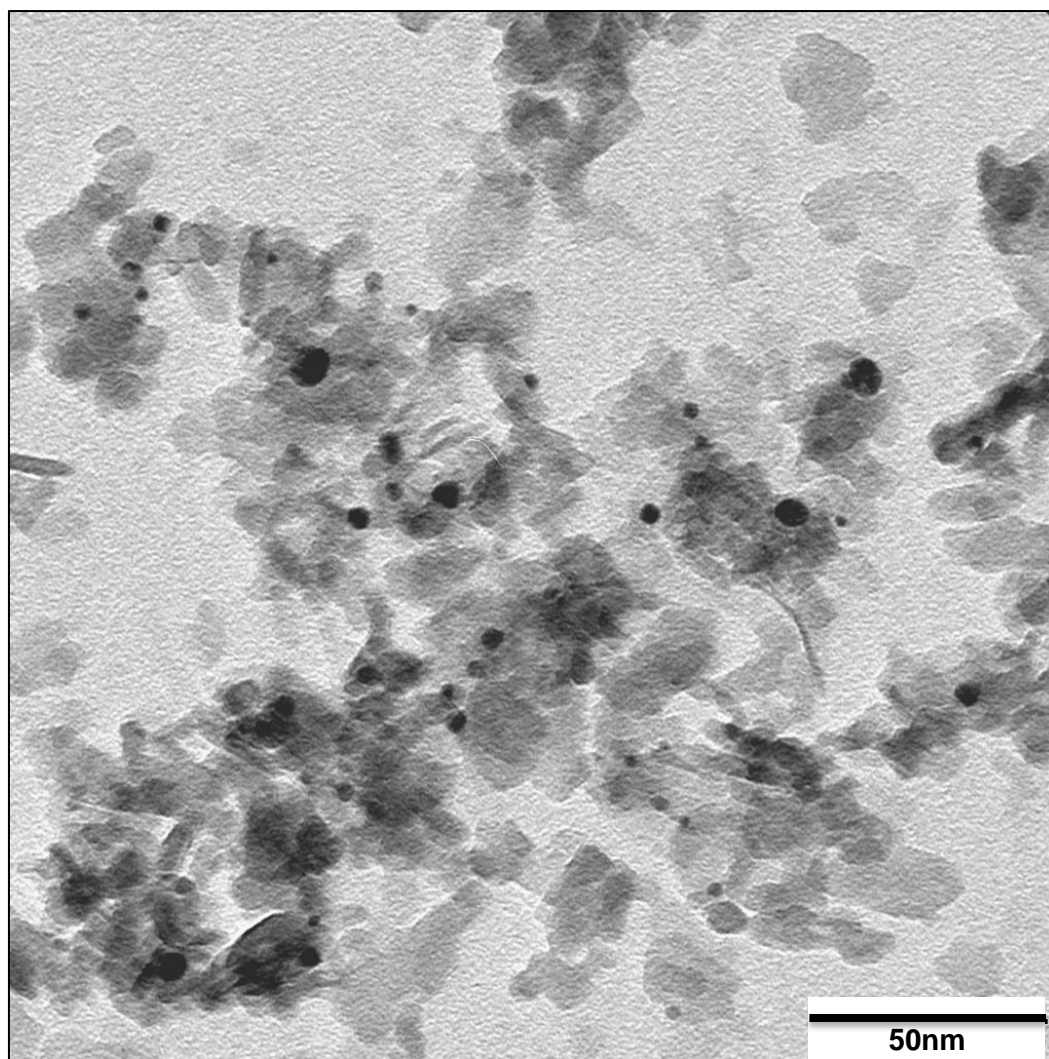


Figure 3-1: Example TEM image (catalyst D200)

Numerous micrographs were taken of each catalyst and all identifiable crystallites were measured to obtain crystallite size distributions (see Figure 3-3 to Figure 3-6). With the exception of those prepared without an ammonia wash, particles were predominantly within or near the 2-5nm range. What appears to be the narrowest size distributions were obtained in Batch C where catalysts were dried in flowing air or in a rotary evaporator as opposed to the usual stationary oven employed for all other batches.

All identifiable crystallites on the images were measured. It is important to measure as many crystallites as possible in order to get a distribution that is representative of the sample and to keep the deviation from the mean as low as possible. Comparison of catalyst samples become statistically relevant when the sample sizes are larger and the deviation from the mean is smaller. Doing statistical tests such as the t-test allows a comparison of the means and to what extent they differ (the full statistical analysis is given in Appendix A - Statistical Analysis).

3.2.1.1 *Batch A – effect of gold concentration in precursor solution and calcination conditions*

The histograms for the gold crystallite size distributions obtained with batch A appear quite similar at a first look (see Figure 3 2). The gold size distributions appear quite broad making the small differences in average size less obvious on the histogram. The catalysts calcined at 200°C show smaller average crystallite sizes than those calcined at 500°C, however, the difference is not always significant. No effect on the crystallite size due to increasing the concentration of the gold in the precursor solution (by a factor of 2 for the A1 series and a factor of 50 for the A2 series) is evident. The use of argon only appears to affect the crystallite size distribution at the lower temperature of 200°C. The calcination gas does not affect the observed crystallite size distributions at the higher temperature of 500°C.

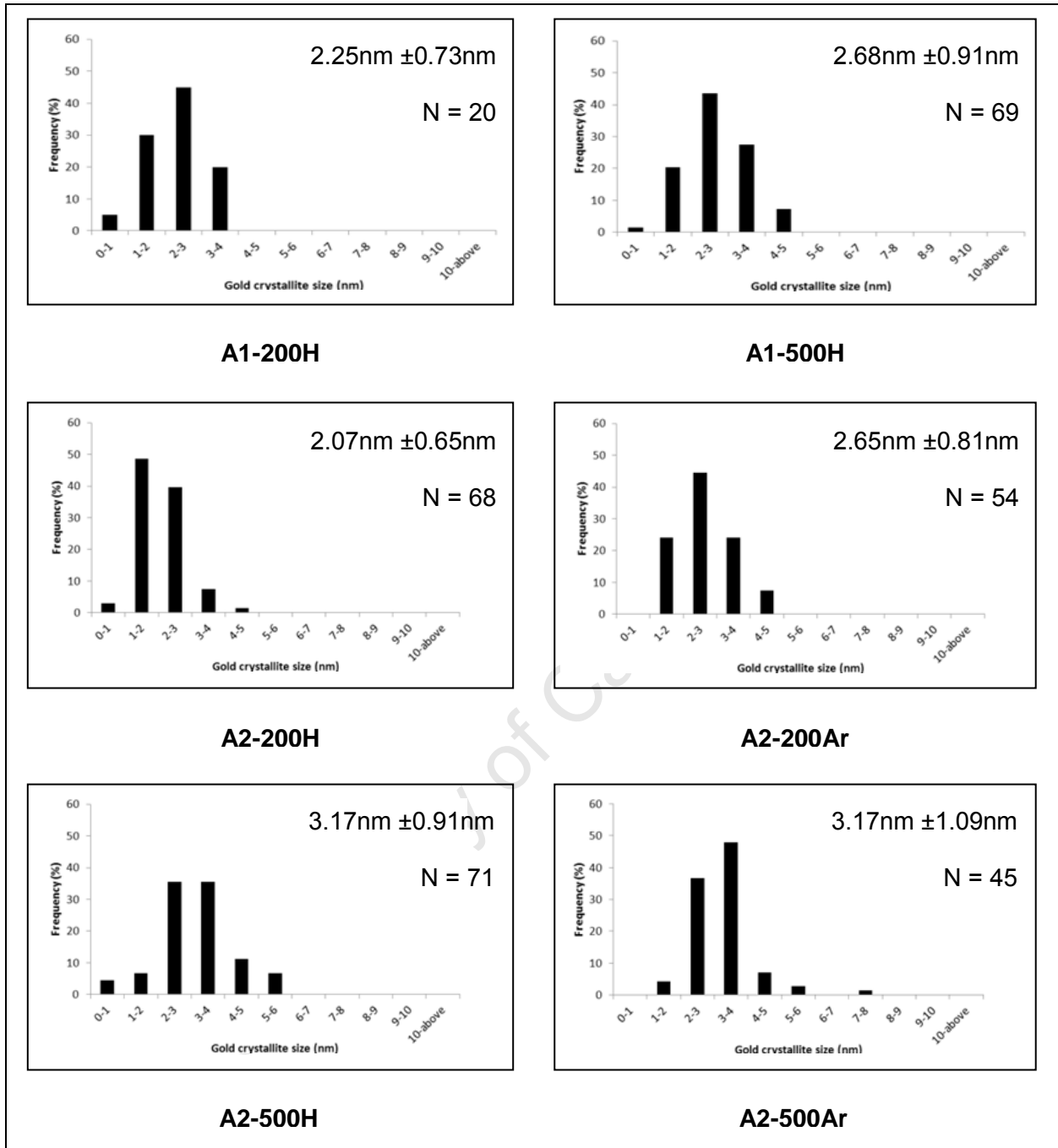


Figure 3-2: Gold crystallite size distributions of Batch A obtained from TEM analysis

3.2.1.2 Batch B – effect of washing procedure

The gold crystallite size distributions obtained for batch B appear to be the widest. When omitting the ammonia wash completely only crystallites with sizes >50 nm are found. The ammonia wash is evidently crucial for the formation of small, uniformly sized gold crystallites. The average crystallite size obtained for the catalyst for which the washing time was shortened to 5 minutes instead of 20 minutes is the largest. The larger average size of the sample B-time (which had the shortest washing time) is of statistical significance: When comparing to B-base and B-conc using a Tukey HSD (honestly significant difference) test at 95% confidence the means are shown to differ, although the number of crystallites counted for sample B-time are much lower than for the other two catalysts. Full results of the statistical analysis can be found in Appendix A - Statistical Analysis. The small difference between catalysts B-conc and B-base is statistically insignificant.

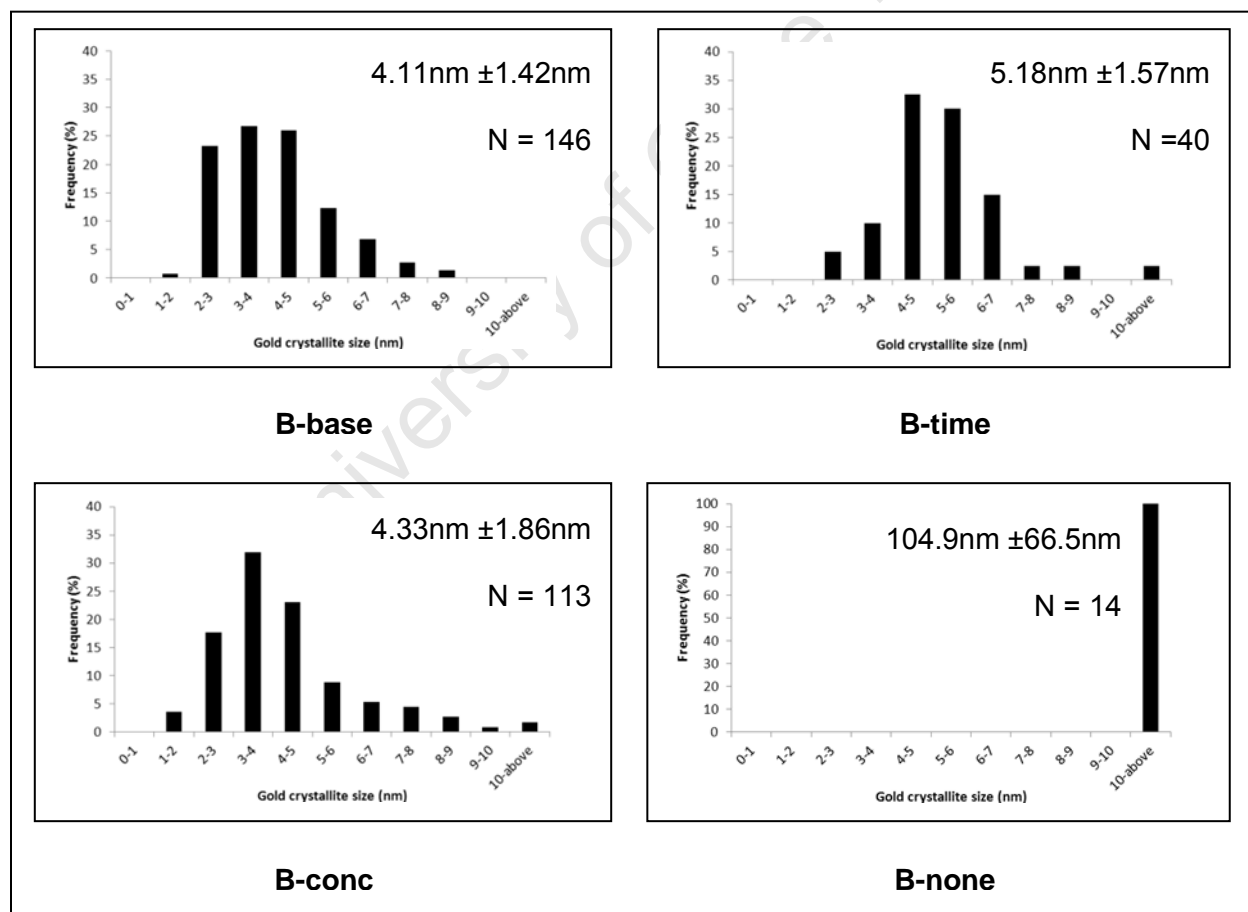


Figure 3-3: Gold crystallite size distributions of Batch B obtained from TEM analysis

3.2.1.3 *Batch C – effect of drying procedure*

The gold crystallite size distributions obtained in batch C appear to be the narrowest. No obvious trend regarding the average crystallite size can be seen with changes in the drying conditions. Drying the catalyst in air that is saturated with water (or not) has no effect on the crystallite size. The size distributions on C-wet and C-dry are no different to those of C100. However, at 95% confidence the mean of C60 is shown to be slightly larger than that of C-wet and C100, but not significantly larger than the mean of C-dry. Sample C80 has a mean that is smaller than all catalysts of batch C at the same level of confidence.

University of Cape Town

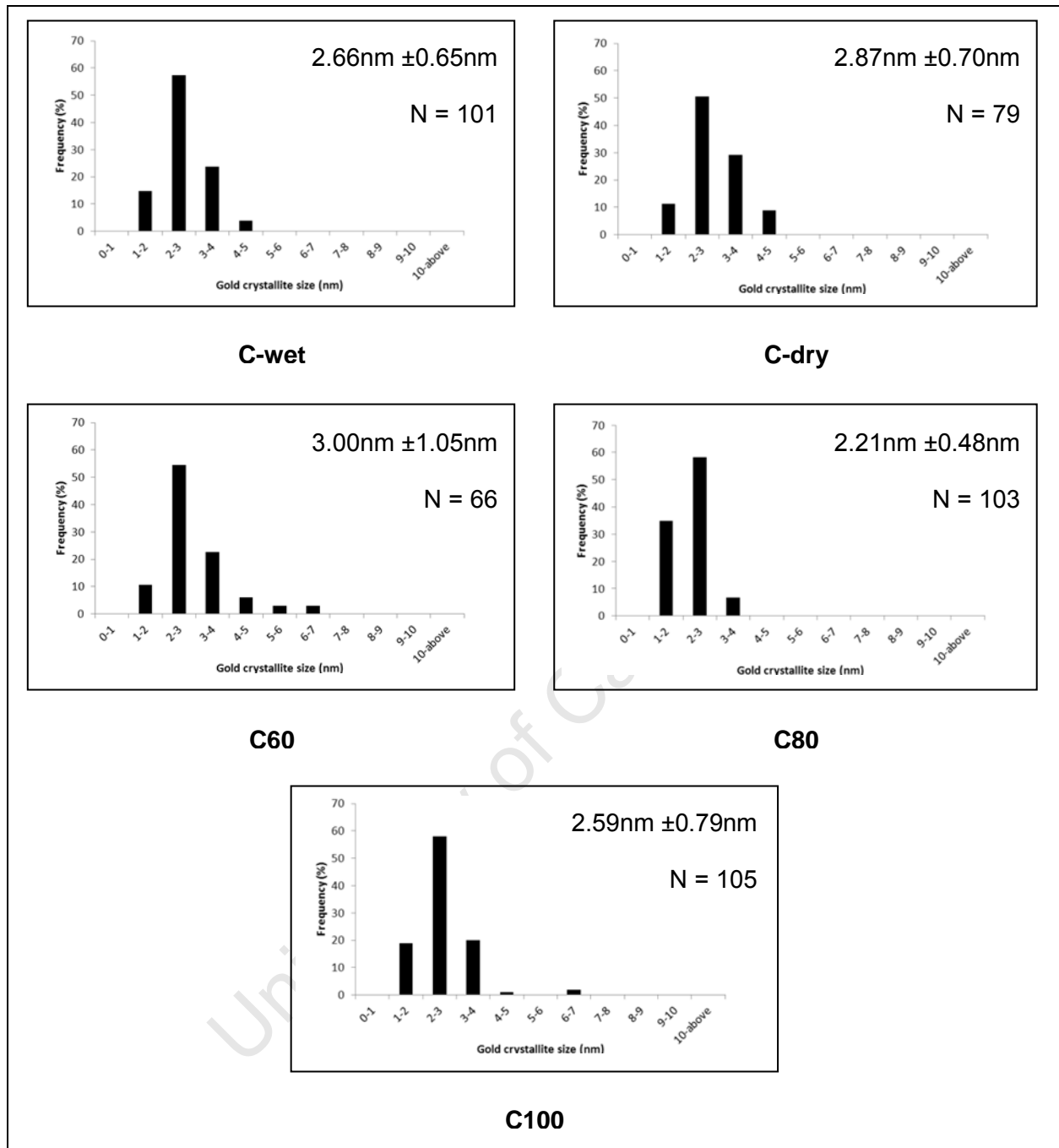


Figure 3-4: Gold crystallite size distributions of Batch C obtained from TEM analysis

3.2.1.4 *Batch D – effect of calcination temperature*

The obtained gold crystallite size distributions in batch D are broad. The effect of calcination temperature on crystallite size is small. Crystallite size distributions of catalysts calcined above 200°C have a smaller average compared to those calcined at 100 and 200°C. There is no difference between the average crystallite sizes obtained for catalysts calcined at 100 or 200°C. The catalysts calcined at 300-500°C are statistically not different from each other. The results of the one-way ANOVA and Tukey HSD tests (at 95% confidence) are given in Appendix A.

University of Cape Town

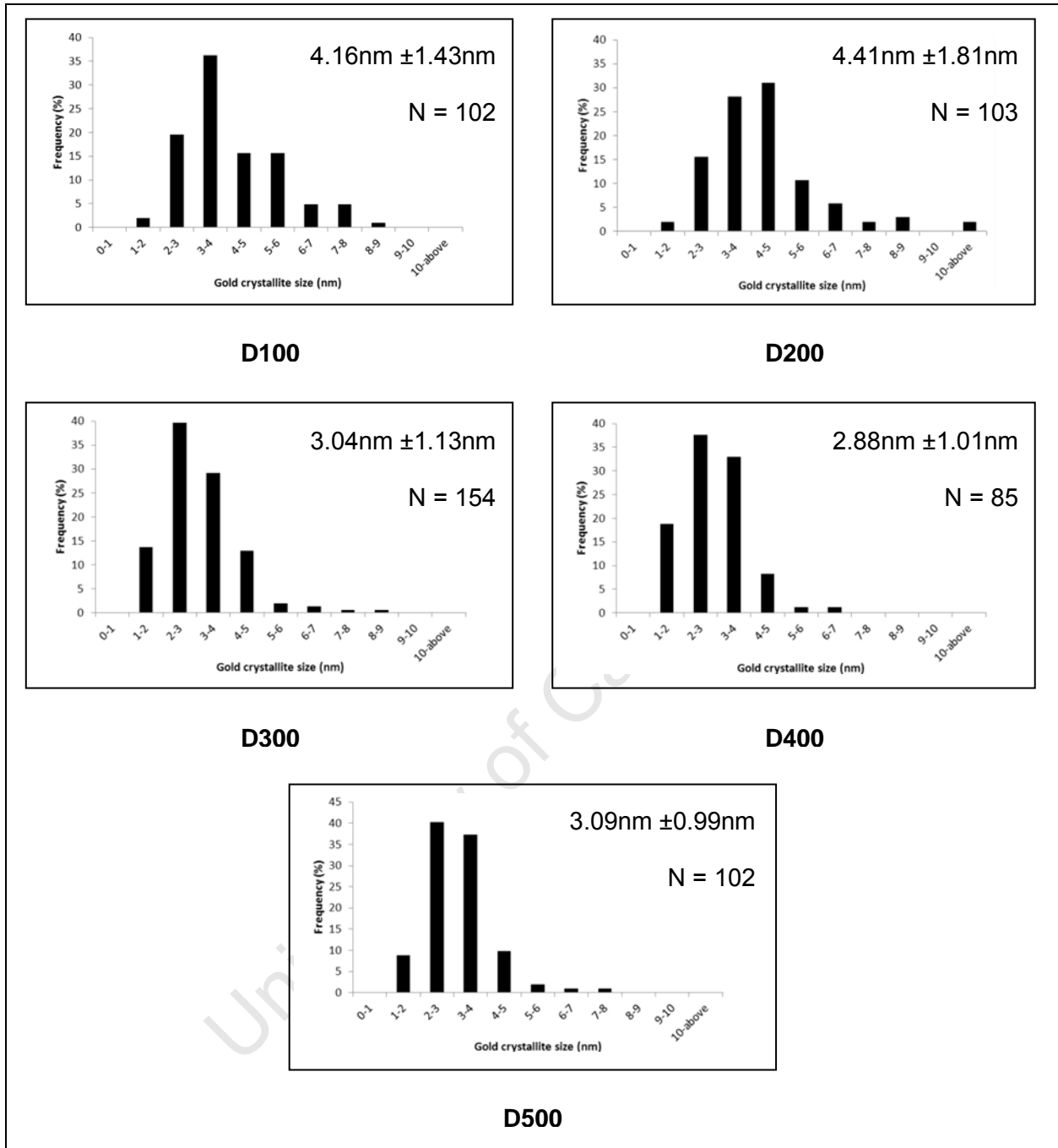


Figure 3-5: Gold crystallite size distributions of Batch D obtained from TEM analysis

3.2.2 HRTEM

On the TEM apparatus employed to it is hard to identify gold particles smaller than $\sim 2\text{nm}$. HRTEM was employed to investigate if there were significant numbers of particles smaller than 2nm present. An example of an HRTEM image is shown in Figure 3-6.

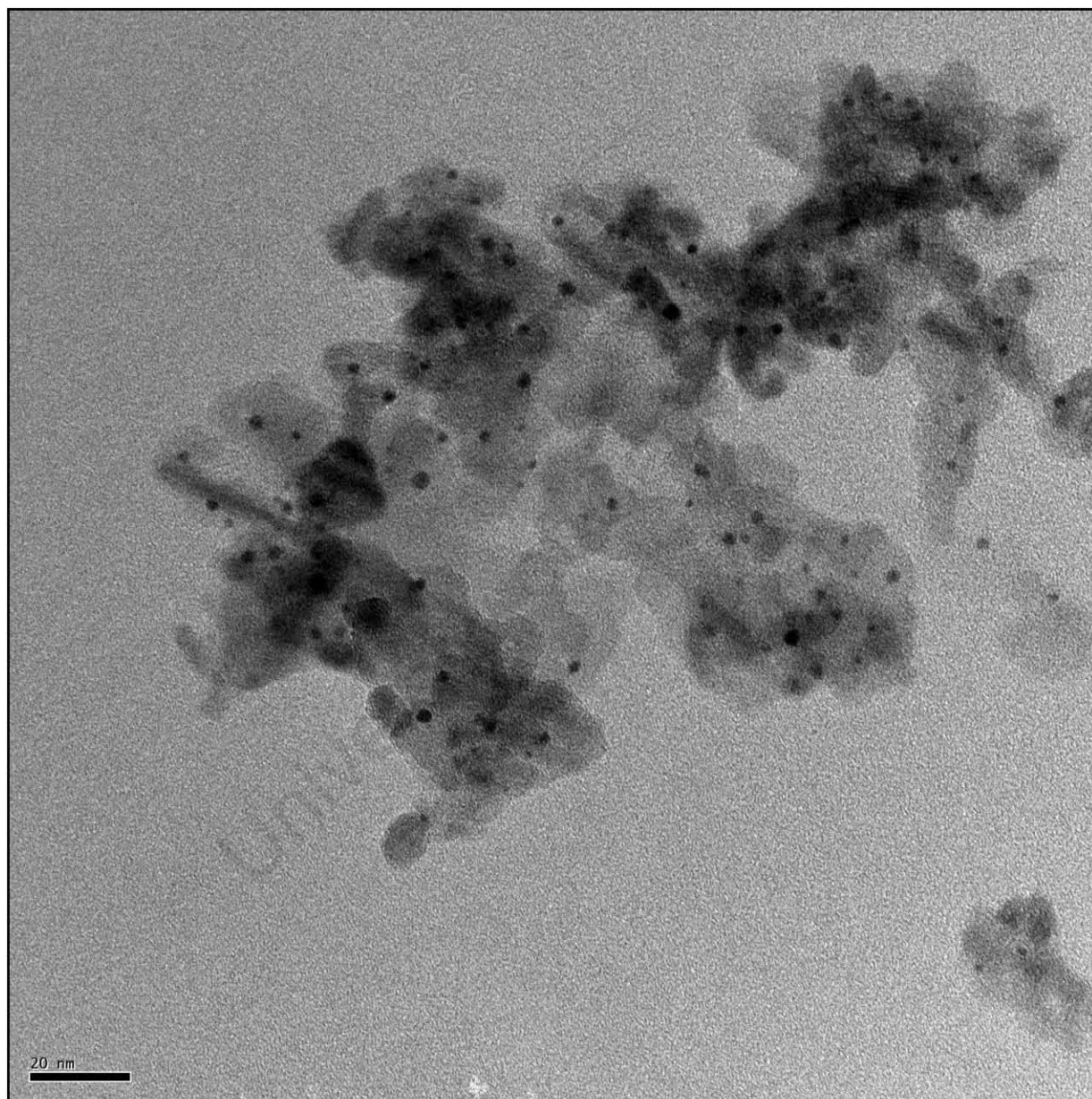


Figure 3-6: Example HRTEM image (catalyst D400)

The samples D200, D300 and D400 were all studied using HRTEM. While there is improved resolution on the HRTEM, there is still a limit to the size of gold crystallite that can be observed. The resultant histograms are plotted on the same axis as the original TEM results (Figure 3-7) and on visual inspection there is not a large difference between the TEM and HRTEM distributions. While the resultant histograms do not indicate any greater number of particles below 1nm, the crystallites below 3nm are more easily identified. This manifests itself on the histograms, especially visible for samples D300 and D400. Distributions obtained on the HRTEM were also narrower with no crystallites above 4nm being observed on catalysts D300 or D400. Statistically the average crystallite sizes and obtained from TEM and HRTEM are different (using a t-test values of P obtained are 0.044, <0.0001 and <0.0001, respectively). However, looking at the confidence intervals the difference with statistical significance, is likely a small difference. At 95% confidence the difference between the means are $0.448 \pm 0.437\text{nm}$, $0.669 \pm 0.218\text{nm}$, $0.579 \pm 0.262\text{nm}$ respectively.

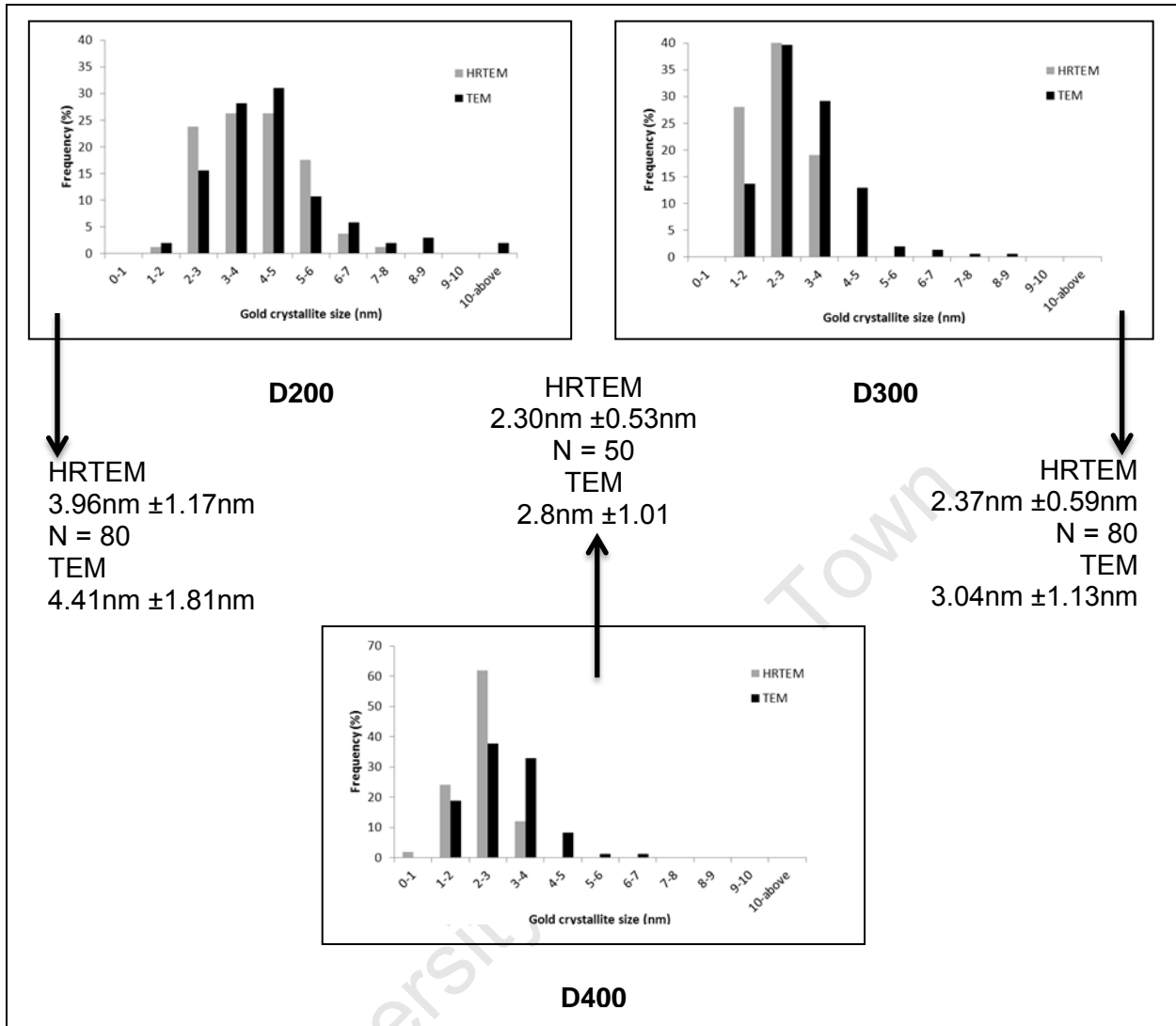


Figure 3-7: Gold crystallite size distributions of Batch D obtained from HRTEM analysis

3.2.3 SEM

SEM images were collected on all catalyst samples. SEM allows us to see the general shape and size of the support particles. However, the resolution is too poor to expect to see the same particles that are typically observed using TEM on samples dispersed in alcohol. All catalysts showed a presence of larger gold crystallites (>50nm) on the surface of the support particles. An example of this is shown in Figure 3-8.

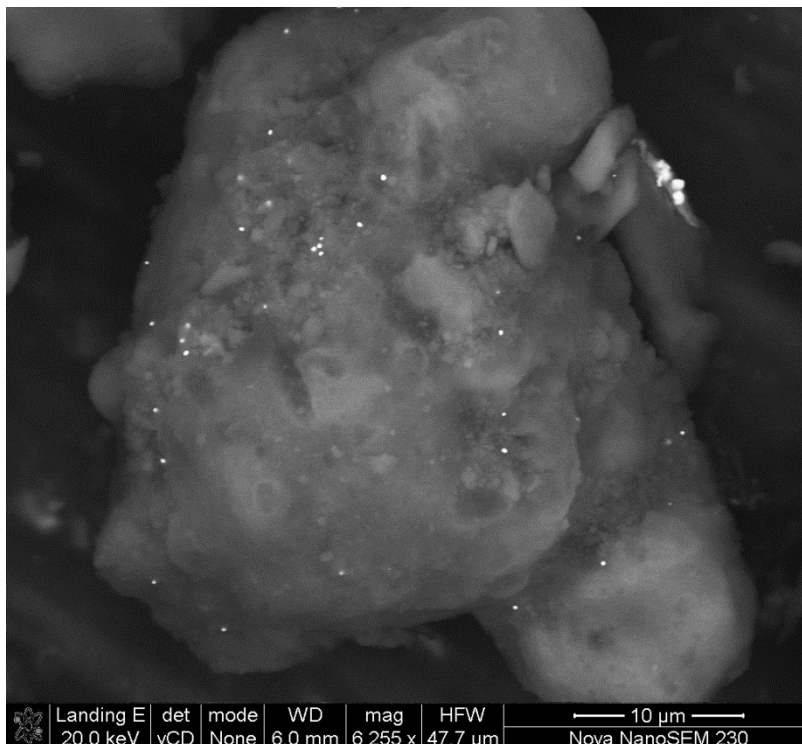


Figure 3-8: Example SEM image (catalyst D100)

These large gold particles (>50nm) were evident on all catalyst samples; however, the amount and distribution differed between and sometimes within batches. Various shapes and sizes were encountered, such as spherical, triangular, hexagonal, elongated and odd shapes, however, these shapes were not characteristic of the catalyst sample on which they were found.

The importance of the number of crystallites that are measured should be mentioned here again. The typical SEM analysis reveals just a few gold particles, and no meaningful distribution can be obtained with such few crystallites. Comparison of size distributions obtained from SEM

is all but impossible. However, there is still useful information in this analysis, namely the frequency with which we observe these particles, as well as how they distribute themselves gives us qualitative information. Sometimes sintering can be quite evident with large fused agglomerations being visible on the SEM.

3.2.3.1 *Batch A – effect of gold concentration in precursor solution and calcination conditions*

Figure 3-9 shows the SEM images and the 'distribution' for the samples in batch A. with the exception of samples A1-500Ar and A2-500H, samples of this batch displayed a small number of isolated individual gold particles. A2-500H showed noticeable sintering and agglomeration, with only one particle being separate and thus measurable. Catalyst A2-500Ar had similar agglomeration/sintering overall, additionally one of the support particles had a significant amount of measurable gold particles on it. This was not homogeneous at all.

University of Cape Town

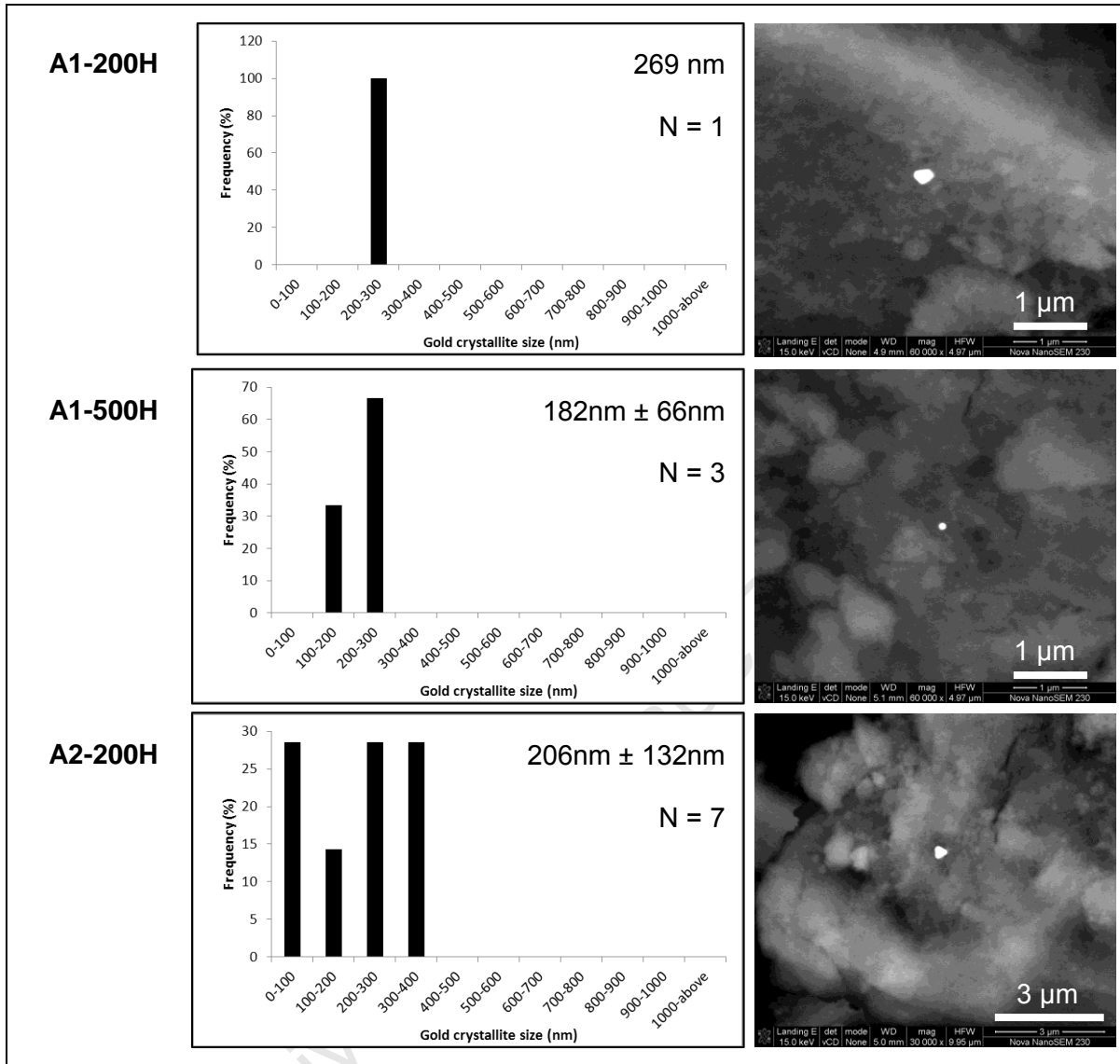


Figure 3-9: Gold crystallite size ‘distributions’ of Batch A obtained from SEM analysis

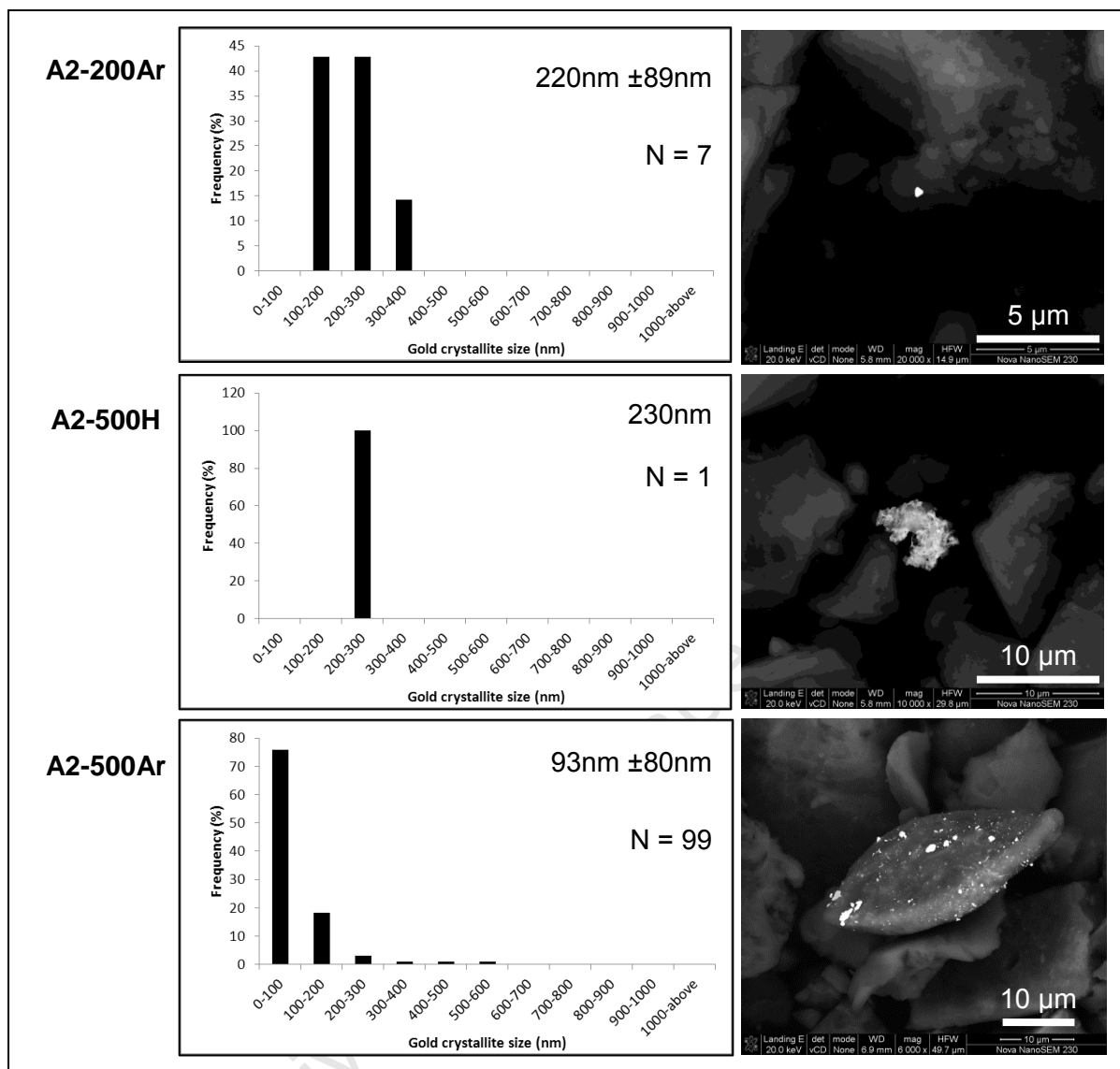


Figure 3-9 (cont.): Gold crystallite size 'distributions' of Batch A obtained from SEM analysis

3.2.3.2 Batch B – effect of washing procedure

The SEM image of sample B-none showed many large particles strewn all over the support. The remaining catalysts in batch B contained scattered single gold particles with the occasional signs of sintered particles and agglomerations. In catalyst B-conc, the largest gold particle with a size of larger than 600nm was found.

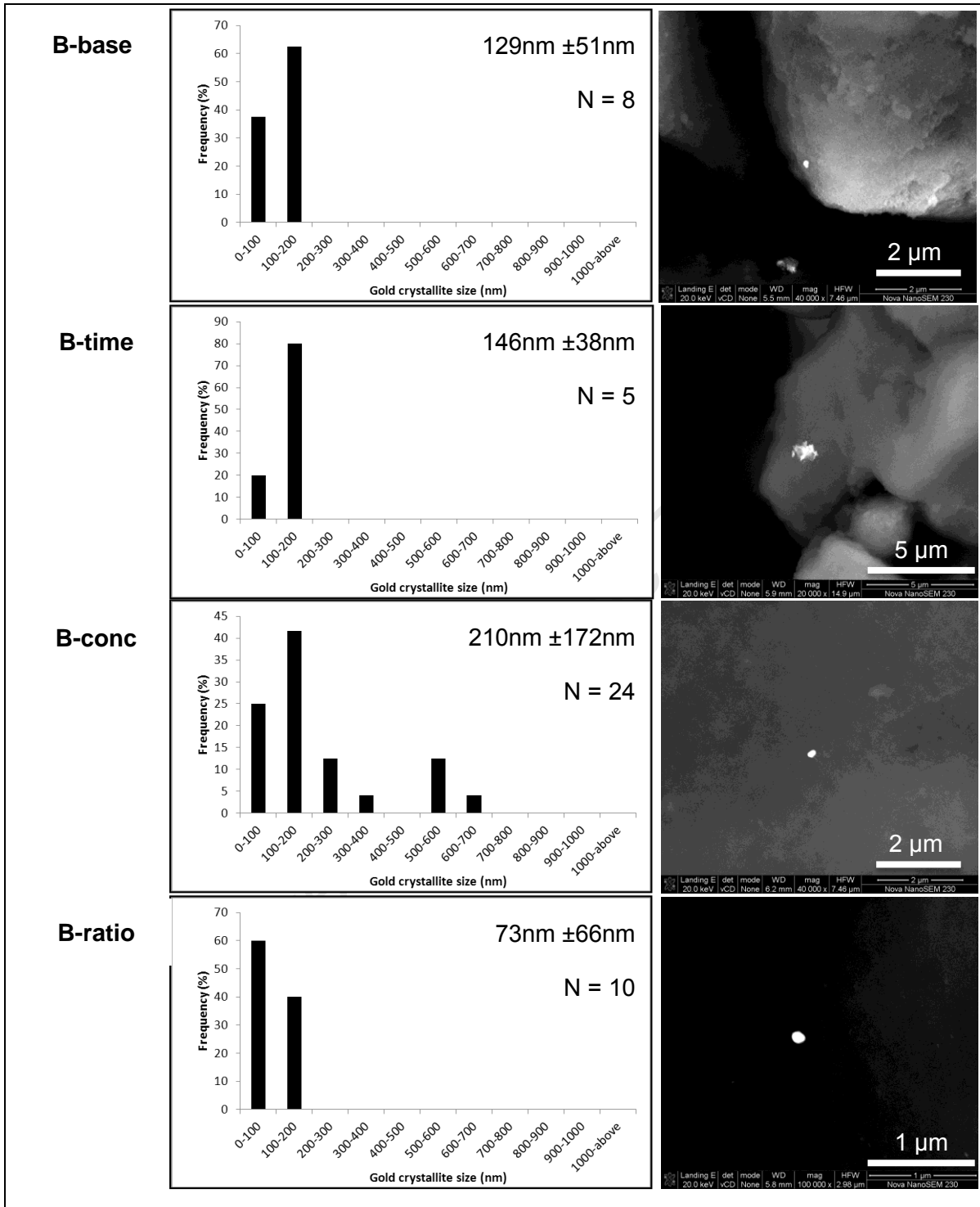


Figure 3-10: Gold crystallite size ‘distributions’ of Batch B obtained from SEM analysis

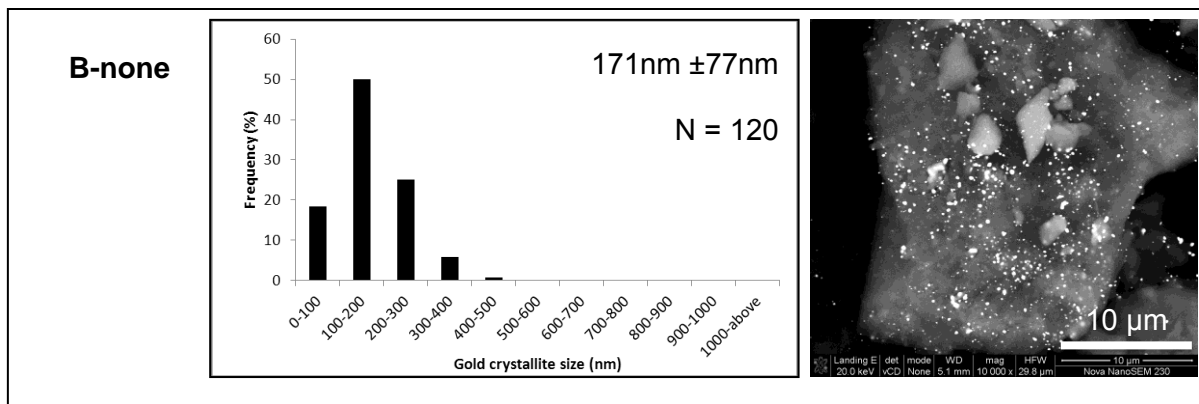


Figure 3-10 (cont.): Gold crystallite size 'distributions' of Batch B obtained from SEM analysis

3.2.3.3 *Batch C – effect of drying procedure*

Catalysts dried in wet hydrogen showed a significantly different image when examined under SEM compared to those dried in dry hydrogen. The catalyst C-dry displayed isolated individual gold particles. On the other hand, large gold particles were far more abundant on the C-wet catalyst. The two gold particles that were observed on the dry catalyst were quite large.

Catalysts dried in the rotary evaporator (C60/80/100) had unique SEM images. The occasional scattered large gold particles were visible (similar to batches A and B). Their frequency and agglomeration increased as the drying temperature increased. At the same time the mean gold particle size measured on these samples appears to decrease with increasing drying temperature. If we plot these sizes (see Figure 3-12), however, we can clearly see that the number of crystallites measured are far too few and statistically we cannot conclude that the drying temperature has an effect on the size of the gold particles. What was also observed is that these catalysts showed a unique "speckled" support background. These speckles are small (<20nm) and likely due to gold crystallites that are near the surface of the catalyst support. Unfortunately the resolution of the SEM is insufficient for these particles to be measured.

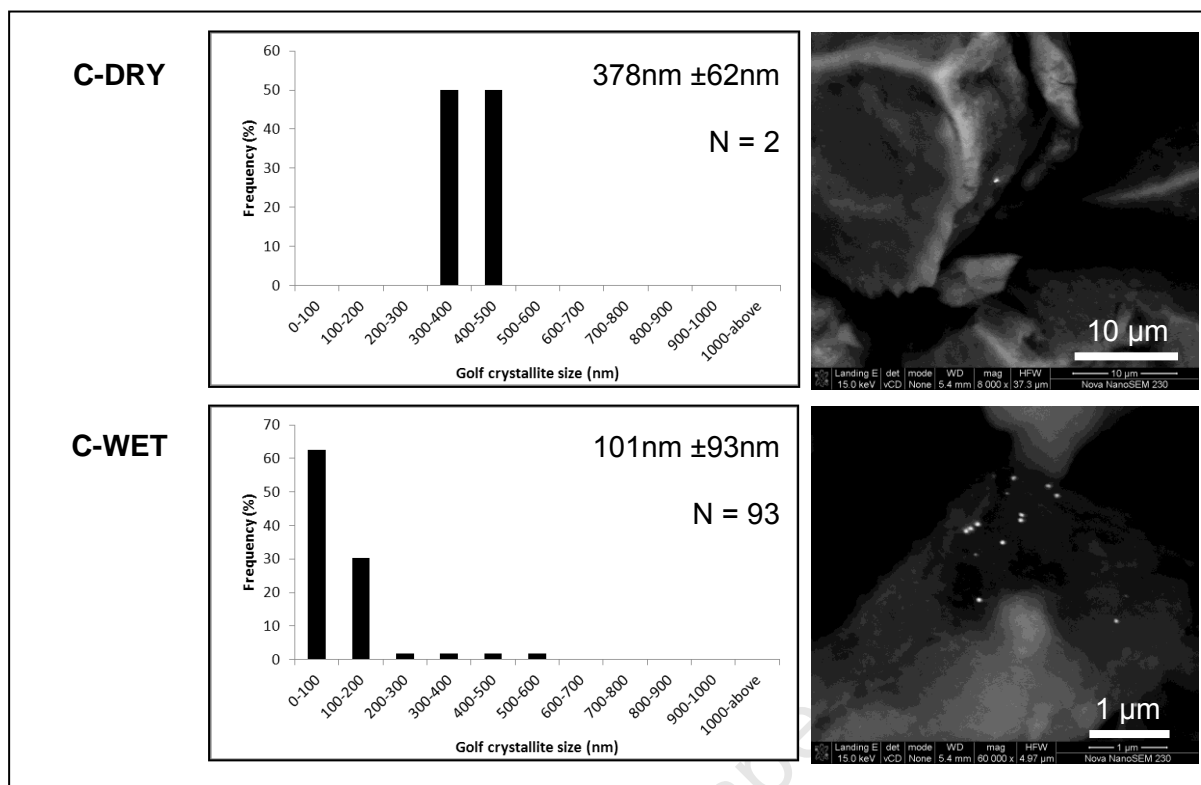


Figure 3-11: Gold crystallite size 'distributions' of Batch C obtained from SEM analysis

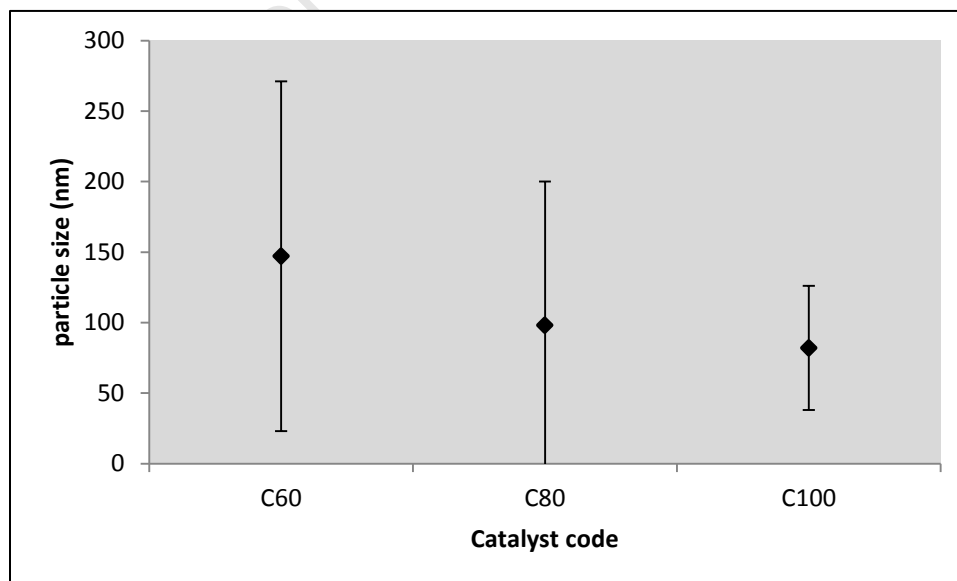


Figure 3-12: SEM average particle sizes for catalysts C60, C80 and C100

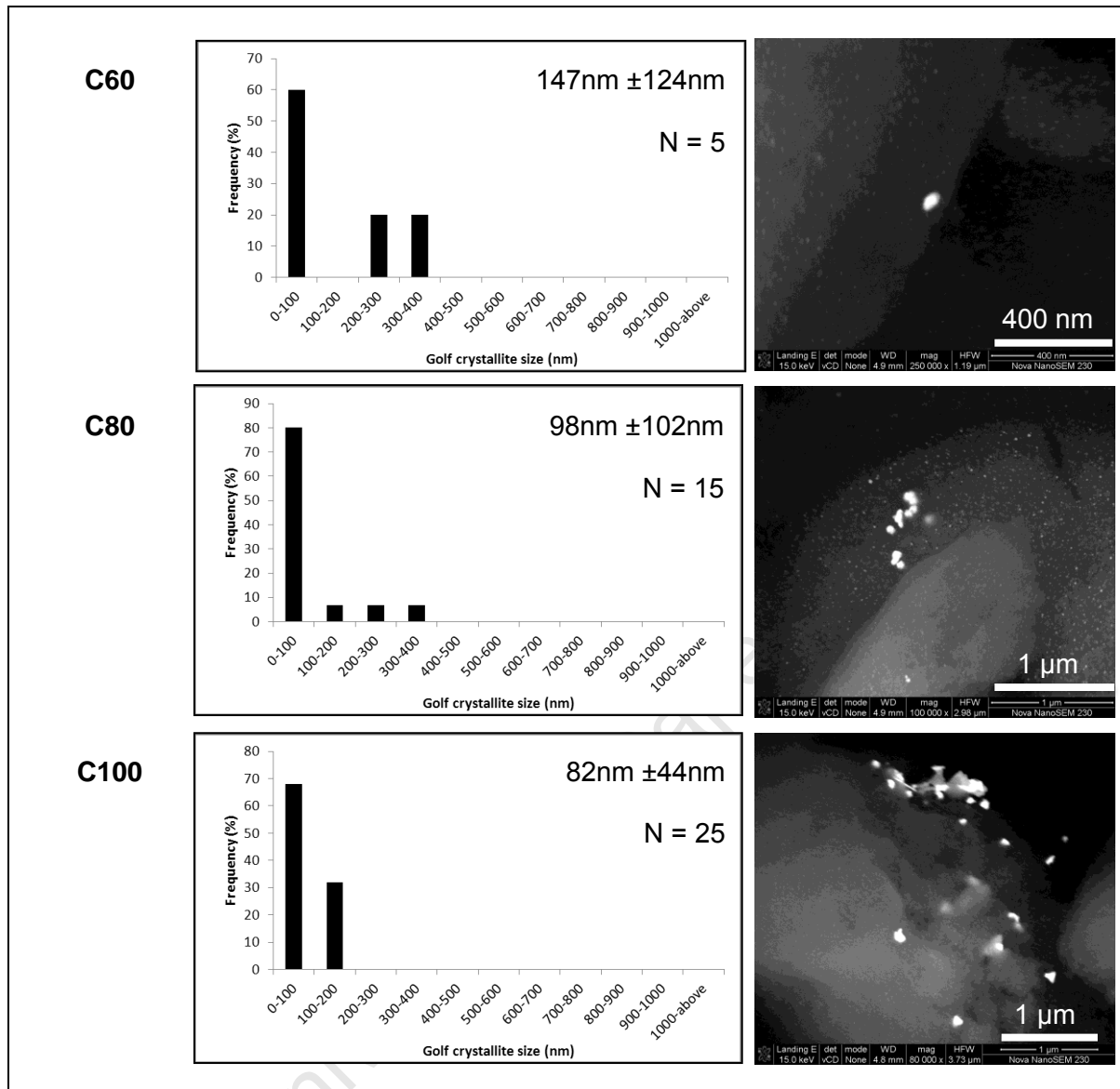


Figure 3-11 (cont.): Gold crystallite sizes of Batch C obtained from SEM analysis

3.2.3.4 Batch D – effect of calcination temperature

The SEM images obtained in samples from Batch D displayed numerous individual particles, with a number of agglomerated particles. There was no clear trend of agglomeration in these samples. It appears that the average gold particle size measured on the SEM images decreases significantly with size (with the exception of catalyst D400) as calcination temperature increases.

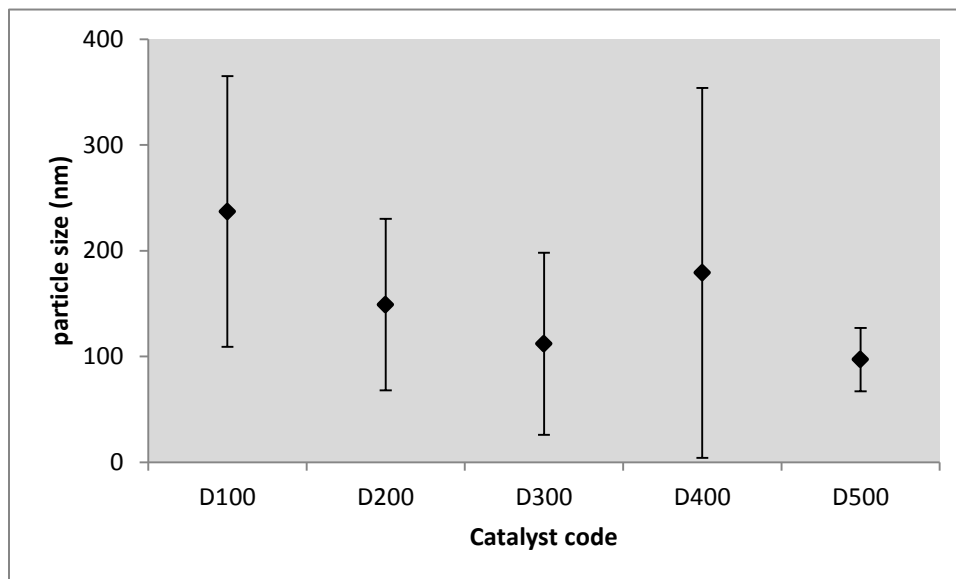


Figure 3-13: SEM average particle sizes for catalysts of Batch D

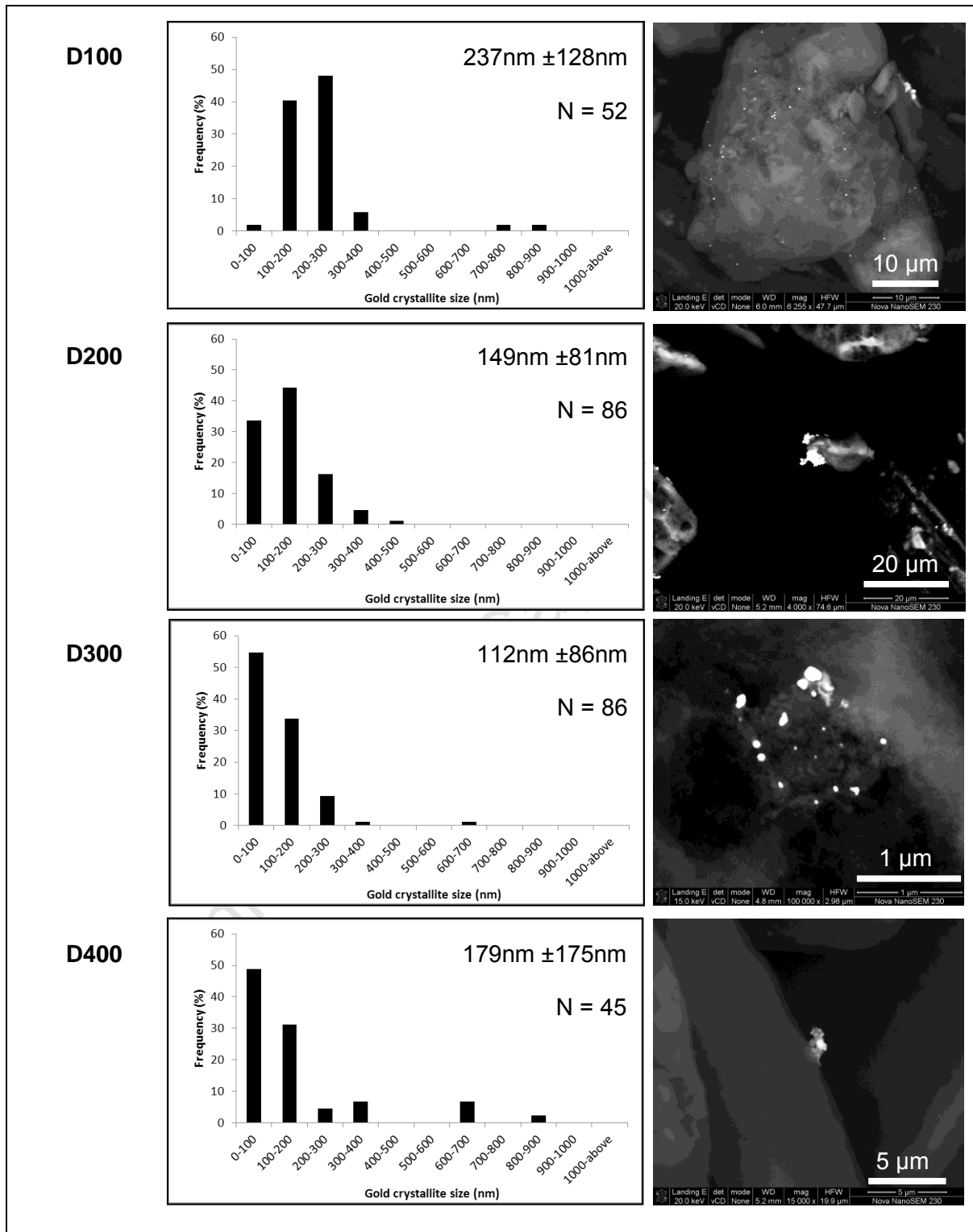


Figure 3-14: Gold crystallite size ‘distributions’ of Batch D obtained from SEM analysis

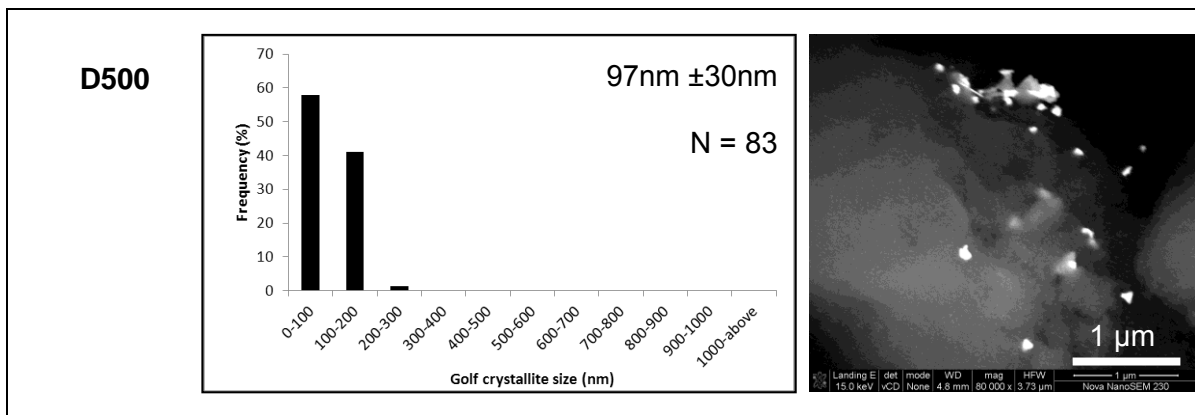


Figure 3-14 (cont.): Gold crystallite sizes of Batch D obtained from SEM analysis

3.3 Chemisorption

The adsorption behaviour of oxygen was investigated on most catalysts. These catalysts were pretreated in hydrogen at 200°C for 16 hours to remove all oxygen as is elaborated on in the experimental section on page 25. At low pressures blank alumina has been shown to not adsorb oxygen (Case, 2009) as well as in this study and is shown as a reference on all figures in this section. No oxygen uptake was detected below 10mmHg.

Oxygen chemisorption on supported gold catalysts shows an initial strong uptake at the lower pressures. This is followed by a slower uptake of oxygen at the higher pressures. The initial uptake is credited to the gold crystallites as it is not a feature in the oxygen chemisorption conducted on γ -alumina. The slower oxygen uptake at increased pressure might be attributed to the alumina support. Comparison of the blank alumina reference isotherm to any catalyst samples isotherm illustrates this point.

In Batch A the Au concentration in the supernatant liquid used to prepare the catalyst is varied, as well as the conditions under which calcination takes place. The oxygen adsorption resulting from these catalysts is shown in Figure 3-15.

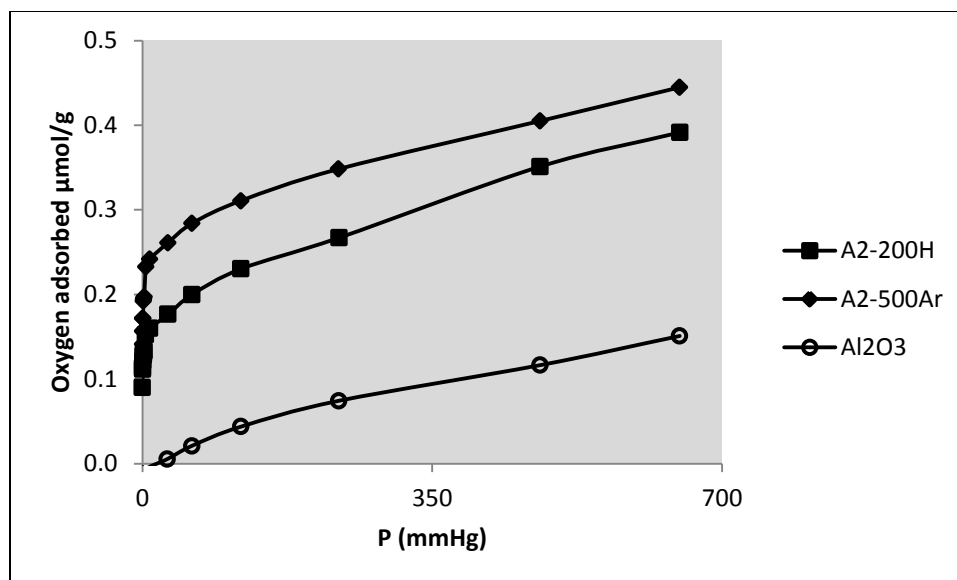


Figure 3-15: Oxygen chemisorption isotherms on catalysts of Batch A at 200°C

Various washing procedures were investigated in Batch B and the oxygen chemisorption results are shown in Figure 3-16. The catalyst using the standard wash is represented as B-base. Varying the washing procedure resulted in large differences in the O₂-uptake as a function of pressure. Reducing the ammonia concentration in the wash is the only change that increases the strong oxygen adsorption. Reducing the duration of the wash or the volume of ammonia with which the catalyst is washed, almost halves the amount of oxygen adsorbed, while eliminating the wash entirely reduces the adsorption significantly.

The drying procedure has a less significant effect on oxygen adsorption as is illustrated in Figure 3-17. The catalyst dried in moist air has a lower oxygen uptake than those dried in dry air. Catalysts dried in the rotary evaporator at 60 and 80°C are nearly identical, while the catalyst dried at 100°C shows a very low adsorption at low pressures, which then increases rapidly.

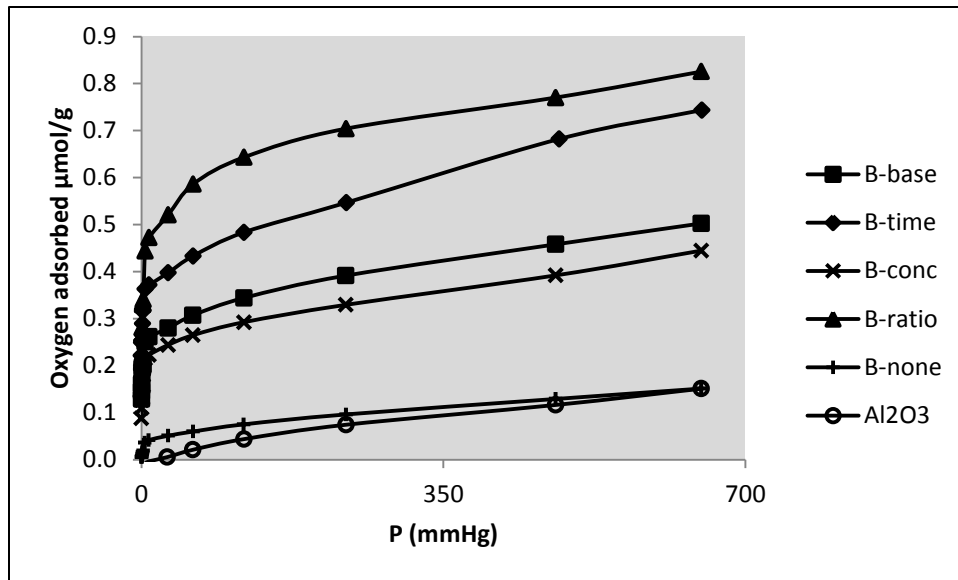


Figure 3-16: Oxygen chemisorption isotherms on catalysts of Batch B at 200°C

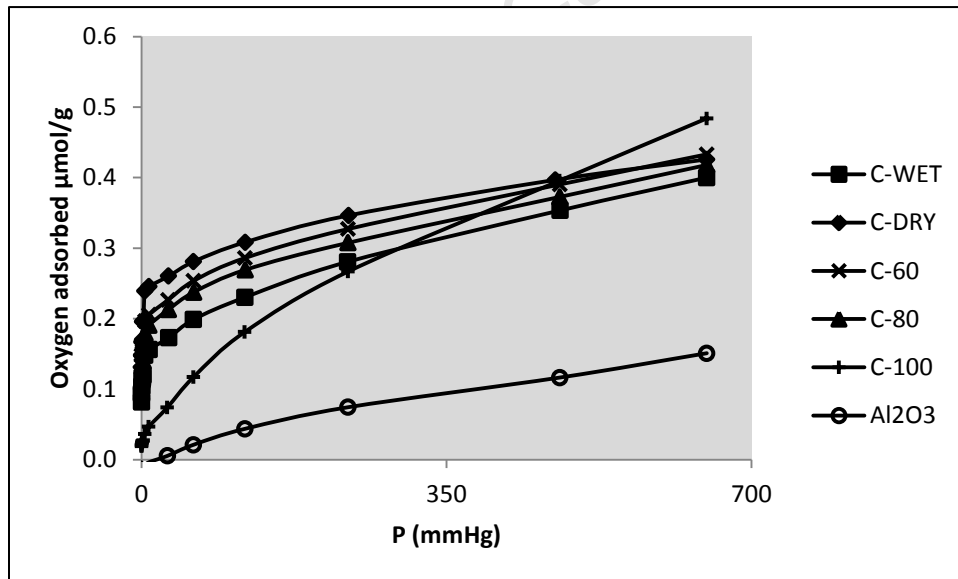


Figure 3-17: Oxygen chemisorption isotherms on catalysts of Batch C at 200°C

The variation in calcination temperature was investigated with batch D. The catalyst calcined at 100°C resulted in the lowest oxygen uptake (see Figure 3-18). The catalyst calcined at 200°C showed the highest uptake of oxygen with the remaining catalysts being grouped quite closely to each other.

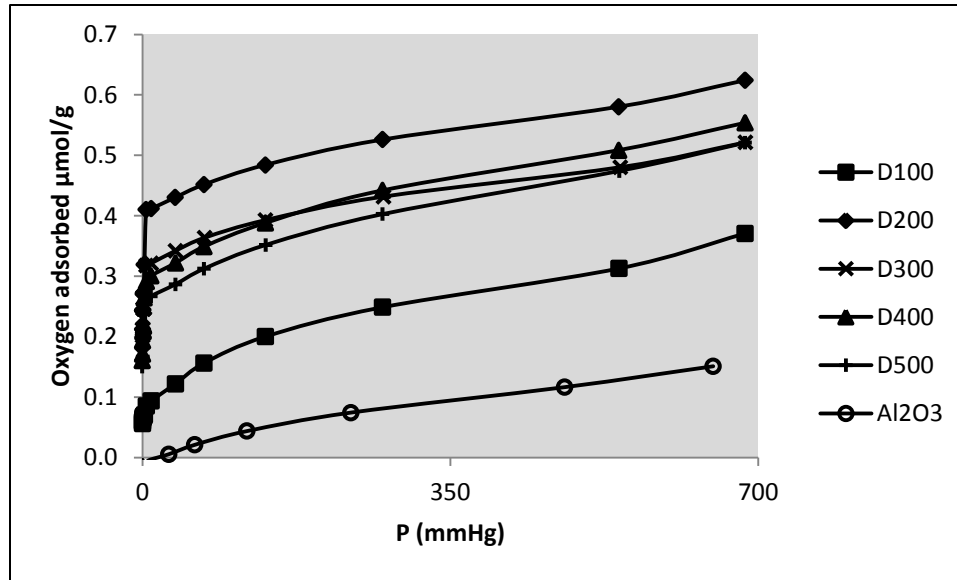


Figure 3-18: Oxygen chemisorption isotherms on catalysts of Batch D at 200°C

It has been shown that oxygen chemisorption data for Au/Al₂O₃ catalysts can be modelled using a dual isotherm (Case, 2009).

$$V_{O_2-adsorbed} = V_{m1} \cdot \frac{K_1 \cdot p_{O_2}}{1 + K_1 \cdot p_{O_2}} + V_{m2} \cdot \frac{K_2 \cdot p_{O_2}}{1 + K_2 \cdot p_{O_2}} \quad (3-1)$$

Where

V_{m1} and V_{m2} are the monolayer volumes in $\mu\text{mol/g}$

K_1 and K_2 are adsorption constants

p_{O_2} is the partial pressure of oxygen in mmHg

The model results of Batch B are displayed in Figure 3-19 and Figure 3-20 below as an example. Figure 3-20 shows the results on a log plot to show the differences at low pressure more clearly.

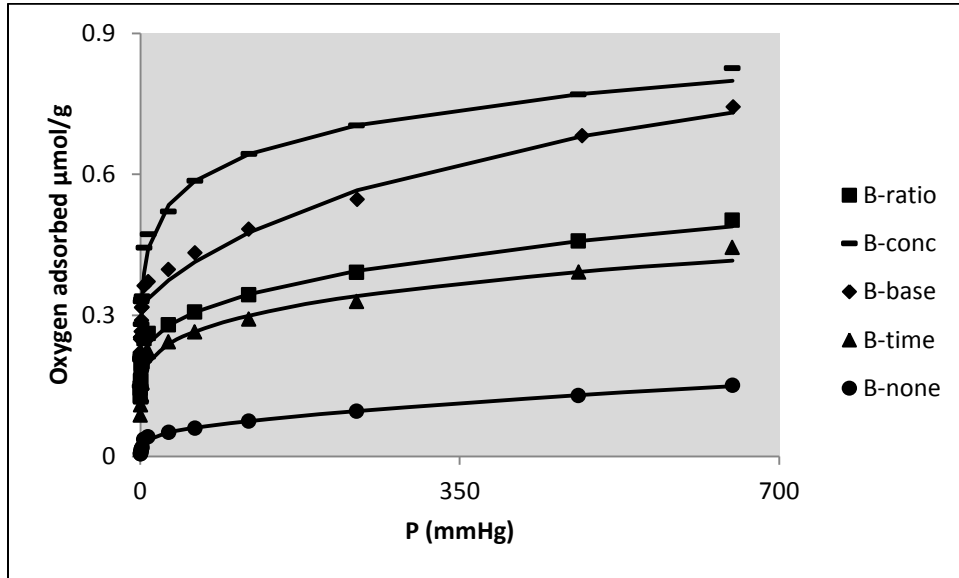


Figure 3-19: Modelled and actual O₂ chemisorption data of gold on alumina support

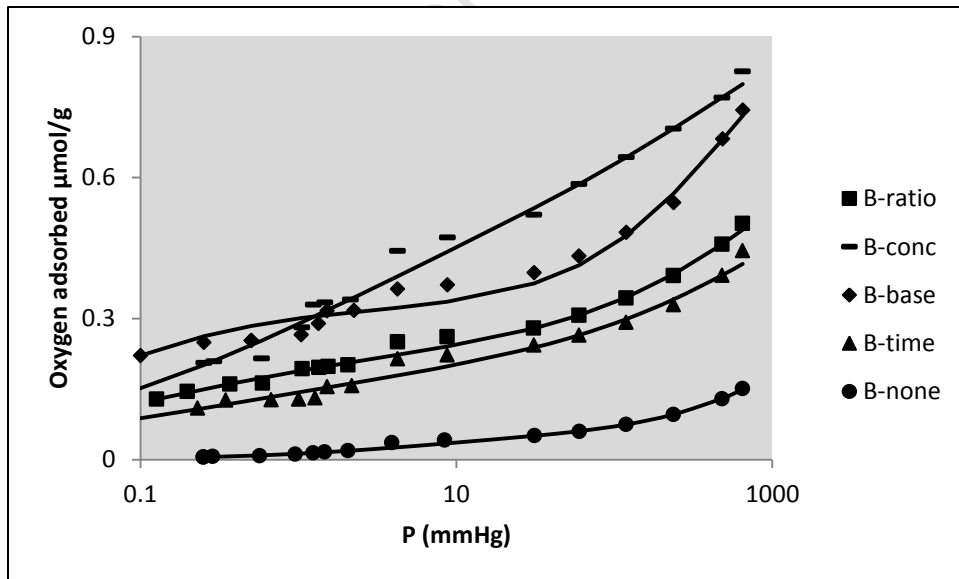


Figure 3-20: Modelled and actual O₂ chemisorption data of gold on alumina support presented on a log scale

The parameters that were found when fitting Equation 1 to the isotherms are given for all catalysts in Table 3-2. The goodness of fit is shown to be generally very good with R^2 never being below 0.92.

With the parameters found from oxygen chemisorption, dispersion and catalyst diameter can be calculated as shown in the equation below. While some of the calculations in the paper by Berndt *et al.* (2003) has been shown to be questionable (see section 1.4.3.3), they have confirmed that the Au:O ratio of 2 gives reasonable agreement to results obtained from TEM as was deduced in previous literature (Fukushima *et al.*, 1979).

$$D_{Au} = 1000 \cdot V_{m1} \cdot \frac{2 \text{ mmol Au}}{\text{mmol O}_2} \cdot \frac{100 \text{ mg cat.}}{\text{Au loading (mass \%)}} \cdot MM(\text{Au}) \quad (3-2)$$

Where V_{m1} is the monolayer volume in $\mu\text{mol/g}$

MM is the molar mass of Au in mg/mmol

Making the assumption that the gold particles are spherical, the diameter can be calculated as follows:

$$d_{Au} = \frac{6 \cdot n \cdot MM(\text{Au})}{D \cdot N_A \cdot \rho} \quad (3-3)$$

Where n is given as 1.15×10^{19} atoms/ m^2 (Berndt *et al.*, 2003)

$\rho = 1.93 \times 10^7$ g/ m^3 for Au

MM is the molar mass of Au in g/mol

N_A is Avogadro's constant (atoms/mol)

The resulting average particle sizes are also given in Table 3-2.

Table 3-2: Parameters calculated for oxygen chemisorption models and particle size calculated from V_{m1} and V_{m2}

Catalyst	V_{m1} ($\mu\text{mol/g}$)	V_{m2} ($\mu\text{mol/g}$)	K_1	$K_2 \times 10^3$	R^2 value	d_{Au} (nm) ^a
A1-200H						
A1-500H						
A2-200H	0.130	0.401	11	2.7	0.973	11.8
A2-200Ar						
A2-500H						
A2-500Ar	0.216	0.297	11	4.1	0.981	7.2
B-ratio	0.420	0.442	2.9	9.4	0.981	2.9
B-base	0.228	0.358	7.1	4.1	0.981	5.3
B-time	0.323	0.600	11	3.1	0.973	3.7
B-conc	0.190	0.327	4.4	4.0	0.961	6.3
B-none	0.051	0.335	0.4	0.7	0.998	30.5
C-Dry	0.207	0.259	9.9	6.1	0.962	6.5
C-Wet	0.134	0.411	9.0	2.6	0.987	13.2
C60	0.175	0.329	11	4.5	0.974	10.1
C80	0.160	0.331	7.9	4.3	0.973	11.1
C100	0.034	0.857	3.8	1.6	0.998	51.3
D100	0.077	0.417	11	2.9	0.992	20.9
D200	0.326	0.300	11	11	0.926	4.5
D300	0.278	0.280	11	5.7	0.966	4.7
D400	0.258	0.379	10	4.1	0.969	6.0
D500	0.222	0.389	11	3.8	0.968	5.9

^a Using equations (3-2) and (3-3)

3.4 Catalyst testing

The catalyst testing procedure has been described in detail in the experimental section (section 2.3). A summary of the important reaction variables is given in Table 3-3. Both the hydrogenation of CO and CO₂ were attempted. When conducting CO hydrogenation it was found that the conversion was very low. The major product was methane. Methanol formation was not detected. The hydrogenation of CO₂ on the other hand yielded significant methanol.

Table 3-3: Reaction parameters for testing supported gold catalysts in CO and CO₂ hydrogenation

<i>Variable</i>	<i>CO hydrogenation</i>	<i>CO₂ hydrogenation</i>
Temperature	200°C → 250°C → 300°C → 350°C	250°C → 300°C → 350°C → 250°C
Pressure	30 bar	30 bar
Mass of catalyst	1 g	1.2 g
Space velocity	3450 ml h ⁻¹ g ⁻¹	3450 ml h ⁻¹ g ⁻¹
CO/CO ₂ /H ₂	1/0/2	0/1/3

3.4.1 CO hydrogenation

CO hydrogenation was conducted using catalyst D400 and the resulting conversions are shown in Table 3-4. Conversion was too low to be detected on the TCD at low temperatures. As temperature was increased to 300°C a conversion of 1.9% was detected for the CO, however, the conversion of hydrogen was not detectable. At 350°C the usage ratio of synthesis gas with a molar inlet ratio of 2, i.e. the amount of H₂ consumed relative to the amount of CO consumed is 2.7, corresponding to methane as a major product in CO hydrogenation with this catalyst at 350°C.

FID analysis was used to identify the formation of any hydrocarbons. Throughout the different testing conditions only methane, ethane, ethene and methanol were ever encountered. For CO hydrogenation, methane and water proved to be the major products (see Table 3-5) with small amounts of ethane, ethene and methanol being detected. Yields of the hydrocarbons were calculated as a C-% using the product concentrations detected on the FID based on the carbon balance.

The methane yield in CO hydrogenation increases strongly with increasing reaction temperature, whereas the methanol yield passes a maximum. The selectivity for methanol decreases with increasing reaction temperature from approximately 9 C-% at 250°C to less than 1 C-% at 350°C.

Table 3-4: Conversion in the CO hydrogenation reaction over a range of temperatures

<i>Catalyst</i>	<i>Conversion (%)</i>			
	200°C	250°C	300°C	350°C
D400 – CO conversion	0.0	0.0	1.9	9.2
– H ₂ conversion	0.0	0.0	0.0	12.3

Table 3-5: Product yield as a function of temperature over Au/Al₂O₃ catalyst D400 in CO hydrogenation

<i>D400</i>	<i>yield (C-%) and [selectivity (C-%)]</i>			
	200°C	250°C	300°C	350°C
Methane	0.2 [86]	0.7 [86]	3.5 [96]	12.0 [97.3]
Ethane	0.06 [14]	0.04 [2.9]	0.06 [0.8]	0.5 [2]
Ethene	0.0 [0]	0.02 [1.6]	0.03 [0.4]	0.02 [0.1]
Methanol	0.0 [0]	0.07 [9.5]	0.1 [2.8]	0.08 [0.6]

3.4.2 CO₂ hydrogenation

Due to difficulties with the online TCD during the CO₂ hydrogenation runs no measured conversion data can be presented. In particular the noise level for the smaller CO₂ peak was a problem.

The products formed during CO₂ hydrogenation were quite different to those formed during CO hydrogenation. Table 3-6 shows the product yields obtained on catalyst D400. The water gas shift reaction takes place and forms CO as a product. Methanol yields are still low; however, they are improved from CO hydrogenation reaction. The yields of the water gas shift products as well as methane increase with temperature, however, the methanol yield decreases over the same range.

Furthermore, the methanol selectivity at 200°C is still less than 9 C-% dropping to approximately 0.6 C-% at 350°C, although the methanol content in the fraction of organic product compounds is significantly higher.

The catalyst deactivation of D400 seems to affect the methanol production more than the methane and carbon monoxide yield. Since the drop in the methanol yield is more severe than the drop in the yield of the two other product compounds.

Table 3-6: Product yield as a function of temperature over Au/Al₂O₃ catalyst D400 in CO₂ hydrogenation

<i>D400</i>	<i>yield (C-%) and [selectivity (C-%)]</i>			
	250°C	300°C	350°C	250°C
Methane	3.3 [20]	7.5 [24]	12.8 [26]	2.8 [24]
Methanol	1.4 [8.6]	0.7 [2.3]	0.3 [0.6]	0.7 [5.9]
Carbon monoxide	11.6 [71]	22.5 [73]	36.5 [74]	8.4 [71]

The CO₂ hydrogenation over catalyst C80 yielded different results. The methanol yield decreases with increasing temperature, however, a much higher yield is obtained than for catalyst D400. The yield of methane is also higher. At the same time the yield of carbon monoxide increases with temperature, however, the yields are much lower than for catalyst D400 at any temperature.

Table 3-7: Product yield as a function of temperature over Au/Al₂O₃ catalyst C80 in CO₂ hydrogenation

C80	<i>yield (C-%) and [selectivity (C-%)]</i>		
	250°C	300°C	350°C
Methane	12.8 [64]	17.4 [59]	9.3 [43]
Methanol	6.0 [30]	4.8 [16]	2.5 [12]
Ethanol	0.1 [0.6]	0.2 [0.8]	0.1 [0.3]
Ethanal	0.5 [2.4]	0.3 [0.9]	0.4 [2.1]
2-Propanone (Acetone)	0.3 [1.3]	0.2 [0.6]	0.2 [0.8]
Ethyl Acetate	0.3 [1.4]	0.2 [0.7]	0.3 [1.3]
Carbon monoxide	0.0 [0.0]	6.5 [22]	9.1 [41]

4 DISCUSSION

4.1 Catalyst Characterization results

4.1.1 Crystallite size analysis

Crystallite sizes were evaluated in numerous ways, primarily using TEM and oxygen chemisorption as well as HRTEM for some cases. SEM was used as an additional characterization for those particles above approximately 50nm.

While obtaining a reasonable level of agreement between chemisorption and TEM results for Au/SiO₂ and Au/MgO catalysts, Fukushima *et al.* (1979) obtained only an order of magnitude agreement on the Au/Al₂O₃ catalyst. More recent studies have reported similar results. It has been shown that crystallite sizes calculated from oxygen chemisorption and those measured on the TEM for Au/Al₂O₃ catalysts have a reasonable level of agreement for the majority of cases (Berndt *et al.*, 2003; Bergh and Van Heerden, 2009; Case, 2009).

In this study the comparison of the oxygen chemisorption and TEM crystallite sizes is visually represented in Figure 4-1. For most catalysts an order of magnitude agreement at least was obtained. Batch C, however, has quite a poor level of agreement.

There can be many factors that lead to these two measurements not always agreeing with each other. The particle size calculated from chemisorption is subject to some assumptions and numerous sources of error. In particular, assumptions around the way oxygen adsorbs onto gold nano particles, the accuracy of the fitted curve, and the accuracy of the loading measured should be noted. These could result in significant changes to the calculated value. The average crystallite size we obtain from TEM is not without fault either, and the presence of very small or large particles could easily go unnoticed as is evident from the images presented on the SEM.

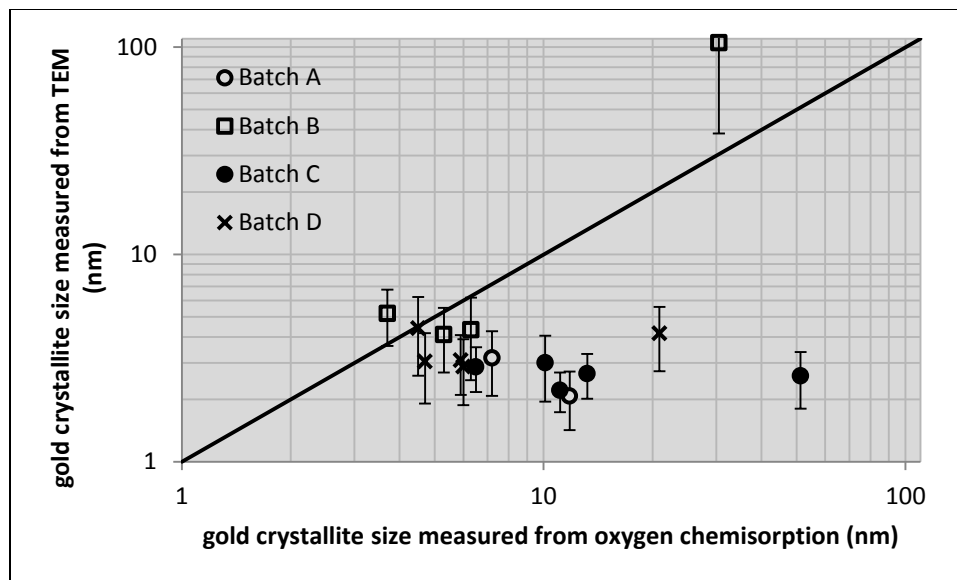


Figure 4-1: Comparison of gold crystallite sizes obtained from oxygen chemisorption using V_{m1} and TEM

Having conducted SEM analysis on most of the catalysts it is clear that there is a bimodal distribution in these catalysts. Using the average crystallite sizes obtained from TEM and SEM analysis as the average sizes of the two nodes their relative amounts can be calculated by making some assumptions. This has already been attempted by Berndt *et al.*, (2003). However, their assumption that large particles contribute in the same manner to the surface area measured by oxygen chemisorption led to an obviously incorrect solution to the simultaneous equations (the solution they presented did not satisfy both equations, and the actual solution to their set of equations yields a negative number of small particles). Following a similar method and assuming that only the smaller crystallites contribute to the chemisorption of oxygen these calculations are repeated for the current catalyst set.

Based on the results obtained by Berndt *et al.*, (2003) we want to calculate the relative amounts of small and large gold crystallites/particles on the supported gold catalysts. However, it is not possible to repeat their calculation and obtain the same results they reported. They calculate the total volume of gold present per gram of catalyst using the density of gold and the loading. It was then said that the total volume is made up of contributions by the small particles as well as the large particles. They used a similar approach to the surface area taking the contribution of

the small and large crystallites into account. The solution to these simultaneous equations, however, results in a negative number of particles (not the positive values they reported). The reason for this is likely due to the large particles not actually contributing to the volume of adsorbed oxygen as above a certain size, gold crystallites will begin to display bulk properties and oxygen would not adsorb.

If the calculations are repeated with the assumption that the large gold crystallites do not adsorb oxygen (and hence do not contribute to the total surface area calculated from oxygen chemisorption) but do contribute to the total volume of gold on the catalyst a more reasonable solution is found. Approximately 90% of the particles are approximately 2nm in size. However, in terms of the mass of gold, the large particles are dominant, taking up 99% of the mass of gold on the catalyst. The TEM results they obtained agree with this. Assuming that the total volume of gold consists of only those particles counted on the histogram they presented and calculate the surface area we would result in a surface area in excess of 100 times larger than that found from their oxygen chemisorption. This would suggest that there is indeed some volume of gold that is not contributing to the oxygen chemisorption.

The oxygen adsorbed in the chemisorption experiments can be used to calculate the surface area of the gold crystallites.

$$S_{Au} = \frac{4 \times O_{2Ads} \times N_L}{1.15 \times 10^{19} Au^S \times m^{-2}} \quad (4-1)$$

Where S_{Au} is the gold surface area in m^2/g

O_{2Ads} is the oxygen adsorbed in $\mu mol O_2/g$

N_L is 6×10^{17} atoms/ μmol

The surface area can also be described by the following equation (large particles are omitted from this equation as it is assumed that they do not contribute to the measured oxygen adsorption):

$$S_{Au} = n_{small} \pi d_{small}^2 \quad (4-2)$$

Where S_{Au} is the gold surface area in m^2/g

n_{small} is the number of small (sized from TEM) gold crystallites in particles/gram

d_{small} is the average diameter of the small particles in m

The volume of gold can be calculated in two ways, in this case the bi-modal distribution plays a role as the volume takes both the large and small particles into consideration.

$$V_{Au} = \frac{m_{Au}}{\rho_{Au}} \quad (4-3)$$

$$V_{Au} = \frac{1}{6} n_{small} \pi d_{small}^3 + \frac{1}{6} n_{large} \pi d_{large}^3 \quad (4-4)$$

Where V_{Au} is the volume of gold in m^3/g

m_{Au} is the mass loading of gold on the catalyst in g_{Au}/g

ρ_{Au} is the density of gold (19.3 g/cm^3)

The number fraction of small particles (x_{small}) is given by:

$$x_{small} = \frac{n_{small}}{n_{small} + n_{large}} \times 100\% \quad (4-5)$$

And the volume fraction of small particles (v_{small}) is given by:

$$v_{small} = \frac{\frac{1}{6} n_{small} \cdot \pi \cdot d_{small}^3}{V_{Au}} \times 100\% \quad (4-6)$$

Calculating n_{small} and n_{large} using these simultaneous equations leads to some interesting results. The calculated values for various catalysts are presented in Table 4-1. Although the small crystallites outnumber the large ones almost 100:1 on most catalysts, the nature of the large crystallites is such that they still account for the majority of the gold present on the catalysts.

Table 4-1: Bi-modal distribution

Catalyst	n_{small} particles / g	n_{large} particles / g	Small particles by no (%)	Small particles by volume (%)
A1-200H ^a				
A1-500H ^a				
A2-200H	4.78E+16	2.65E+13	99.94	0.18
A2-200Ar ^a				
A2-500H ^a				
A2-500Ar	2.02E+16	2.92E+14	98.57	0.59
B-ratio ^a				
B-base	2.13E+16	8.36E+13	99.61	0.82
B-time	1.90E+16	5.73E+13	99.70	1.46
B-conc	1.60E+16	1.94E+13	99.88	0.72
B-none	7.31E+12	4.54E+13	13.87**	3.59 ^b
C-Dry	3.96E+16	3.72E+12	99.99	0.46
C-Wet	2.99E+16	2.58E+14	99.14	0.21
C60	3.07E+16	5.04E+13	99.84	0.31
C80	5.16E+16	2.86E+14	99.45	0.21
C100	7.99E+15	4.77E+14	94.36	0.05
D100	7.01E+15	1.82E+13	99.74	0.21
D200	2.64E+16	6.56E+13	99.75	1.03
D300	4.74E+16	1.39E+14	99.71	0.68
D400	4.90E+16	4.08E+13	99.92	0.50
D500	3.67E+16	2.16E+14	99.41	0.55

^achemisorption was not conducted on these catalysts

^bsmall particles in this context are defined as those observed on TEM images. For catalyst B-none these are greater than 100nm in size.

Case (2009) concluded from a plot of gold loading against monolayer volume that the loading of gold within the investigated range is not a determinant for crystallite size. A similar plot with no more of a trend results from this study (Figure 4-2) and it is evident that the loading does not determine the crystallite / particle size determined from TEM / SEM (see Figure 4-4).

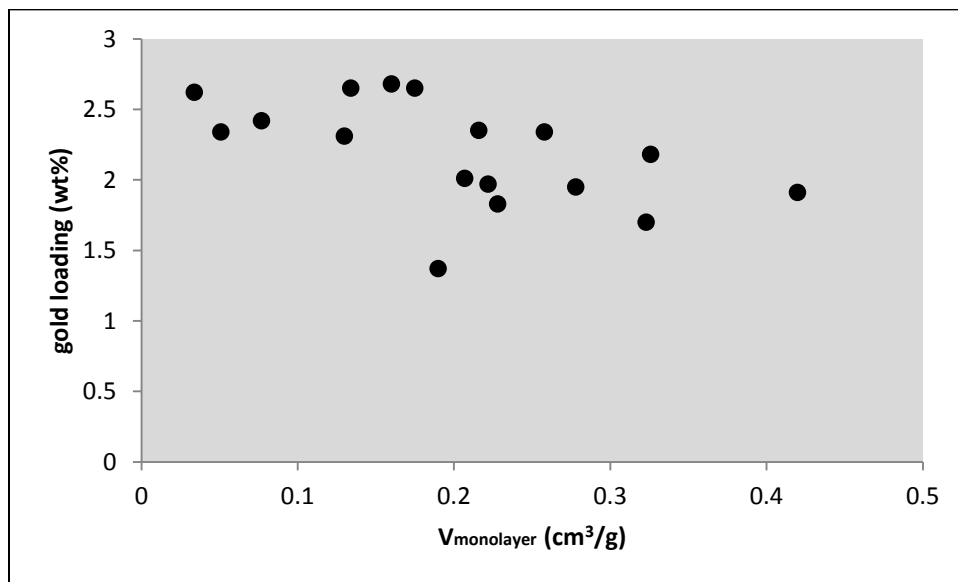


Figure 4-2: Monolayer volume plotted against gold loading

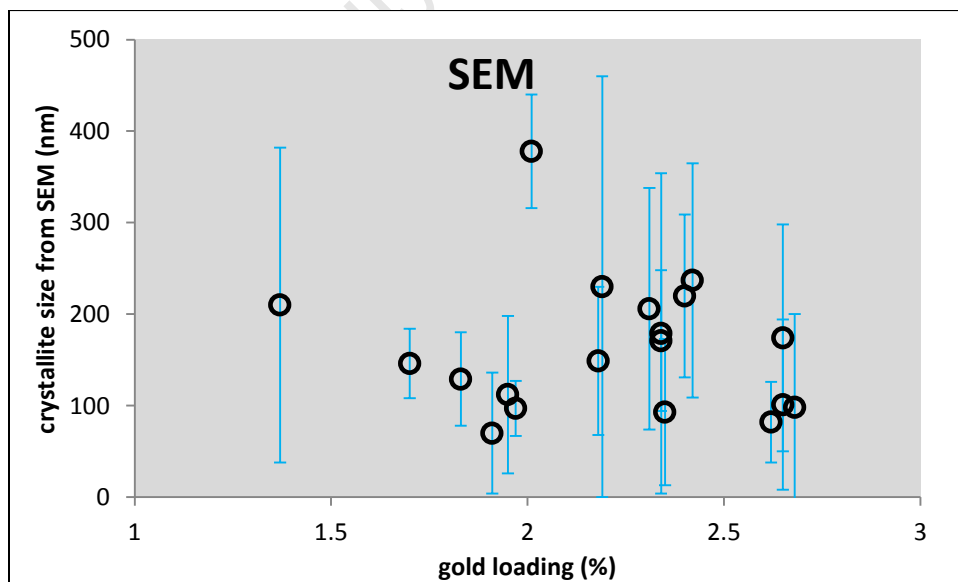


Figure 4-3: Gold loading vs crystallite sizes from SEM

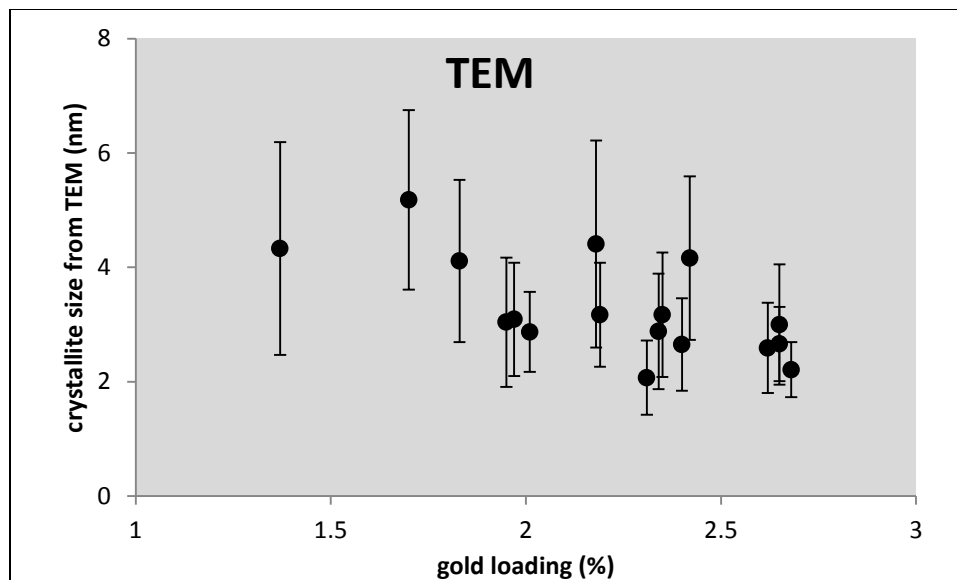


Figure 4-4: Gold loading vs crystallite sizes from TEM

An interesting thing to look at is how the loading influences the amount of small crystallites present on the catalyst (see Figure 4-5). There is a more or less downward trend evident on the graph. An increase in loading corresponds to a decrease in the volume of small gold crystallites. This is likely due to sintering and agglomeration when more gold is present on the catalyst. Catalyst B-none is omitted from this figure as the 'small' crystallites measured on the TEM were of a size greater than 100nm.

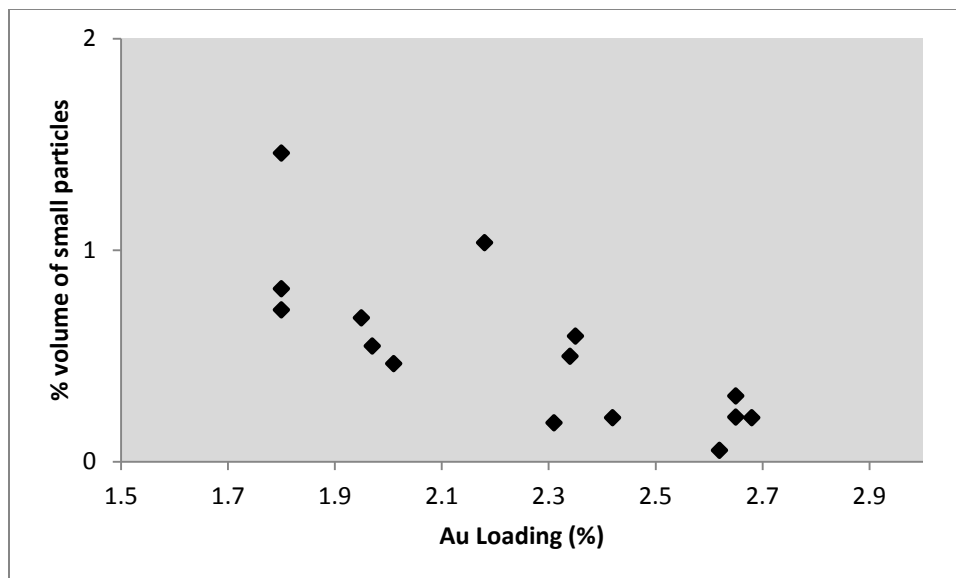


Figure 4-5: Effect of Au loading on volume % of small particles

4.1.2 Effect of precursor concentration and calcination gas

The influence of pre-cursor concentration on the various catalyst characteristics was investigated with catalysts in Batch A. Catalysts were prepared with concentrations of double and 50 times that of the 'standard' method. No effect on the loading of gold with variation in the concentration of gold in the precursor solution between 0.5 and 25 g/L was observed (see Figure 4-6).

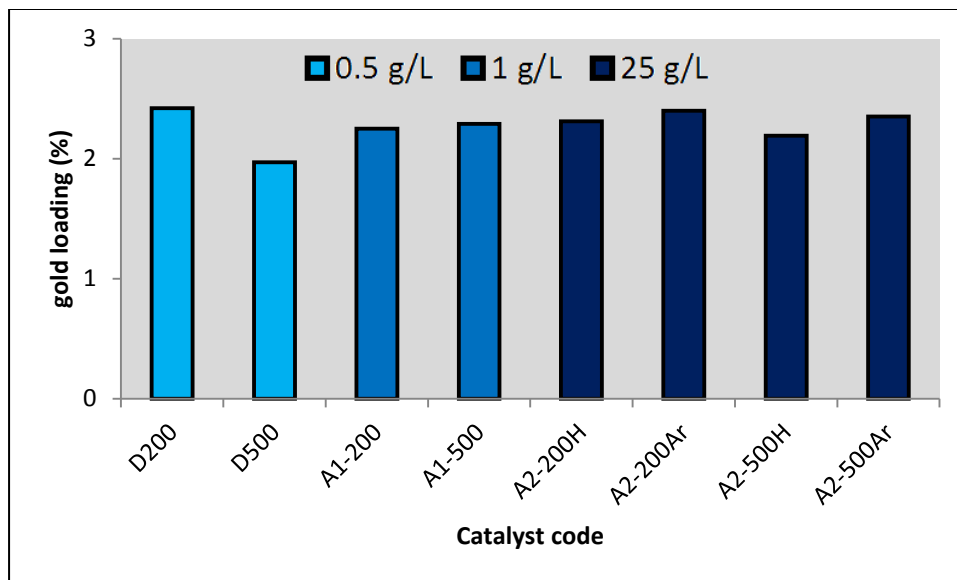


Figure 4-6: Effect of gold precursor concentration, keeping Au : support ratio constant, on loading

Crystallite size, however, does appear to have been affected to a certain extent by the concentration of the precursor. The catalysts that were calcined at the lower temperature in hydrogen (200°C) showed an initial decrease in crystallite size with increasing gold concentration in the precursor solution. The catalyst calcined in argon shows an increased particle size compared to that of its hydrogen equivalent (see Figure 4-7). The same cannot be seen with the catalysts calcined at higher temperature. At a calcination temperature of 500°C the crystallite size is not significantly affected by the gold concentration in the precursor solution or the choice between argon and hydrogen as a calcination gas. This is shown in Figure 4-8.

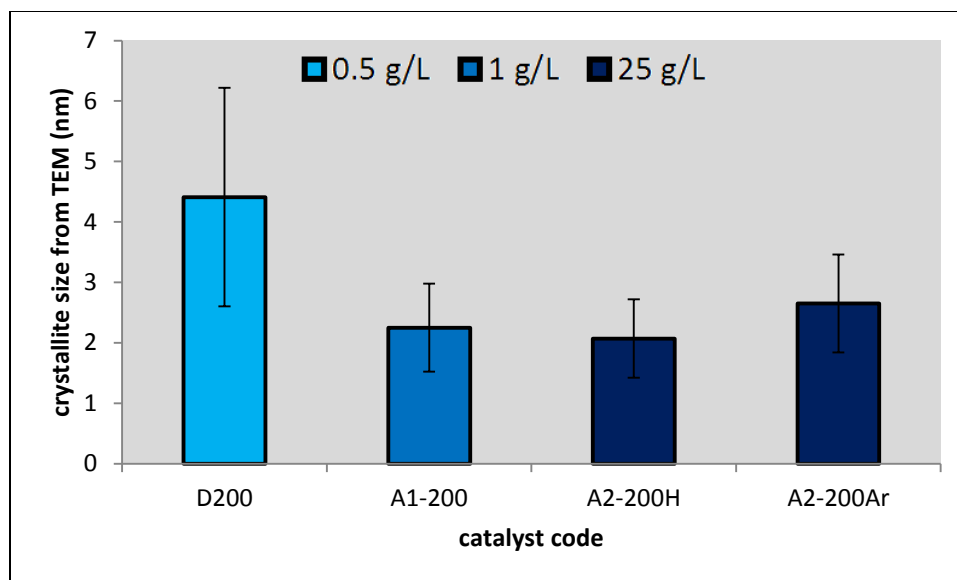


Figure 4-7: Effect of gold precursor concentration, keeping Au : support ratio constant, on crystallite size of catalysts calcined at 200°C

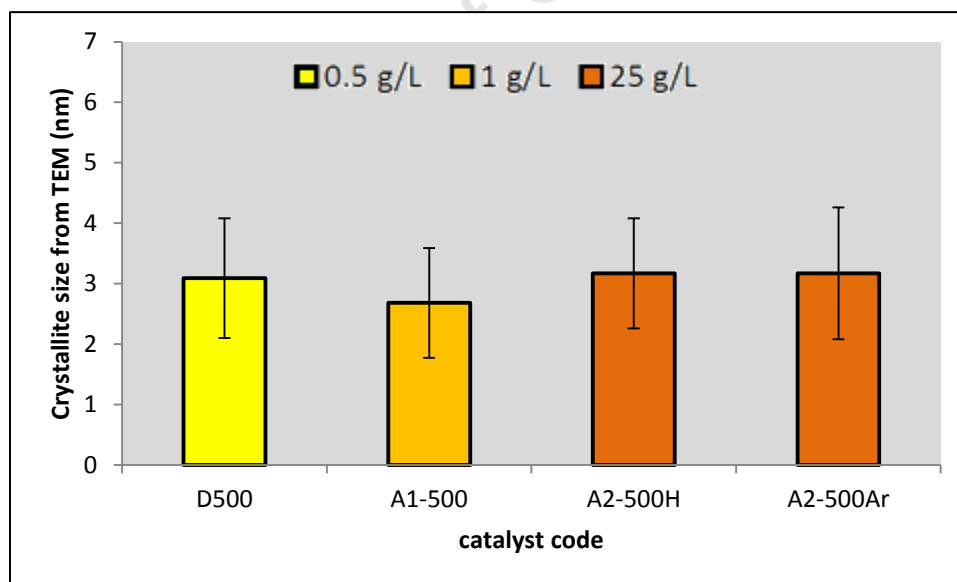


Figure 4-8: Effect of gold precursor concentration, keeping Au : support ratio constant, on crystallite size of catalysts calcined at 500°C

4.1.3 Effect of washing procedure

The washing step is crucial in removing any unattached gold in order to prevent sintering at a later stage in the preparation procedure. It is also likely that the washing procedure could affect the final gold loading onto the catalyst. Figure 4-9 illustrates that the omission of the ammonia wash will result in a higher loading, most likely due to the ammonia wash not only removing the chloride, but also some of the more weakly attached gold. In the work reported by Case (2009) it was shown that up to 6.8% (of the gold present in the initial solution) is lost from the catalyst during the ammonia wash step. The catalyst washed in the lower concentration ammonia showed a noticeable drop in loading. It is unclear what might have caused this.

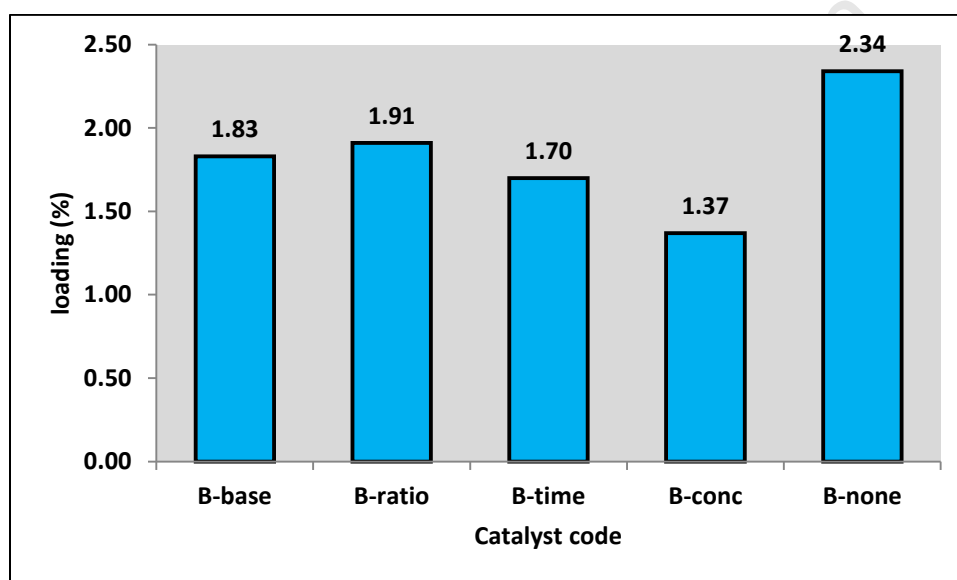


Figure 4-9: Effect of washing procedure on obtained gold loading

Other than the effect on loading demonstrated above, the washing procedure has been shown to be vitally important in the formation of small crystallites when using ion-exchange to prepare supported gold catalysts (Ivanova *et al.*, 2005). Both the TEM and chemisorption results of catalysts in Batch B show that the crystallite size is affected by the ammonia wash, most significantly by its omission. The crystallite size distribution is essentially unaffected by changes to the washing time, concentration or the solid/liquid ratio in the wash. The results from TEM and chemisorption are shown again in Figure 4-10.

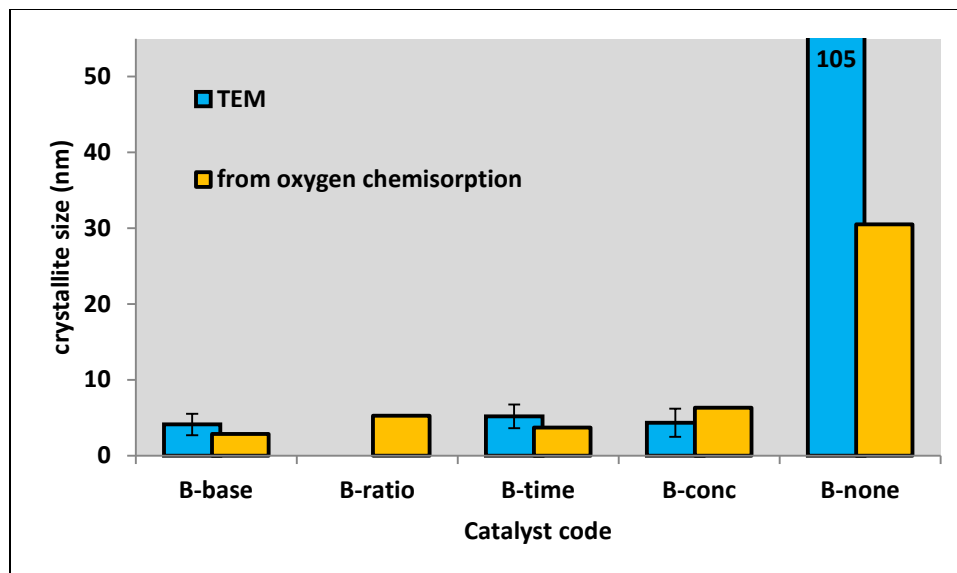


Figure 4-10: Effect of washing procedure on crystallite size

It might appear that the washing procedure affects the size of the large crystallites (see Figure 4-11); however, the number of particles isn't sufficient in most cases to consider the average as representative of the sample. Nonetheless it is interesting to notice that the number of particles observed is similar for catalysts in batch B with the catalysts washed for a shorter time having slightly more and the catalyst where the wash was omitted having a significant presence of large particles.

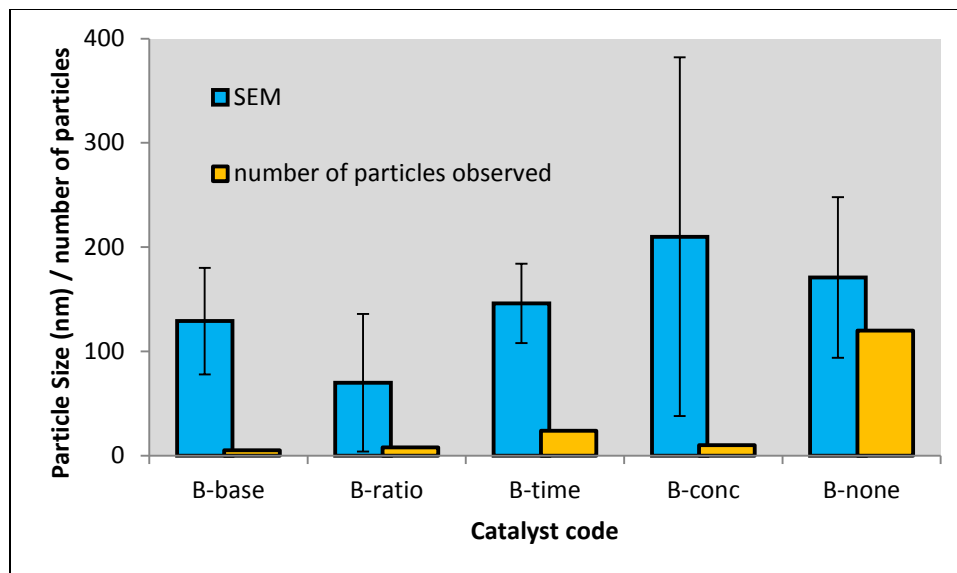


Figure 4-11: Effect of washing procedure on size and frequency of large gold crystallites

4.1.4 Effect of drying procedure

The importance of the drying procedure on the catalyst profile has been shown in particular for catalysts produced using impregnation (Lekhal *et al.*, 2001).

No effect on loading was observed, as is expected. As is shown in Figure 4-12 below, there is no clear effect from the drying procedure on the average gold crystallite size observed on TEM other than a decrease in the average crystallite size from the static drying technique used in batch D.

However, using the oxygen chemisorption results, drying of the catalyst in wet air rather than dry air results in a noticeable increase in the average crystallite size. Drying in the rotary evaporator at elevated temperatures (100°C) led to a drastic increase in the calculated average gold crystallite size.

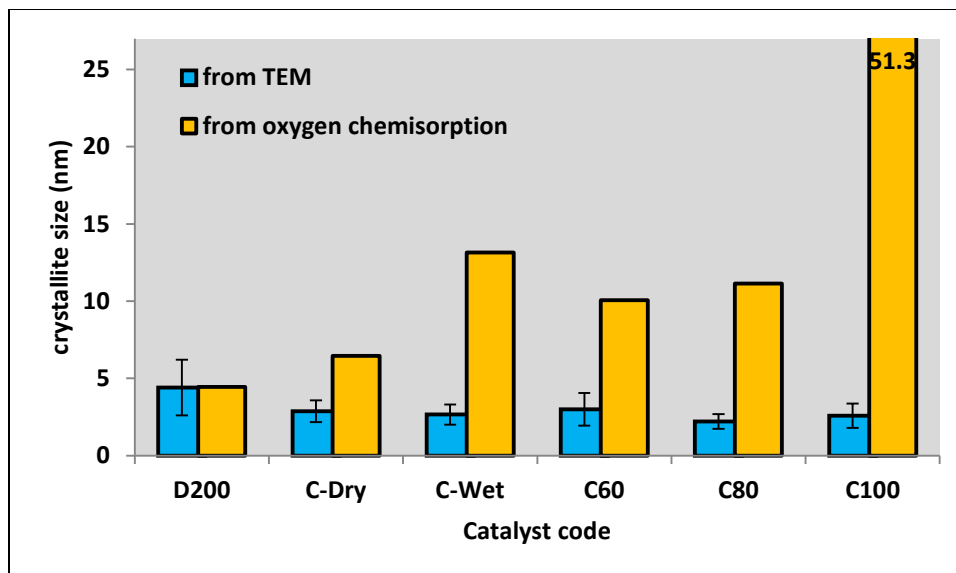


Figure 4-12: Effect of drying procedure on crystallite size

SEM images also show significant differences when investigating this batch of catalysts. While not much meaning from the average crystallite sizes measured from the SEM images can be obtained (these are displayed in Figure 4-13), it is interesting to note that the use of non-static drying techniques led to much less large crystallites being observed. Additionally, the presence of additional moisture during drying drastically increases the number of large crystallites that are observed, while increasing the drying temperature from 60-80-100°C leads to a gradual increase in the number of large particles observed.

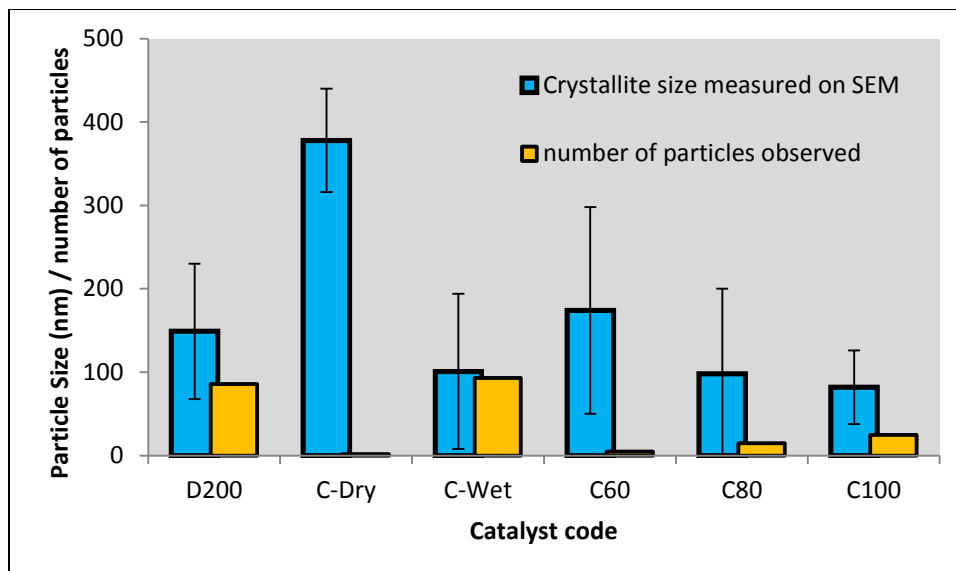


Figure 4-13: effect of drying procedure on size and frequency of large gold crystallites

Another observation from the SEM images was that the three catalysts dried in the rotary evaporator had unique features on their images. It appeared that the surface of the support was covered in small well distributed gold crystallites. Due to resolution limitations of the SEM these crystallites could not be measured with any kind of accuracy, however, their size could be estimated to be in the range of 10-20nm, a size that corresponds with the oxygen chemisorption analysis. Some example SEM images are given in Figure 4-14.

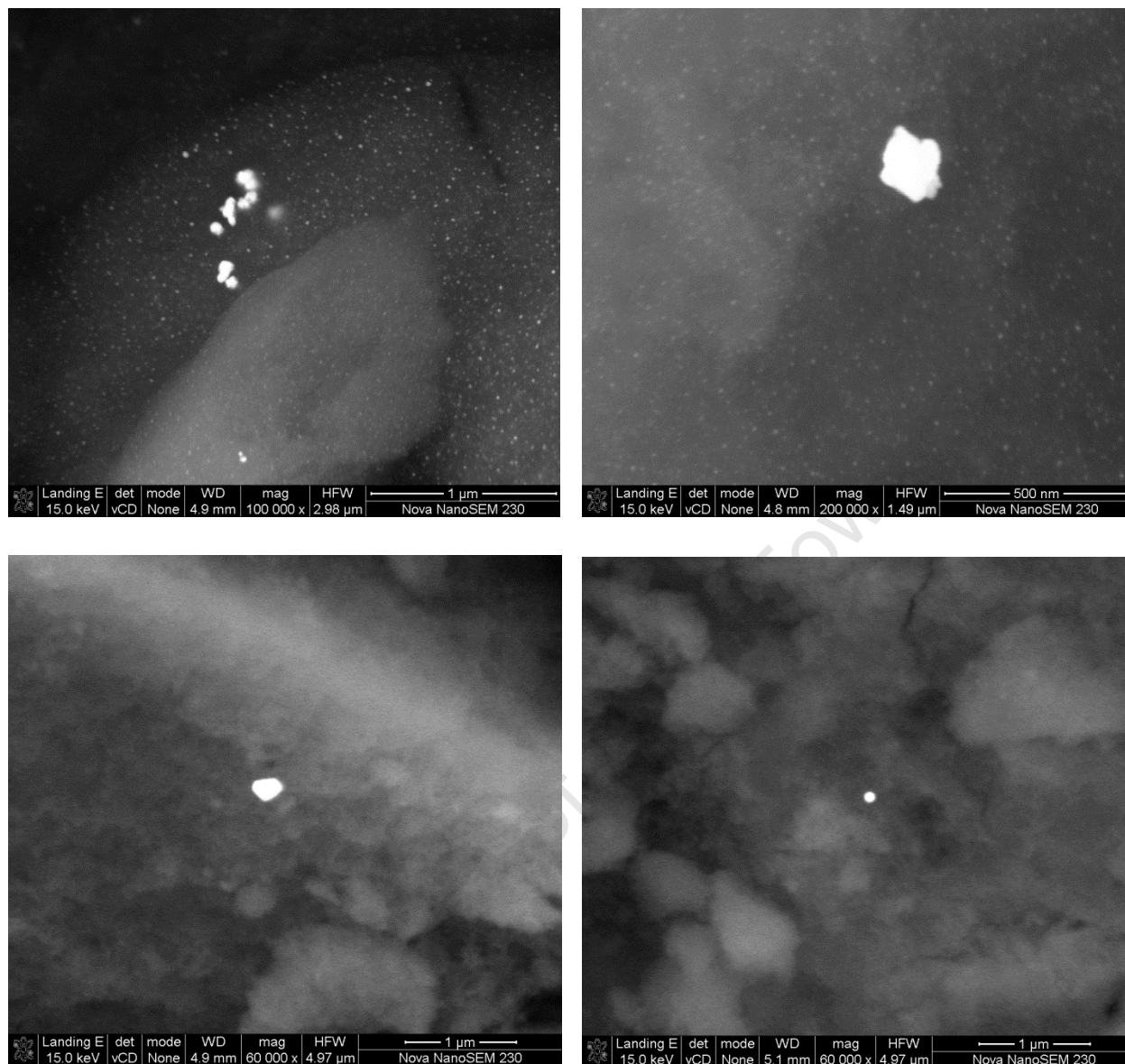


Figure 4-14: Example SEM images. Catalyst labels clockwise from top left - C80, C100, CDRY, CDRY

4.1.5 Effect of calcination temperature

The calcination temperature is not considered to be a determining factor for the loading of gold. Rather the fact that each catalyst in this batch was prepared separately, together with errors in measuring the loading, has resulted in the fluctuations in loading observed in Figure 4-15.

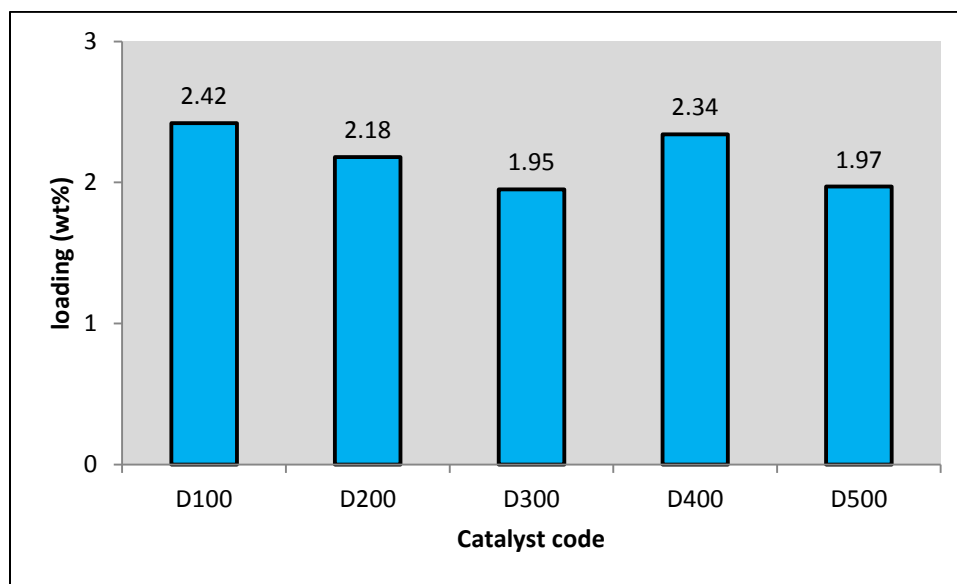


Figure 4-15: Effect of calcination temperature on gold loading

When looking at the TEM results two distinct sizes are observed. Catalysts calcined at 100 or 200°C have a larger average crystallite size above 4nm while catalysts calcined at higher temperatures show smaller sizes, near 3nm. It was thought that this was due to the crystallites below 3nm being harder to identify and measure on the TEM. HRTEM on catalysts D200-D400 resulted in lower average crystallite sizes than observed on TEM. Statistically this difference was shown to be significant for all three catalysts at 95% confidence (using a t-test). However, at 99% confidence only D300 and D400 had significant differences. This implies that the larger average crystallite size measured on catalysts D100 and D200 is not just an effect of the resolution limitations of the TEM, and that in fact the difference in size between D100-200 and D300-500 may be larger than measured by TEM rather than smaller.

Oxygen chemisorption sizes show a somewhat different trend to that of the TEM measured crystallites (see Figure 4-16). The catalyst calcined at 100°C has a much larger crystallite size than the rest of the batch. For the remainder of the samples an overall increase in crystallite size with increasing calcination temperature was observed, rather than a decrease.

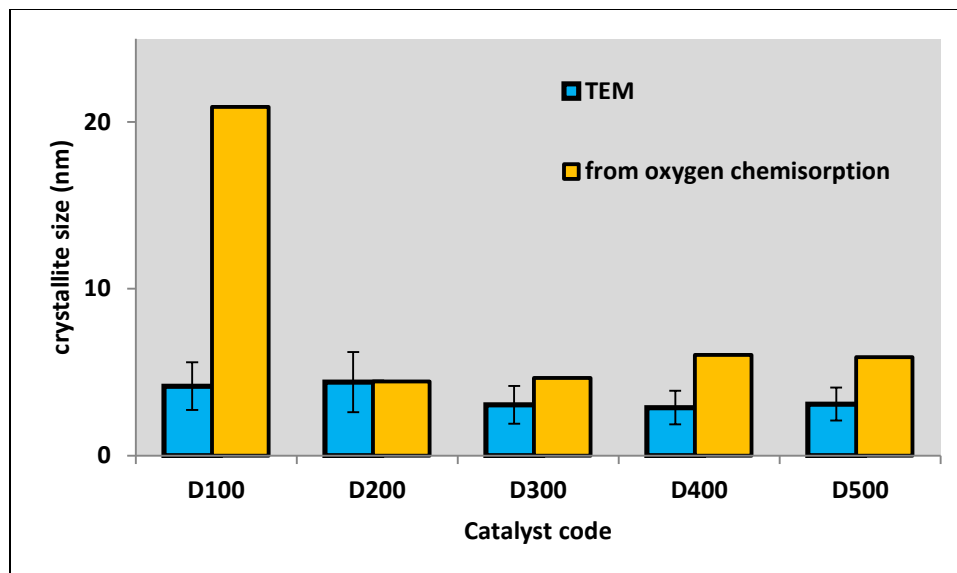


Figure 4-16: Effect of calcination temperature on crystallite size

SEM images for this batch showed a significant number of gold particles on the support. Even with the exception of the catalyst D400 sample there appears to be a steady decline in gold particle size as the calcination temperature is increased (see Figure 4-17). This might seem counterintuitive, as an increase in agglomeration and sintering is expected with increased temperature. It is possible that the samples were simply not exposed to these high temperatures for long enough for this to affect the SEM visible particles with calcination having a duration of 2 hours.

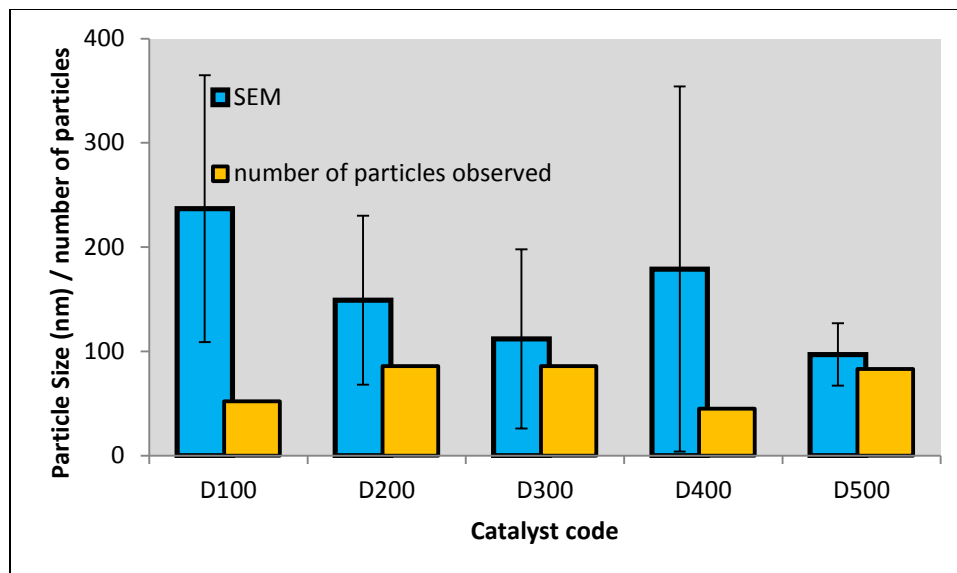


Figure 4-17: effect of calcination temperature on size and frequency of large gold crystallites

4.2 Catalyst testing

Catalyst D400 was tested for both CO and CO₂ hydrogenation activity at similar conditions. The activity for CO₂ hydrogenation was found to be significantly higher than for CO hydrogenation. Product distribution differs significantly between the reactions where CO hydrogenation formed primarily methane, as well as some ethane, ethane and methanol. Yields are low and methanol has a maximum selectivity of 9% at 250°C. CO₂ hydrogenation over the same catalyst results in higher yields of methanol (1.4 C-% as opposed to 0.7 C-% at 250°C), however, the selectivity to methanol is still below 9% due to formation of CO from the water gas shift reaction, while the formation of ethane and ethene is no longer observed.

Catalyst C80 was also tested for activity in CO₂ hydrogenation. It was found to have higher yields of methane and methanol than catalyst D400 at temperatures up to 300°C, with the additional presence of ethanol, ethanal, acetone, and ethyl acetate as products. Primarily due to much lower formation of CO from water gas shift, the methanol yields are as high as 30%, decreasing with increasing reaction temperature. Characterization of catalysts C80 and D400 did not yield significant differences. TEM results were very similar (2.2nm and 2.8nm respectively). Chemisorption results showed a higher oxygen adsorption on catalyst D400 (and thus a smaller calculated gold crystallite size). However, the biggest difference in characteristics

of these two catalysts was observed on the SEM. Catalyst C80 had visibly homogenous / well dispersed gold crystallites of below 20nm in size appear on the SEM images, while only the large (>50nm) gold particles and agglomerations were visible on the D400 sample.

During testing of catalyst D400 the reaction temperature was returned to 250°C at the end of the run to investigate what effect the likely deactivation of the catalyst would have on the product yields. The yields for all products drop compared to their earlier evaluation at the same temperature. However, the methanol yield drops most severely, being most affected by the deactivation of the catalyst.

Sakurai & Haruta, (1995, 1996) showed that for CO and CO₂ hydrogenation maximum yields of methanol are achieved near 250°C for most supported gold catalysts they tested over a temperature range of 150-400°C (Au/ZnO, Au/Fe₂O₃, Au/TiO₂). The presence or absence of products other than methane, methanol and carbon monoxide for CO₂ hydrogenation was not reported nor the gold loading or crystallite size for some of the catalysts.

Sakurai & Haruta, (1995) reported the formation of small amounts C₂ and C₃ products as well as CO₂ during CO hydrogenation. Zhao *et al.* (2007) conducted CO hydrogenation at 25 bar and 300°C, and C₁₀+ products were formed in measurable quantities.

There is no literature with results of CO hydrogenation specifically on a Au/Al₂O₃ catalyst. A comparison of relevant catalysts that have been tested is given in Table 4-2. While the Au/ZnO catalysts perform better than the catalyst tested in this study, ZnO is a known methanol synthesis catalyst and has a significant effect in the results obtained from those catalysts.

Table 4-2: Comparison of methanol yields and selectivity's for CO hydrogenation at 250°C of catalysts D400 and C80 with supported gold catalysts from literature

<i>Catalyst description Au content in wt%</i>	<i>d_{Au} (nm)</i>	<i>Testing conditions</i>	<i>Yield and [selectivity] of MeOH (C-%)</i>	<i>Reference</i>
2.3% Au/Al ₂ O ₃ [D400]	2.8 ^a	30 bar CO/H ₂ = 1/2 3450 ml h ⁻¹ g ⁻¹	0.07 [9.5]	-
11% Au/ZnO	3.5 ^c	50 bar CO/H ₂ /Ar = 30/60/10	~2.5 [70.3]	(Sakurai and Haruta, 1995)
Au/Fe ₂ O ₃	3.3 ^c	3000 ml h ⁻¹ g ⁻¹	~1 [16.3]	(Sakurai and Haruta, 1995)
5% Au/ZnO ^b	-	25 bar [300°C] CO/H ₂ /N ₂ = 47.5/47.5/5	[87] ^d	(Zhao <i>et al.</i> , 2007)
5% Au/Fe ₂ O ₃ ^b	-	Unknown space velocity	[0.2]	(Zhao <i>et al.</i> , 2007)

^a measured from TEM

^b Sizes and yields not given in paper

^c measured from XRD

^d selectivity excludes possible formation of carbon dioxide and methane

While the testing conditions are somewhat different for CO₂ hydrogenation, with increased pressures and lower space velocities, it is clear that the catalysts in this study perform as well as, if not better than catalysts in literature (Table 4-3). When looking at catalyst C80, only the Au/ZnO catalyst performs slightly better in terms of selectivity.

Table 4-3: Comparison of methanol yields and selectivity's for CO₂ hydrogenation at 250°C of catalysts D400 and C80 with supported gold catalysts from literature

<i>Catalyst description Au content in wt%</i>	<i>d_{Au} (nm)</i>	<i>Testing conditions</i>	<i>Yield and [selectivity] of MeOH (C-%)</i>	<i>Reference</i>
2.3% Au/Al ₂ O ₃ [D400]	2.8 ^a	30 bar	1.4 [8.6]	-
2.6% Au/Al ₂ O ₃ [C80]	2.2 ^a	CO ₂ /H ₂ = 1/3 3450 ml h ⁻¹ g ⁻¹	6.0 [30]	-
Au/Al ₂ O ₃ ^b	-		~2 [12]	(Sakurai and Haruta, 1996)
11% Au/ZnO	3.5 ^c	50 bar	~4 [49]	(Sakurai and Haruta, 1996)
Au/Fe ₂ O ₃ ^b	3.3 ^c	CO ₂ /H ₂ /Ar = 23/67/10 3000 ml h ⁻¹ g ⁻¹	~5 [30]	(Sakurai and Haruta, 1996)
Au/TiO ₂ ^b	-		~2 [12]	(Sakurai and Haruta, 1996)

^a measured from TEM

^b Sizes not given in paper

^c measured from XRD

5 CONCLUSIONS

The aims of this study were threefold. One of the aims was to investigate the use of oxygen chemisorption as an alternative characterization technique to TEM. A second target of this study was to investigate the effect of numerous preparation variables on the characteristics of supported gold catalysts. The effects of variations in the concentration of gold in the precursor solution, the washing procedure, the conditions of drying as well as the temperature of calcination were investigated. Lastly how the key preparation variables influence the yields and selectivities during catalyst testing in methanol synthesis is investigated and compared to testing reported in literature.

5.1 Oxygen chemisorption as an alternative to TEM

TEM and HRTEM are widely accepted and utilized techniques for characterizing crystallite size distributions. While in certain situations other techniques such as XRD can be used to validate the results of TEM analysis this is generally not possible for supported gold catalysts due to their characteristic low loadings and small gold crystallite sizes. Oxygen chemisorption has been identified as a possible alternate method for gold crystallite size determination in the nanometer range.

TEM has clear weaknesses due to the sample size and the resolution limitations of the microscope. While oxygen chemisorption has neither of these problems, it has serious drawbacks of its own. Numerous assumptions are made when calculating the average crystallite size from the adsorption measurement, and numerous sources of error are present.

This study has shown that over a wide range of variations in catalyst preparation technique, the results of TEM and oxygen chemisorption agree only in the order of magnitude sense. Trends observed on TEM do not always match those observed for oxygen chemisorption. Neither result should be discarded, however, until the relationship between gold crystallite size distribution and their oxygen chemisorption is better understood, they should be considered separately.

Oxygen chemisorption results were used to calculate the mass fraction of gold present as nano-crystallites. It was found that this fraction is typically less than 1%.

5.2 The effect of preparation method on catalyst characteristics

5.2.1 Loading efficiency

The loading efficiency of gold onto the support is not affected by increases in the concentration of the gold precursor. As was expected, variations in the drying and calcination procedure had no effect on the gold loading efficiency either.

What did play a significant role was the ammonia wash step. Omitting this wash resulted in a higher loading efficiency as there was less opportunity for gold losses, while a drop in the concentration of ammonia used in this wash, also resulted in a drop in the gold loading. However, it should be noted that omitting the wash also resulted in a catalyst that had no gold crystallites below 10nm in size. It is clear that the washing procedure plays a vital role in the formation of small well dispersed gold crystallites, as well as the efficiency of this process.

5.2.2 Gold crystallite size

Gold crystallite size is affected by many of the variables, some more significantly than others. At a low temperature calcination (200°C) increasing the concentration of the gold in the precursor solution resulted in smaller gold crystallite sizes measured from TEM images. At a calcination temperature of 500°C no significant effect on gold crystallite size is observed.

As has been mentioned already the washing procedure is critical in allowing well dispersed gold nano-particles to form. The omission of the ammonia wash results in large (>50nm) gold particles. Both TEM and oxygen chemisorption are in agreement with no effect on crystallite sizes with variation in the washing time, concentration or solid/liquid ratio.

The drying process plays a small role in the gold crystallite size obtained. Drying the catalyst in flowing gas or in a rotary evaporator resulted in smaller gold crystallites than static drying techniques.

An increase in the calcination temperature from 200 to 300°C resulted in an unexpected decrease in gold crystallite size measured on the TEM. There was no significant change in the average crystallite size up to 500°C. An increase in the calcination temperature was expected to cause sintering and an increase in the average gold crystallite size. Calcination was conducted

for 2 hours; it is likely that increasing this time would result in an increase in the gold crystallite size as expected.

5.2.3 SEM visible gold particles

As much as 99% of the gold loaded onto the catalyst takes the form of large gold particles and agglomerations that are visible with SEM. Variations in the preparation of the catalysts did not have any significant effects on the SEM visible particles for the most part. Omitting the ammonia wash from the preparation of these catalysts resulted in the presence of many more large particles on the surface of the support. This was also observed on the TEM images where no small crystallites were observed.

Drying the catalysts in a rotary evaporator at reduced pressures led to small barely SEM visible gold crystallites homogeneously distributed over the surface of the support.

5.3 Catalytic testing in CO and CO₂ hydrogenation

Supported gold catalysts have been shown in this study to exhibit significant activity in the synthesis of methanol from CO and CO₂ hydrogenation. Methanol yields and selectivities are comparable and even surpass those of similar catalysts studied in literature. It is found that for CO₂ hydrogenation the yield of methanol and other alcohols is significantly higher than for CO hydrogenation over the same catalyst. Comparison of different catalysts for CO₂ hydrogenation leads to the conclusion that the preparation of gold catalysts play a significant role in the product distribution and yields obtained. In particular, a small change in the drying procedure, that had no effect on the gold crystallite size observed on TEM images, resulted in an increase in the yield and selectivity of methanol

It is clear that there is still a large room for improvement in the preparation of supported gold catalysts. The washing and drying of the catalysts during preparation were identified as key steps in the resultant characteristics of the catalyst. It was shown that variation in the drying procedure affects the product yields and selectivities during methanol synthesis significantly.

This study was limited to one type of catalyst preparation. Similar investigation into other preparation methods such as impregnation and deposition-precipitation might yield further insight into the importance of catalyst preparation on its characteristics and performance during reaction.

University of Cape Town

7 REFERENCES

- Beeming, B.A., 2008. Synthesis and characterisation of carbon supported gold catalysts prepared by ion-exchange. MSc thesis, University of Cape Town, Cape Town.
- Beeming, B.A., Bialek, K., 2006. Synthesis and testing of gold catalyst prepared by ion-exchange. 4th year thesis, University of Cape Town, Cape Town.
- Bergh, C., Van Heerden, T., 2009. Synthesis and characterization of supported gold catalysts by anionic exchange for the oxidation of alcohols. 4th year thesis, University of Cape Town, Cape Town.
- Berndt, H., Pitsch, I., Evert, S., Struve, K., Pohl, M., Radnik, J., Martin, A., 2003. Oxygen adsorption on Au/Al₂O₃ catalysts and relation to the catalytic oxidation of ethylene glycol to glycolic acid. *Applied Catalysis A: General* 244, 169-179.
- Bond, G.C., 1972. The catalytic properties of gold. *Gold Bulletin* 5, 11-13.
- Bond, G.C., Louis, C., Thompson, D., 2006. *Catalysis by Gold*. Imperial College Press.
- Bond, G.C., Thompson, D.T., 1999. Catalysis by gold. *Catalysis Review - Science and Engineering* 41, 319-388.
- Brunelle, J.P., 1978. Preparation of catalysts by metallic complex adsorption on mineral oxides. *Pure and Applied Chemistry* 50, 1211-1229.
- Bus, E., Miller, J.T., van Bokhoven, J.A., 2005. Hydrogen chemisorption on Al₂O₃-supported gold catalysts. *The journal of physical chemistry. B* 109, 14581-14587.
- Case, J.M., 2009. Gold catalysts prepared by ion exchange for use in ethylene glycol oxidation: An exploratory study. MSc thesis, University of Cape Town, Cape Town.
- Centeno, M.A., Hadjiivanov, K., Venkov, T., Klimev, H., Odriozola, J.A., 2006. Comparative study of Au/Al₂O₃ and Au/CeO₂-Al₂O₃ catalysts. *Journal of Molecular Catalysis* 252, 142-149.
- Choi, Y., Futagami, K., Fujitani, T., Nakamura, J., 2001. The role of ZnO in Cu/ZnO methanol synthesis catalysts — morphology effect or active site model? *Applied Catalysis A: General* 208, 163-167.
- Claus, P., 2005. Heterogeneously catalysed hydrogenation using gold catalysts. *Applied Catalysis A: General* 291, 222-229.

- Comotti, M., Li, W.-C., Spliethoff, B., Schüth, F., 2006. Support effect in high activity gold catalysts for CO Oxidation. *Journal of the American Chemical Society* 128, 917-924.
- English, A., Brown, J., Rovner, J., Davies, S., Davy Process Technology, 1992. Methanol, in: *Kirk-Othmer Encyclopedia of Chemical Technology*.
- Fujitani, T., Saito, M., Kanai, Y., Kakumoto, T., Watanabe, T., Nakamura, J., Uchijima, T., 1994. The role of metal oxides in promoting a copper catalyst for methanol synthesis. *Catalysis Letters* 25, 271-276.
- Fukushima, T., Galvagno, S., Parravano, G., 1979. Oxygen chemisorption on supported gold. *Journal of Catalysis* 57, 177-182.
- Grabowski, R., Kozłowska, a., Olszewski, P., Stoch, J., Skrzypek, J., Lachowska, M., Słoczyński, J., 2004. Catalytic activity of the $M/(3ZnO \cdot ZrO_2)$ system ($M=Cu, Ag, Au$) in the hydrogenation of CO_2 to methanol. *Applied Catalysis A: General* 278, 11-23.
- Haruta, M., 1997. Size-and support dependency in the catalysis of gold. *Catalysis Today* 36, 153-166.
- Haruta, M., 2004. Gold as a novel catalyst in the 21st century : preparation, working mechanism and applications. *Gold Bulletin* 37, 27-36.
- Haruta, M., Yamada, N., Kobayashi, T., Iijima, S., 1989. Gold catalysts prepared by coprecipitation for low-temperature oxidation of hydrogen and of carbon monoxide. *Journal of Catalysis* 115, 301-309.
- Hugon, A., Kolli, N.E., Louis, C., 2010. Advances in the preparation of supported gold catalysts: Mechanism of deposition, simplification of the procedures and relevance of the elimination of chlorine. *Journal of Catalysis* 274, 239-250.
- Ivanova, S., Petit, C., Pitchon, V., 2004. A new preparation method for the formation of gold nanoparticles on an oxide support. *Applied Catalysis A: General* 267, 191-201.
- Ivanova, S., Pitchon, V., Zimmermann, Y., Petit, C., 2005. Preparation of alumina supported gold catalysts: Influence of washing procedures, mechanism of particles size growth. *Applied Catalysis A: General* 298, 57-64.
- Kartusch, C., Bokhoven, J.A.V., Bond, G.C., Louis, C., 2009. Hydrogenation over gold catalysts: The interaction of gold with hydrogen. *Gold Bulletin* 42, 343-348.

- Kurtz, M., Wilmer, H., Genger, T., Hinrichsen, O., Muhler, M., 2003. Deactivation of supported copper catalysts for methanol synthesis. *Catalysis Letters* 86, 77-80.
- Lekhal, A., Glasser, B.J., Khinast, J.G., 2001. Impact of drying on the catalyst profile in supported impregnation catalysts. *Chemical Engineering Science* 56, 4473-4487.
- Lemire, C., Meyer, R., Shaikhutdinov, S., 2004. Do quantum size effects control CO adsorption on gold nanoparticles? *Angewandte Chemie International Edition* 43, 118 -121.
- Lemire, C., Meyer, R., Shaikhutdinov, S.K., Freund, H., 2004. CO adsorption on oxide supported gold: from small clusters to monolayer islands and three-dimensional nanoparticles. *Surface Science* 552, 27-34.
- the Methanol Institute, 2011. Methanol Institute milestones [WWW Document]. URL <http://www.methanol.org/Files/About-Us/2011-Milestones.aspx>
- Meyer, R., Lemire, C., Shaikhutdinov, S.K., Freund, H., 2004. Surface chemistry of catalysis by gold. *Gold Bulletin* 37, 72-124.
- Mihaylov, M., Knözinger, H., Hadjiivanov, K., Gates, B.C., Weitkamp, J., 2007. Characterization of the oxidation states of supported gold species by IR spectroscopy of adsorbed CO. *Chemie Ingenieur Technik* 79, 795-806.
- Oh, H.-S., Yang, J.H., Costello, C.K., Wang, Y.M., Bare, S.R., Kung, H.H., Kung, M.C., 2002. Selective catalytic oxidation of CO: Effect of chloride on supported Au catalysts. *Journal of Catalysis* 210, 375-386.
- Outka, D.A., Madix, R.J., 1987. The oxidation of carbon monoxide on the Au(110) surface. *Surface Science* 179, 351-360.
- Porta, F., Prati, L., Rossi, M., Coluccia, S., Martra, G., 2000. Metal sols as a useful tool for heterogeneous gold catalyst preparation: reinvestigation of a liquid phase oxidation 61, 165-172.
- Reuss, G., Disteldorf, W., Gamer, A.O., Hild, A., 2002. Formaldehyde, in: *Ullmann's Encyclopedia of Industrial Chemistry*. Wiley-VCH, Weinheim.
- Ruggiero, C., Hollins, P., 1996. Adsorption of carbon monoxide on the gold (332) surface. *Journal of the Chemical Society, Faraday Transactions* 92, 4829-4834.

- SRI Consulting, 2010. WP report [WWW Document]. URL <http://www.ihs.com/products/chemical/planning/ceh/methanol.aspx>
- Sakurai, H., Haruta, M., 1995. Carbon dioxide and carbon monoxide hydrogenation over gold supported on titanium, iron, and zinc oxides. *Applied Catalysis A: General* 127, p93-105.
- Sakurai, H., Haruta, M., 1996. Synergism in methanol synthesis from carbon dioxide over gold catalysts supported on metal oxides. *Catalysis Today* 29, p361-365.
- Scherrer, P., 1918. Bestimmung der Grösse und der inneren Struktur von Kolloidteilchen mittels Röntgenstrahlen. *Nachr. Ges. Wiss. Göttingen* 26, 98-100.
- Shaikhutdinov, S.K., Meyer, R., Naschitzki, M., Ba, M., Freund, H., 2003. Size and support effects for CO adsorption on gold model catalysts. *Catalysis Letters* 86, 211-219.
- Shibata, M., Kawata, N.N., Masumoto, T., Kimura, H., 1985. CO Hydrogenation over an amorphous gold-zirconium alloy. *Chemistry Letters* 1605-1608.
- Steinhauser, G., Evers, J., Jakob, S., Klapötke, T.M., Oehlinger, G., 2008. A review on fulminating gold (Knallgold). *Gold Bulletin* 41, 305-317.
- Strunk, J., Kahler, K., Xia, X., Comotti, M., Shuth, F., Reineke, T., Muhler, M., 2009. Au/ZnO as catalyst for methanol synthesis: The role of oxygen vacancies. *Applied catalysis A: General* 359, 121-128.
- Van Steen, E., 2009. Modelling of speciation in gold containing solutions. Personal communication [e-mail]
- Venkov, T., Klimev, H., Centeno, M.A., Odriozola, J.A., Hadjiivanov, K., 2006. State of gold on an Au/Al₂O₃ catalyst subjected to different pre-treatments: An FTIR study. *Catalysis Communications* 7, 308-313.
- Weirauch, W., 2006. China is the source of most global methanol demand growth [WWW Document]. *Hydrocarbon Processing*. URL <http://www.highbeam.com/doc/1G1-146220572.html>
- Williams, D.B., Carter, C.B., 2009. *Transmission electron microscopy: a textbook for materials science*, 2nd ed. Springer.
- Wolf, A., Schüth, F., 2002. A systematic study of the synthesis conditions for the preparation of highly active gold catalysts. *Applied Catalysis A: General* 226, 1-13.
- Xu, Q., Kharas, K.C.C., Datye, A.K., 2003. The preparation of highly dispersed Au/Al₂O₃ by aqueous impregnation. *Catalysis Letters* 85, 229-235.
- Yang, J. H., Henao, J. D., Costello, C., Kung, M. C., Kung, H. H., Miller, J. T., Kropf, A. J., Kim,

J. -G., Regalbuto, J. R., Bore, M. T., Pham, H. M., Datye, A. K., Laeger, J. D., Kharas. K., 2005. Understanding preparation variables in the synthesis of Au/Al₂O₃ using EXAFS and electron microscopy. *Applied Catalysis A: General* 291, 73-84.

Zhao, Y., Mpela, A., Enache, D.I., Taylor, S.H., Hildebrandt, D., Glasser, D., Hutchings, G.J., Atkins, M.P., Scurrel, M.S., 2007. Study of carbon monoxide hydrogenation over supported Au catalysts. *Studies in Surface Science and Catalysis* 163, 141-151.

Zwane, S., 2004. Vanadia-promoted Co-Al₂O₃ Fischer-Tropsch catalysts. Phd thesis, University of Cape Town, Cape Town.

University of Cape Town

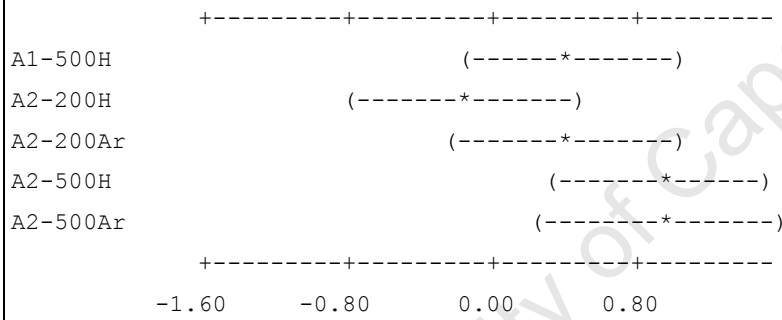
Tukey 95% Simultaneous Confidence Intervals

All Pairwise Comparisons

Individual confidence level = 99.53%

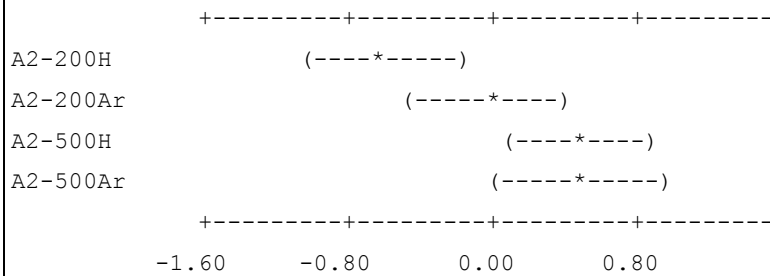
A1-200H subtracted from:

	Lower	Center	Upper
A1-500H	-0.1939	0.4321	1.0581
A2-200H	-0.8101	-0.1831	0.4440
A2-200Ar	-0.2450	0.4003	1.0456
A2-500H	0.2980	0.9220	1.5461
A2-500Ar	0.2591	0.9216	1.5841

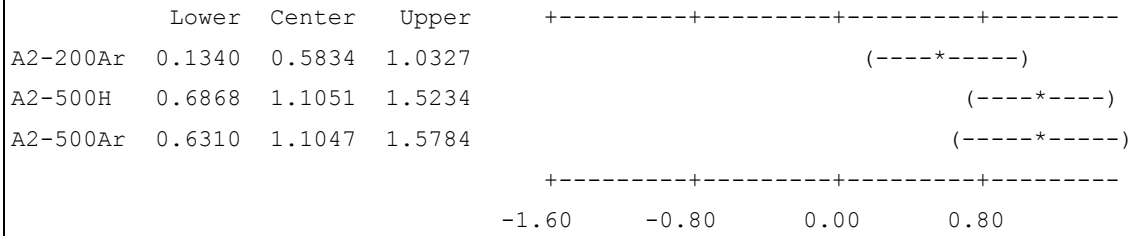


A1-500H subtracted from:

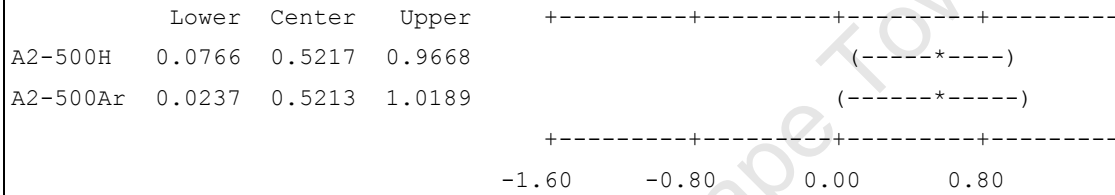
	Lower	Center	Upper
A2-200H	-1.0364	-0.6152	-0.1939
A2-200Ar	-0.4797	-0.0318	0.4161
A2-500H	0.0732	0.4899	0.9067
A2-500Ar	0.0172	0.4895	0.9619



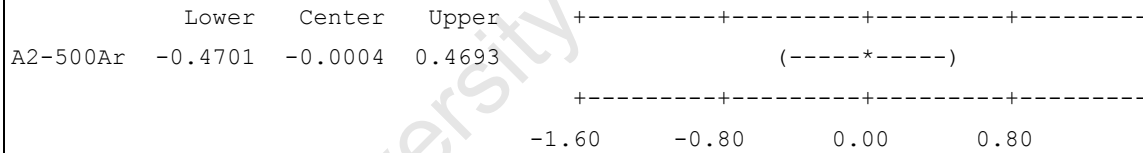
A2-200H subtracted from:



A2-200Ar subtracted from:



A2-500H subtracted from:

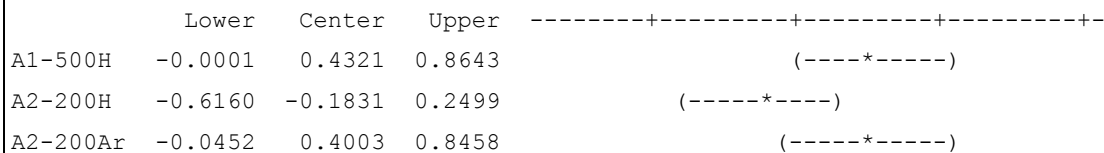


Fisher 95% Individual Confidence Intervals

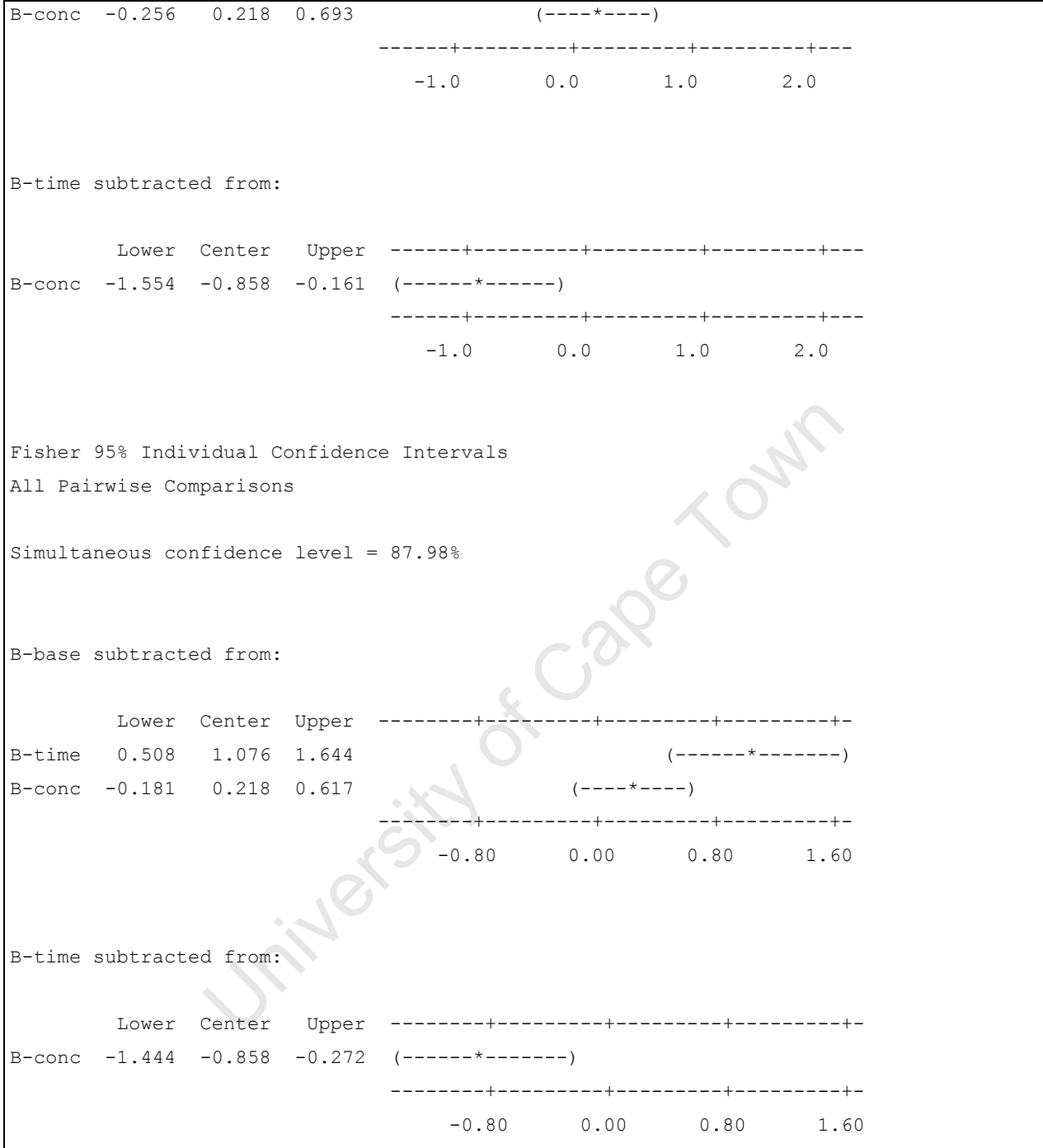
All Pairwise Comparisons

Simultaneous confidence level = 63.88%

A1-200H subtracted from:



Appendix A



Batch C

One-way ANOVA: C-wet, C-dry, C60, C80, C100

Appendix A

Source	DF	SS	MS	F	P
Factor	4	31.797	7.949	14.83	0.000
Error	449	240.705	0.536		
Total	453	272.502			

S = 0.7322 R-Sq = 11.67% R-Sq(adj) = 10.88%

Individual 99% CIs For Mean Based on Pooled StDev

Level	N	Mean	StDev
C-wet	101	2.6582	0.6528
C-dry	79	2.8718	0.6993
C60	66	3.0031	1.0529
C80	103	2.2148	0.4820
C100	105	2.5922	0.7857

2.10 2.45 2.80 3.15

Pooled StDev = 0.7322

Tukey 95% Simultaneous Confidence Intervals
All Pairwise Comparisons

Individual confidence level = 99.34%

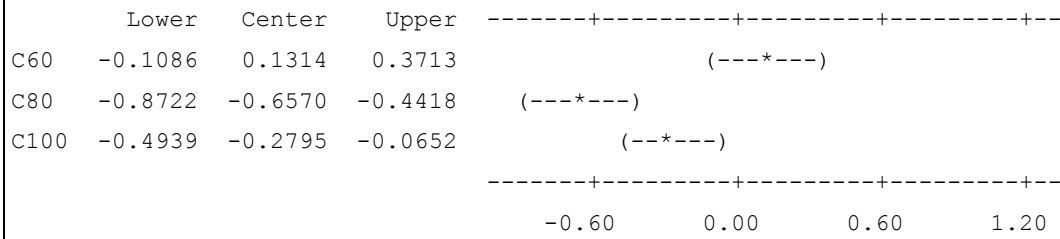
C-wet subtracted from:

	Lower	Center	Upper
C-dry	-0.0866	0.2135	0.5137
C60	0.0286	0.3449	0.6612
C80	-0.7233	-0.4435	-0.1636
C100	-0.3445	-0.0660	0.2125

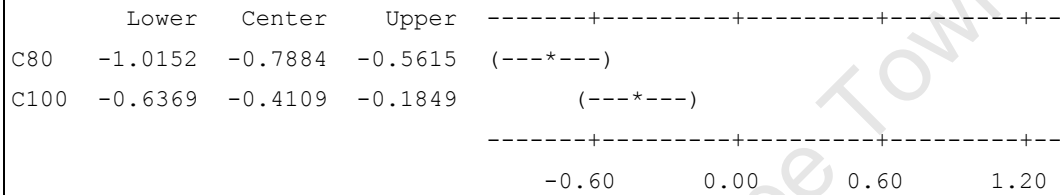
-0.60 0.00 0.60 1.20

C-dry subtracted from:

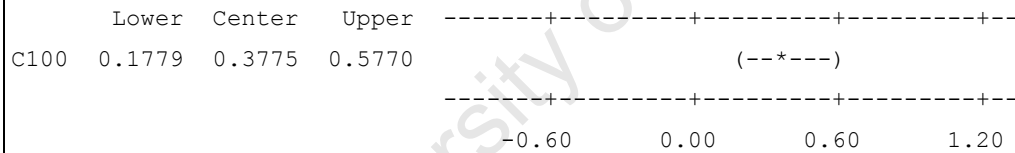
C-dry subtracted from:



C60 subtracted from:



C80 subtracted from:



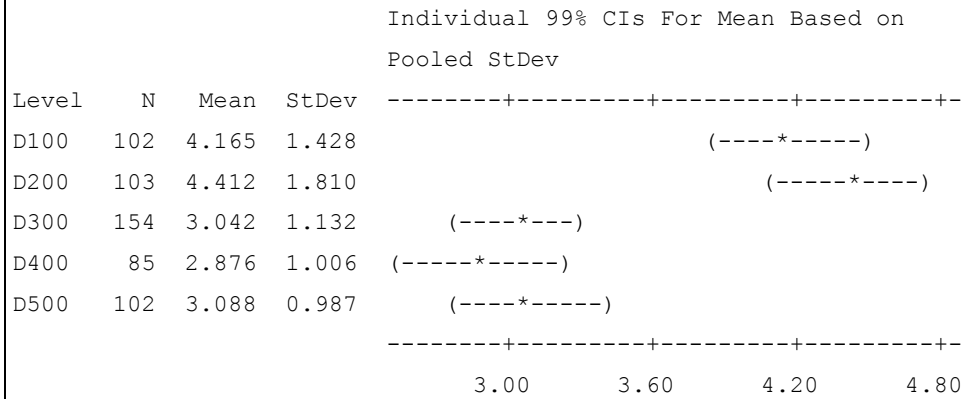
Batch D

One-way ANOVA: D100, D200, D300, D400, D500

Source	DF	SS	MS	F	P
Factor	4	213.47	53.37	31.39	0.000
Error	541	919.66	1.70		
Total	545	1133.12			

S = 1.304 R-Sq = 18.84% R-Sq(adj) = 18.24%

Appendix A



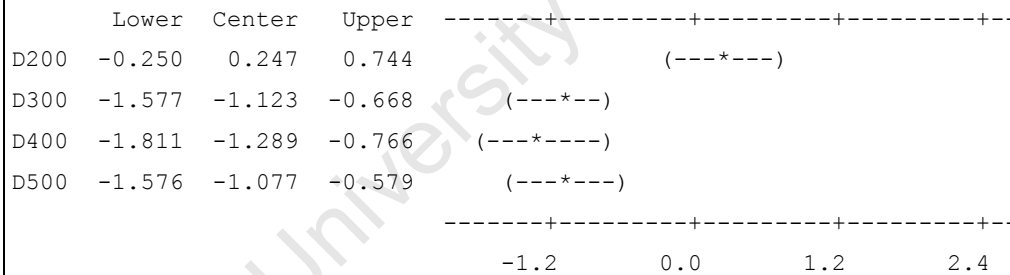
Pooled StDev = 1.304

Tukey 95% Simultaneous Confidence Intervals

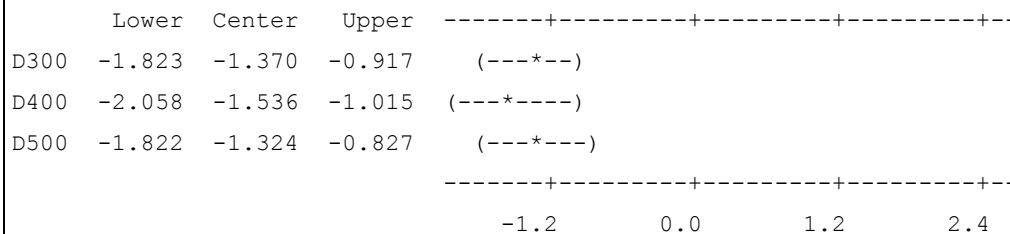
All Pairwise Comparisons

Individual confidence level = 99.34%

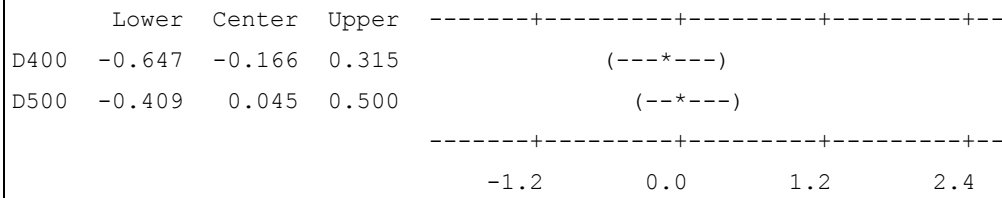
D100 subtracted from:



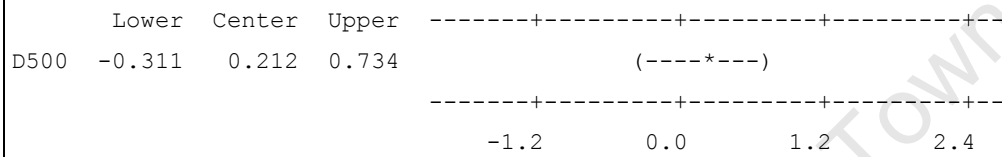
D200 subtracted from:



D300 subtracted from:



D400 subtracted from:

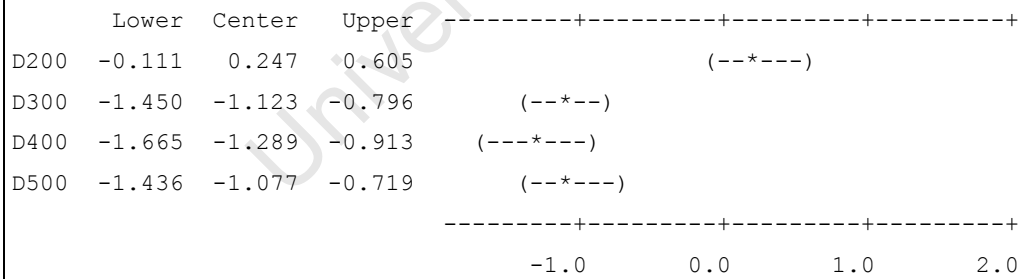


Fisher 95% Individual Confidence Intervals

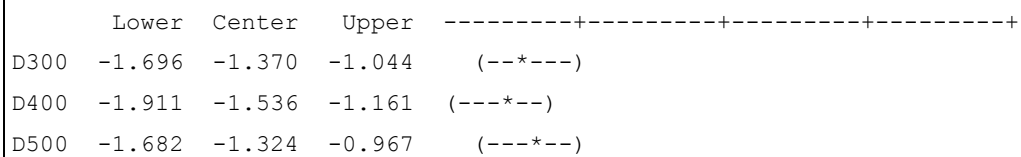
All Pairwise Comparisons

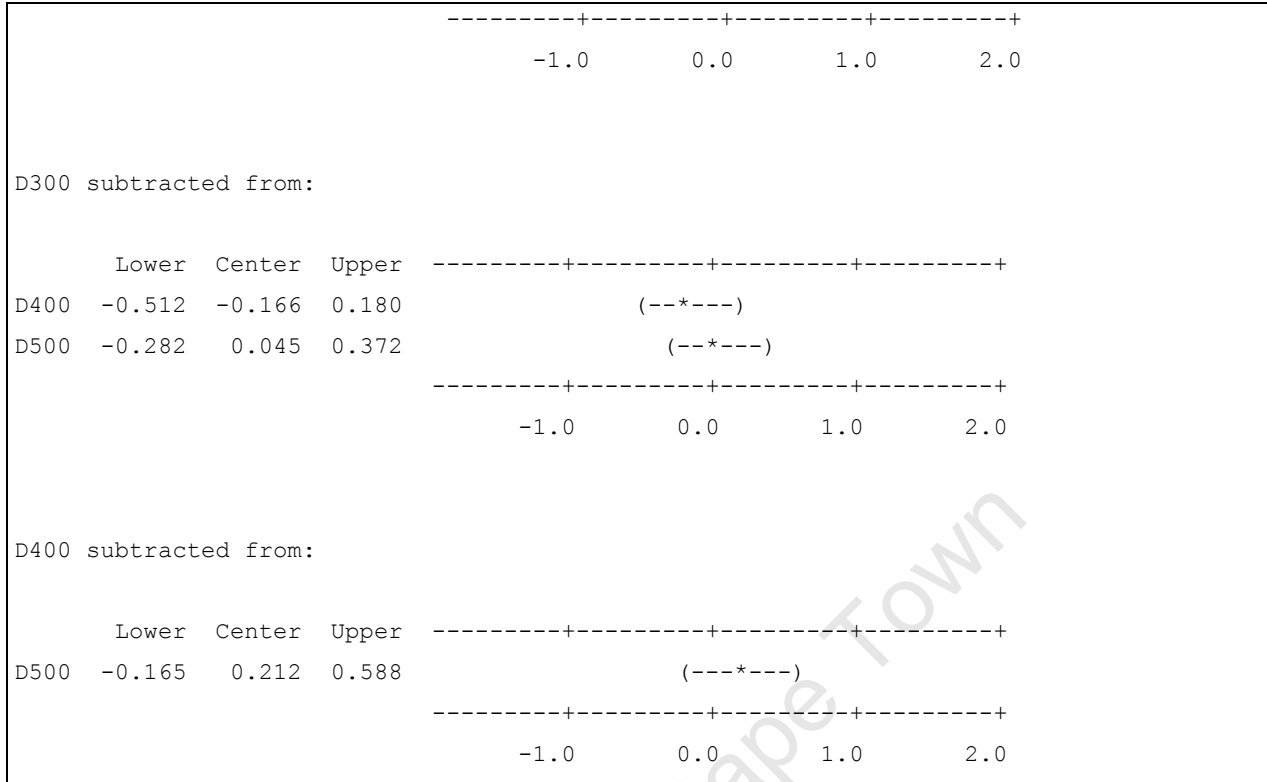
Simultaneous confidence level = 71.64%

D100 subtracted from:



D200 subtracted from:





8.2 T-test comparison of TEM and HRTEM

D200

Two-Sample T-Test and CI: HRTEM, TEM

Two-sample T for HRTEM vs TEM

	N	Mean	StDev	SE Mean
HRTEM	80	3.96	1.17	0.13
TEM	103	4.41	1.81	0.18

Difference = mu (HRTEM) - mu (TEM)

Estimate for difference: -0.448

95% CI for difference: (-0.885, -0.011)

T-Test of difference = 0 (vs not =): T-Value = -2.03 P-Value = 0.044 DF = 175

Two-Sample T-Test and CI: HRTEM, TEM

Two-sample T for HRTEM vs TEM

	N	Mean	StDev	SE Mean
HRTEM	80	3.96	1.17	0.13
TEM	103	4.41	1.81	0.18

Difference = mu (HRTEM) - mu (TEM)

Estimate for difference: -0.448

99% CI for difference: (-1.024, 0.128)

T-Test of difference = 0 (vs not =): T-Value = -2.03 P-Value = 0.044 DF = 175

D300**Two-Sample T-Test and CI: HRTEM, TEM**

Two-sample T for HRTEM vs TEM

	N	Mean	StDev	SE Mean
HRTEM	89	2.373	0.595	0.063
TEM	154	3.04	1.13	0.091

Difference = mu (HRTEM) - mu (TEM)

Estimate for difference: -0.669

95% CI for difference: (-0.887, -0.451)

T-Test of difference = 0 (vs not =): T-Value = -6.03 P-Value = 0.000 DF = 239

Two-Sample T-Test and CI: HRTEM, TEM

Two-sample T for HRTEM vs TEM

	N	Mean	StDev	SE Mean
HRTEM	89	2.373	0.595	0.063
TEM	154	3.04	1.13	0.091

Difference = μ (HRTEM) - μ (TEM)
 Estimate for difference: -0.669
 99% CI for difference: (-0.957, -0.381)
 T-Test of difference = 0 (vs not =): T-Value = -6.03 P-Value = 0.000 DF = 239

D400

Two-Sample T-Test and CI: HRTEM, TEM

Two-sample T for HRTEM vs TEM

	N	Mean	StDev	SE Mean
HRTEM	50	2.297	0.530	0.075
TEM	85	2.88	1.01	0.11

Difference = μ (HRTEM) - μ (TEM)
 Estimate for difference: -0.579
 95% CI for difference: (-0.841, -0.317)
 T-Test of difference = 0 (vs not =): T-Value = -4.37 P-Value = 0.000 DF = 131

Two-Sample T-Test and CI: HRTEM, TEM

Two-sample T for HRTEM vs TEM

	N	Mean	StDev	SE Mean
HRTEM	50	2.297	0.530	0.075
TEM	85	2.88	1.01	0.11

Difference = μ (HRTEM) - μ (TEM)
 Estimate for difference: -0.579
 99% CI for difference: (-0.925, -0.233)
 T-Test of difference = 0 (vs not =): T-Value = -4.37 P-Value = 0.000 DF = 131

University of Cape Town